5-2024

An in Vitro Investigation of Urothelial Cell Function in Response to Hypoxia and Pressure in Relation to Bladder Outlet Obstruction

Britney Hudson
britneh@g.clemson.edu

AN IN VITRO INVESTIGATION OF UROTHELIAL CELL FUNCTION IN
RESPONSE TO HYPOXIA AND PRESSURE IN RELATION TO
BLADDER OUTLET OBSTRUCTION

_____

A Dissertation,
Presented to
the Graduate School of
Clemson University

_____

In Partial Fulfillment
of the Requirements for the Degree
Doctor of Philosophy
Bioengineering

_____

by
Britney Nicolette Hudson
May 2024

_____

Accepted by:
Dr. Jiro Nagatomi, Committee Chair
Dr. Sarah Harcum
Dr. J. Todd Purves
Dr. F. Monty Hughes

ABSTRACT

Bladder outlet obstruction (BOO) is a urological condition affecting around 18.5% of the population and is caused by a narrowing of the urethra. The urethral blockage is accompanied by lower urinary tract symptoms (LUTS) such as hesitancy and weak stream, which are generated by inflammation leading to fibrosis and degraded bladder tissue compliance. The obstruction leads to abnormal chemical and mechanical changes such as high-pressure voiding, high-pressure storage, and tissue ischemia, which are thought to be the trigger of inflammation. Previous work has shown that urothelial cells (UCs) lining the lumen of the bladder respond to high levels of hydrostatic pressure and thus contribute to NLRP3 inflammasome and epithelial-mesenchymal transition (EMT) changes. However, not much work has been conducted to understand the role hypoxia in the initiation of inflammation and the development of BOO pathology. Although this bladder disease can be diagnosed through measuring the pressure of the bladder, this method is invasive and involves the use of catheters. In addition, characterizing the EMT or other bladder tissue changes is not feasible as a tissue biopsy would be necessary. Thus, there needs to be a non-invasive method to determine EMT changes in bladder tissues.

The goal of the current study includes to elucidate the role of hypoxia in the initiation of inflammation in urothelial cells and to characterize the effects of pressure on extracellular vesicle release from urothelial cells as a non-invasive method to detect EMT bladder tissue changes. These goals will be achieved through three specific aims: 1) characterize a two-enzyme system for creating an *in vitro* hypoxic environment, 2)

quantify the urothelial cell response to hypoxia and identify inflammasome activation mechanisms, and 3) characterize exosome release from UCs in response to pressure and hypoxia.

To create an *in vitro* hypoxic environment, the enzymes glucose oxidase (GOX) and catalase (CAT) effects on oxygen and cell viability were quantified. The two-enzyme system was able to effectively reduce oxygen tension in culture media without impacting rat urothelial cell viability. In addition, enzyme-induced hypoxia was able to illicit a hypoxic cell response from the urothelial cells as seen through the stabilization of HIF-1α and increase in extracellular nitric oxide.

Second, the two-enzyme system was used to elucidate the role of hypoxia in the initiation of NLRP3 inflammasome. It was determined that hypoxia led to NLRP3 inflammasome activation in a time-dependent manner. Shorter time periods of hypoxic exposure did not lead to the activation of the NLRP3 inflammasome; however, longer time periods of hypoxic exposure did. In the later stage of BOO, high pressure storage can lead to the compression of blood vessels which create a prolonged hypoxic environment. These results provide further evidence of the dangers occurring during the storage period in the later stages of BOO and the importance of maintaining a lower storage pressure.

Lastly, rat and human urothelial cells were exposed to a pressure cycling regime that mimicked the later stages of BOO via a custom pressure chamber (storage pressure of 15 cm H_2O for 175 minutes and a voiding pressure of 75 cm$H_2$0 for 5 minutes) for various time periods. Extracellular vesicles (EVs) released by the UCs into the media

were harvested using three different methods and compared: classical ultracentrifugation, capillary-channeled fiber spin down-tips, and a commercially available Total Exosome Isolation kit. Analysis of RNAseq data from human UCs exposed to elevated pressure cycling released EVs that contained genes that are mainly expressed in cancer, indicative of EMT, and several novel lncRNA transcripts.

In summary, we have provided evidence of the ability of enzymes to easily create an *in vitro* hypoxic environment and shown that UCs can sense and respond appropriately. Also, we have also shown that UCs initiate inflammation through a different pathway than pressure and that the inflammasome is activated in a time dependent manner. More specifically, instead of the ATP-mediated pathway that pressure invokes, hypoxia leads to inflammation through the ROX/TXNIP/NLRP3 pathway. Furthermore, we have demonstrated that UCs secrete more exosomes as a result of elevated pressure cycling and that pressure cycling can bring about changes in exosomal cargo. These results contribute to the study of how chemical and mechanical stimuli influence bladder pathology as it relates to inflammation and exosome release. This knowledge can aid in the development of new therapeutic targets. In addition, understanding how elevated pressure impacts extracellular vesicle release can lead to the advancement of non-invasive methods to diagnose BOO.

DEDICATION

This work is dedicated to my mother, Nicole, who has always been a guiding force on my academic journey. Thank you for your encouragement, unwavering support, and fostering in me the confidence to become a researcher and engineer. Every success I achieve is a testament to your sacrifices and boundless love.

ACKNOWLEDGMENTS

First, I would like to thank my research advisor Dr. Jiro Nagatomi. This dissertation would not be possible without his support, guidance, patience, and mentorship throughout my graduate career. I am forever grateful to Dr. Nagatomi for providing a challenging learning experience that allowed me to become the engineer and researcher I am today.

Secondly, I would like to thank my committee members and collaborators Dr. Todd Purves and Dr. Monty Hughes, who not only provided guidance and insight but challenged me to become more confident in my research. I would also like to thank Dr. Sarah Harcum who provided invaluable support and connections that helped complete this project. I am very fortunate to have had the opportunity to learn from all of you.

I would also like to thank past and present fellow lab members for their companionship and support. Specifically, Dr. Cody Dunton for passing down his knowledge to me and previous work that helped with the basis of this project. Additional thanks go out to the Clemson Bioengineering Department, specially Maria Torres for helping me get acquainted with graduate school, Cassie Gregory for always answering my questions, Dr. Pattie Tate, Dr. Agnes Nagy-Mehesz for teaching me various protocols, and Dr. Guzeliya Korneva for teaching me how to use various equipment.

Lastly, I would like to thank my friends and family for their support including but not limited to Sarah Mbiki, K. Lora Alatise, and Brenda Okereke.

TABLE OF CONTENTS

LIST OF TABLES

LIST OF FIGURES

List of Figures (Continued)

CHAPTER ONE

Introduction and Background

1.1 Clinical Significance

Bladder outlet obstruction (BOO) is a urological condition affecting around 21.8% of adults over the age of 20 and can be caused by functional and anatomical abnormalities.[1] As a result of inflammation and subsequent fibrosis, BOO leads to the development of lower urinary tract symptoms (LUTS) such as hesitancy, weak stream, incomplete bladder emptying, and irritative symptoms such as frequency, urge incontinence, and nocturia.[2] A hallmark characterization of BOO is increased detrusor pressure, and decreased in urine flow rate.[3] Additionally, bladder tissues become ischemic, partially due to impaired blood flow caused by the obstruction and elevated pressures.[4]

The gold standard for BOO diagnosis is urodynamic testing which involves a combination of noninvasive methods such as uroflowmetry, and invasive methods such as cystometry and pressure-flow measurements.[5] Although the International Continence Society (ICS) advise guidelines to standardize urodynamic testing, factors such as patient anatomy, equipment calibration, and catheter diameter can affect pressure measurements.[6–8] Additionally, invasive urodynamics are associated with high levels of embarrassment, some pain, and patients often don't seek treatment until conditions are irreversible.[9]

Commonly, the first step in the treatment of BOO is the use of medications such as α1 adrenoreceptor antagonists to relax muscles of the prostate and the bladder neck and 5α-reductase inhibitors which reduce enlarged prostates.[10–12] After other medical methods are exhausted, surgical methods are employed to remove the obstruction via transurethral resection of the prostate (TURP) or transurethral incision of the prostate (TUIP).[13] Although surgical

techniques improve urodynamics parameters, cell signaling pathways are not fully restored and symptoms may still persist.[14–16]

Previously, our lab investigated the role of mechanical stimuli in BOO (elevated storage and voiding pressures) and how pressure is not only involved in the development of inflammation and fibrosis in BOO pathology but epithelial mesenchymal transition as well.[17,18] However, the role of hypoxia in inflammation due to BOO has not been well expounded. Therefore, determining how hypoxia leads to inflammation and the role of hypoxia in progression of BOO is fundamental in the development of effective treatment options for BOO patients. Additionally, understanding how pressure and hypoxia lead to changes in vesicles released from urothelial cells may help in the development of less invasive diagnostic tools.

1.2 Bladder Anatomy and Physiology

Anatomy

The bladder is a hollow distensible muscular organ with the primary function to store and void urine. Located above the bladder are the ureters, which collect urine from the kidneys and insert into the trigone of the bladder. Located below the bladder is the urethra, where urine passes through during voiding. There are three regions of the bladder: 1) dome or apex which is the top of the bladder, 2) bladder wall, which consists of the sides of the bladder, and 3) trigone, a triangle-shaped region between the ureteral orifices and the urethral meatus.[19] The bladder wall consists of 3 main cell layers: detrusor muscle, submucosa, and the urothelium.

The urothelium refers to the transitional epithelium layer that lines the lower urinary tract including the lumen of the bladder. It is composed of epithelial cells that express various receptors or ion channels that are responsive to mechanical and chemical changes such as purines

(P2X), and transient receptor potential (TRP) channels.[20,21] The urothelium can be subdivided into three distinct cell layers: apical, intermediate, and basal. The apical or superficial layer is a single layer of hexagonal shaped umbrella cells. The size and morphology of umbrella cells is dependent upon the bladder's state of filling and can range from 50-129 μm across.[22] In a relaxed state, umbrella cells are cuboidal in shape; when filled the cells become stretched. [23] There are two morphological features of the apical layer: a scalloped-shaped plaque and a high density of cytoplasmic vesicles within umbrella cells.[22] This plaque consists of four types of uroplakins that play the barrier function of the urothelium. The intermediate layer lies beneath the umbrella cells and contains polygonal shaped cells that mature into umbrella cells. The basal layer anchors the urothelium to underlying tissues.[24]

The submucosa layer (also known as the lamina propria) is a thin layer of connective tissue that surrounds the urothelium and is connected to the basement membrane. This layer is comprised of elastic fibers, vasculature, nerve endings, and interstitial cells. The detrusor layer is comprised of smooth muscle fibers that are oriented in different directions, granting the bladder the ability to stretch and contract. Primarily, the role of the detrusor is to contract to void urine and to relax to allow for urine storage.

Physiology

The bladder serves as a storage site for urine until the initiation of voiding, which expels metabolic products and toxic wastes. As the bladder fills, pressure increases and creates a sensation of fullness, and the tissue stretches to accommodate the increase in volume. While whether bladder blood flow decreases during filling is up for discussion, there is a consensus that at capacity, the bladder does experience a drop in bladder blood flow and creates transient tissue

ischemia. These changes in pressure, stretch, and oxygen tension can be sensed by the urothelium. During the normal micturition cycle, spinal sympathetic reflexes that travel to the base of the bladder and urethra through β3 adrenergic receptors allow the bladder smooth muscles to relax. In contrast, the urethral smooth muscle contracts to help facilitate the storage of urine through spinal reflexes traveling to the urethra through α1 adrenergic receptors. At capacity, increased afferent signals are processed and if appropriate, bladder emptying reflex is initiated.[19,25] It has been established that the bladder releases signaling molecules in response to changes in mechanical stimuli such as ATP, acetylcholine (ACh), and nitric oxide (NO).[26] Mediators such as ATP and ACh initiate bladder depolarization and signal bladder fullness, thus triggering voiding. Conversely, NO relaxes bladder smooth muscle cells, helps regulate bladder blood flow, and can serve as a modulator in inflammation.[27]

1.3 Pathology of Bladder outlet obstruction

Bladder outlet obstruction (BOO) is primarily characterized by a urethral blockage and can be caused by different functional and anatomic abnormalities. In men, the most common cause is an anatomical obstruction resulting from benign prostatic hyperplasia (BPH), where the enlarged prostate narrows the urethra. An obstruction resulting from stress urinary incontinence surgery, is the most common cause in women.[2]

The disease can be characterized into three stages: hypertrophy, compensation, and decompensation. The bladder's initial response to urethral resistance can be summarized as a period of rapid bladder growth. The hypertrophy phase is characterized by increased smooth muscle cells (SMCs) hyperplasia and urothelial cell proliferation. A hypoxic response can be seen with a decrease in bladder blood flow and an increase in HIF-1α and vascular endothelial

growth factor (VEGF). Additionally, increased ECM deposition begins in this phase and can be

characterized by an accumulation of collagen and elastic fibers. The compensation phase,

bladder growth stops, and ECM deposition continue. If the obstruction in not resolved, the

bladder enters the decompensation phase, where there is neuron and smooth muscle cell

degeneration, urothelial dysfunction and high levels of fibrosis.[28] Proposed theory of BOO

progression is depicted in **Figure 1.1**.
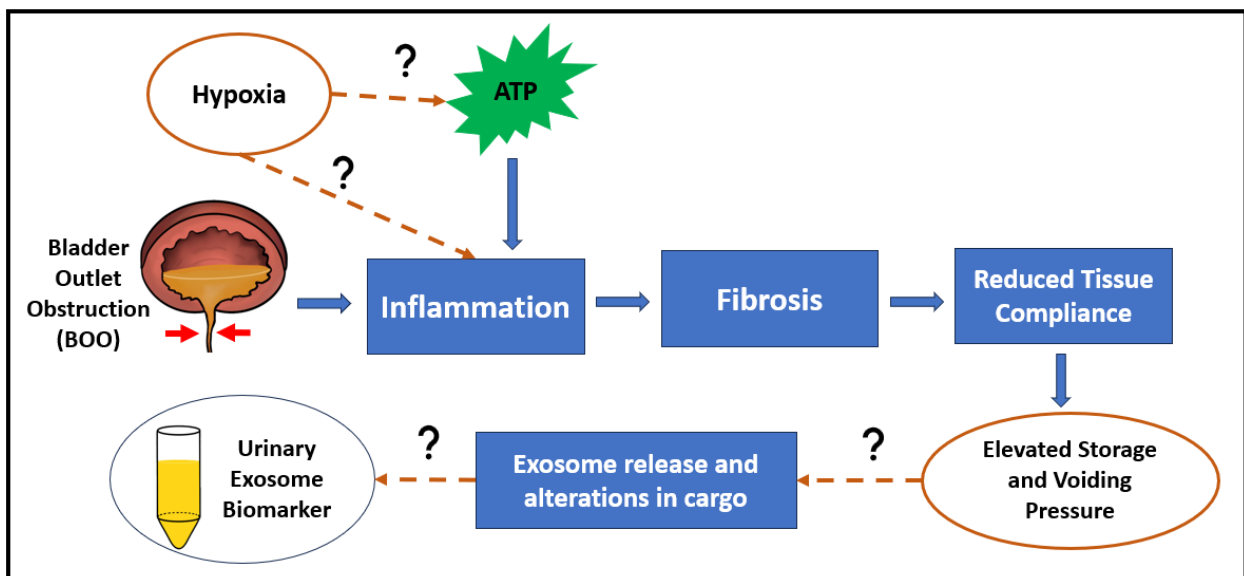
Figure 1.1 Proposed theory on BOO progression

NLRP3 Inflammasome

Inflammation seen in bladder outlet obstruction has been shown to be primarily driven

through a member of pattern-recognition receptors (PRRs), specifically nod-like receptor protein

3 or NLRP3 inflammasome. NLRP3 consists of 3 domains: an amino-terminal pyrin domain

(PYD), a nucleotide-binding and oligomerization domain (NOD), and a C-terminal leucine-rich

repeat domain (LRR). NLRP3 activates via binding with an associated-spec-like protein (ASC),

which cleaves pro-caspase-1 to caspase-1. Caspase-1 serves as a regulator of interleukin family

of pro-inflammatory cytokines and subsequently leads to the production of IL-1β and IL-18.[29]

NLRP3 can be activated by a diverse range of pathogen-associated molecular patters (PAMPs) or damage-associated molecular patterns (DAMPs). In the bladder, a DAMP of particular interest is ATP, which under mechanical stressors such as pressure, increases extracellularly and can lead to NLRP3 activation. One proposed pathway of ATP-mediated NLRP3 inflammation starts with small amounts of ATP release through the urothelium via pannexin-1 channels alongside exocytosis in response to mechanical stressors. This released ATP binds to purinergic P_2X_7 receptors, which in turn amplifies extracellular ATP release. Once amplified, ATP then acts on P_2X_4 receptors leading to the activation of NLRP3 inflammasome. [17]

Another DAMP of interest is reactive oxygen species (ROS). Under normoxic conditions thioredoxin interacting protein (TXNIP) is bound to antioxidant thioredoxin (TRX). Under oxidative stress, TXNIP dissociates from TRX, where the unbound TXNIP associates with NLRP3, and promotes NLRP3 activation. Several studies have shown the link between TXNIP and NLRP3.[29] One *in vitro* study used known DAMPs calcium pyrophosphate (CPPD) and monosodium urate (MSU) to activate NLRP3 in urothelial cells and found significant increases in caspase-1 activity. The authors found that TXNIP inhibitor verapamil was able to reduce NLRP3 activation as indicated by lower levels of caspase-1. Additionally, ROS inhibitor N-acetylcysteine (NAC) also reduced DAMP induced caspase-1 activity.[30]

Epithelial to Mesenchymal Transition

Epithelial to mesenchymal transition (EMT) is a complex biological process, where epithelial cells undergo a functional transition into a mesenchymal cell phenotype. More specifically, cells lose their epithelial characteristics (polarity and attachment to basement

membrane) and markers (E-cadherin, cytokeratin, etc.) and gain mesenchymal characteristics (increase migratory and invasive properties) and markers (N-cadherin, vimentin, etc.). Although EMT is commonly associated with cancer, recent studies have linked EMT with an obstructed bladder. Recently, Dunton et al. has linked pressure profiles associated with BOO to increased EMT gene expression changes in urothelial cells.[18] Additionally, in a rat model of BOO, Zhang et al. found an association between the PI3K-ACK-mTOR pathway and EMT.[31] Oxidative stress contributes to EMT in bladder smooth muscle cells through TGFβ2.[32]

1.4 Effects of Hypoxia on the Bladder

Hypoxia inducible factors (HIFs) are a family of heterodimeric transcriptions factors and are the main regulators of the hypoxic response within the body. There are three known HIFs (HIF-1, HIF-2, and HIF-3) and they are comprised of an alpha and beta subunit. HIF-1α is ubiquitously expressed in human tissues and increases during acute hypoxic exposures. HIF-2α is generally expressed in the liver, pancreas, and kidneys and increases with prolonged hypoxia. Whereas HIF-3α is expressed in the heart, lungs, and eyes with its exact role not yet fully expounded.[33] Under normoxia, HIF-α mRNA is rapidly degraded via proteasomal degradation that is mediately by prolyl-4-hydroxylases (PHDs). The PHDs use oxygen and iron to hydroxylate proline residues on the HIF-α subunit. Hydroxylated HIF-α is recognized by Von Hippel-Lindau protein (pVHL), which binds to the subunit, causing ubiquitination and proteasomal degradation.[34,35] The absence of oxygen prevents the hydroxylation of the HIF-α subunit. Once stabilized, HIF-α accumulates above basal levels and translocates to the nucleus and dimerizes with HIF-β.[35]

During BOO, the bladder tissues including the urothelium, experience a hypoxic environment. Bladder tissue ischemia begins with blood flow reduction caused by pinching of vasculature due to high-pressure voiding and high-pressure storage during BOO. Immunostaining of hypoxic adducts with hypoxyprobe-1 in BOO rats found a strong hypoxic response in the urothelium at 3 days post obstruction.[36] In another study, increased nuclear HIF-1α reactivity was found in the urothelial layer of bladder sections from human patients with BOO.[37] These studies establish that the urothelium experiences a hypoxic environment as a result of BOO, and thus the effect of hypoxia on the urothelium should be investigated.

In Vivo Urothelial Response

To investigate the role of hypoxia in the bladder *in vivo*, tissue ischemia is induced by surgically reducing blood flow. This is achieved by injuring the main vascular supply to the bladder which is generally the internal iliac artery.[4] Several studies have linked ischemia with bladder dysfunction. In a rabbit bladder model, ischemia caused by injury to iliac arteries caused an increased release of leukotrienes in the urothelium.[38] Tissues from an ischemic rat bladder demonstrated that hypoxia led to a significant increase in tight junction and gap junction proteins in the urothelium, which are involved in cellular communication and remodeling mechanisms.[39] Bladder ischemia caused by inducing arterial atherosclerosis increased HIF gene expression in the tissues of rabbit bladders. Additionally, rabbit bladder ischemia led to a thickened urothelium with partial mitochondrial membrane loss.[40] Together these studies show that low oxygen can contribute to bladder dysfunction within the urothelium and that hypoxia may cause the urothelium to initiate an inflammatory response.

In Vitro Urothelial Response

There are limited studies investigating the response of urothelial cells to hypoxia *in vitro* (**Table 1.1**). In one study, human urothelial cells extracted from urological tissues were exposed to 2% O_2 for 2 days using a hypoxia chamber. The hypoxic environment increased the passage number by one compared to UCs cultured in normoxic conditions. In addition, the ability of the UCs to form a differentiated urothelium layer when generating a bladder mucosa substitute was increased when the UCs were cultured under hypoxic conditions.[41] Chemical stabilization of HIF-1α via treatment with AKB-4924 (an inhibitor of PHDs) was able to protect human urothelial cells from infection from uro-pathogenic *E. coli* (UPEC) invasion and reduced UC cell death.[42] In a diabetic model, TERT-NHUC normal human urothelial cells received a high glucose dose and were exposed to 1% O_2 for 24, which led to the stabilization of HIF-1. This HIF-1 stabilization subsequently increased activation of pro-inflammatory cytokines IL-1β and IL-8.[43] These findings show that UCs experience and respond to hypoxia. In addition, these studies indicate that hypoxia not only serves as a protective mechanism to pathogens but can play a role in the initiation of inflammation. However, the exact mechanism of inflammation initiation in UCs has not been established and more research needs to be conducted to ascertain the role of hypoxia and inflammation in BOO pathology.

Table 1.1: Responses of urothelial cells to hypoxia *in vivo* and *in vitro*

	Key Findings	Cells/Tissue Source	Methods	Reference
In vivo	Increased leukotrienes in the urothelium which is associated with inflammation	Rabbit bladder	Injury to iliac artery 8 weeks	Azadzoi et al. 2004
	Alterations in cellular communication and remodeling via increased tight junctions and gap junctions	Rat bladder	Injury to iliac artery 8 weeks	Sunagawa et al. 2015
	Thickened urothelium and increased HIF-1α expression	Rabbit bladder	Injury to iliac artery 12 weeks	C. Liu et al. 2018
In vitro	Increased passage number by one and created a differentiated urothelium layer when generating a bladder mucosa substitute (BMS).	UCs extracted from human urological tissues	2% O_2 for days using hypoxia chamber	Chabaud et al. 2017
	NLRP3 activation through ROS/TXNIP pathway	Rat urothelial cells	5% O_2 for 6 hours using enzymes	Hudson et al. 2023
	HIF-1α protected cells from pathogen invasion and pathogen induced cell death	Human uroepithelial cells	Chemically induced HIF-1α stabilization via AKB-4924 and treated with E.coli (UTI model)	Lin et al. 2015
	Hypoxia exposure led to increased activation of IL-1β and IL-8 in human urothelial cells treated with high glucose	Human urothelial cells TERT-NHUC	1% O_2 via a hypoxia chamber for 24 hours and high glucose doses (diabetic model)	Mohanty et al. 2022

Nitric Oxide and Hypoxia

Nitric oxide (NO) is a signaling molecule that plays a role in mediating bladder blood flow and defense. NO is generated by a family of nitric oxide synthases or NOS: neuronal NOS (nNOS), inducible NOS (iNOS), and endothelial NOS (eNOS). NOS enzymes can produce NO through two main pathways. The first pathway is oxygen dependent where the NO enzymes use L-arginine and oxygen as a substrate to generate NO. Whereas the nitrate-nitrite-NO pathway can be activated without oxygen.[44] NO concentrations are elevated to induce vasodilation and restore oxygen delivery to ischemic tissues following a reduction in oxygen. Thus, a prominent hypothesis is that NO plays a role in protecting the bladder and inhibiting bladder dysfunction in BOO pathology.

In BOO pathology, NO has been implicated as a protector from oxidative stress in an obstructed bladder. In an *in vivo* study, New Zealand White male rabbits with surgically induced BOO were treated with universal NOS inhibitor, L-NAME (N(ω)-nitro-L-arginine methyl ester). Initially the absence of NO negatively impacted blader function as bladder contractility decreased and increased the level of hypoxia compared to untreated bladders.[45] In another study, female Sprague-Dawley rats with surgically induced BOO were also given L-NAME. Treatment with L-NAME amplified bladder dysfunction compared to the untreated BOO bladders as frequency of bladder contractions and residual volume increased. In addition, the bladder tissues with L-NAME treatment exhibited an upregulation of HIF-1 protein.[46] Male C57BL6 mice with obstructed bladders and L-NAME treatment demonstrated increased non-voiding contractions compared to untreated BOO animals. These studies indicated that the absence of NO contributes to worsening bladder function in BOO and that NO is essential in protecting the bladder from oxidative stress.[47]

1.5 Hypoxia and Activation of NLRP3

The link between hypoxia and NLRP3 inflammasome activation has been elucidated in different organ systems. In an *in vivo* study of 2 hours of hypoxia followed by reperfusion, Jiang et al. found an increase in HIF-1α and NLRP3 mRNA when modeling a stroke in the brains of Sprague-Dawley rats. Another *in vivo* study where wild type mice were placed in a hypobaric hypoxia chamber (10.16% O_2), there was an increase in both NLRP3 and caspase-1 mRNA and protein in brain tissues.[48] In pancreatic rat islets exposed to 24 hours of 1% oxygen tension, there was a noted increase in NLRP3 and caspase-1 mRNA. In the same study, treatment with antioxidant NAC inhibited this hypoxic induced NLRP3 increase, which implicates the

involvement of ROS in NLRP3 inflammasome activation.[49] In an *in vitro* study, HUVEC cells exposed to chronic intermittent hypoxia led TXNIP mediated NLRP3 inflammasome activation and subsequent increase in IL-1β.[50] Inflammatory response due to hypoxia (1% O_2) in mouse insulinoma cells was driven through the ROS/TXNIP/NLRP3 pathway.[51] Another *in vitro* study observed a time dependent increase in inflammatory cytokines IL-1β, TGFβ, and TNFα in human bladder smooth muscle cells that were exposed to 3% oxygen via a hypoxia chamber.[52] As previously mentioned, Hughes et al. established that NLRP3 is the main driver of inflammation in BOO. Thus, bladder induced hypoxia might also lead to inflammasome activation through the ROS/TXNIP/NLRP3 pathway.

Nitric oxide has roles in immune responses including inhibition of NLRP3. In an *in vivo* study, Mishra et al. found that NO inhibited the assembly of the NLRP3 inflammasome.[53] An *in vitro* study, treating mouse macrophages with NO donor SNAP (S-nitroso-N-acetyl penicillamine), significantly inhibited IL-1β secretion when NLRP3 inflammasome activation was stimulated via LPS-priming and ATP. In addition, SNAP reduced caspase-1 activation. In that same study, using THP-1 cells, NLRP3 inflammasome activation was stimulated via LPS and DAMP nigericin, and SNAP treatment reduced caspase-1 and IL-1β production.[54] These studies indicate that NO has a role in protection through modulating potential destruction caused by NLRP3 activation. The proposed pathway for NLRP3 inflammasome activation due to BOO-induced hypoxia is depicted in **Figure 1.2**.
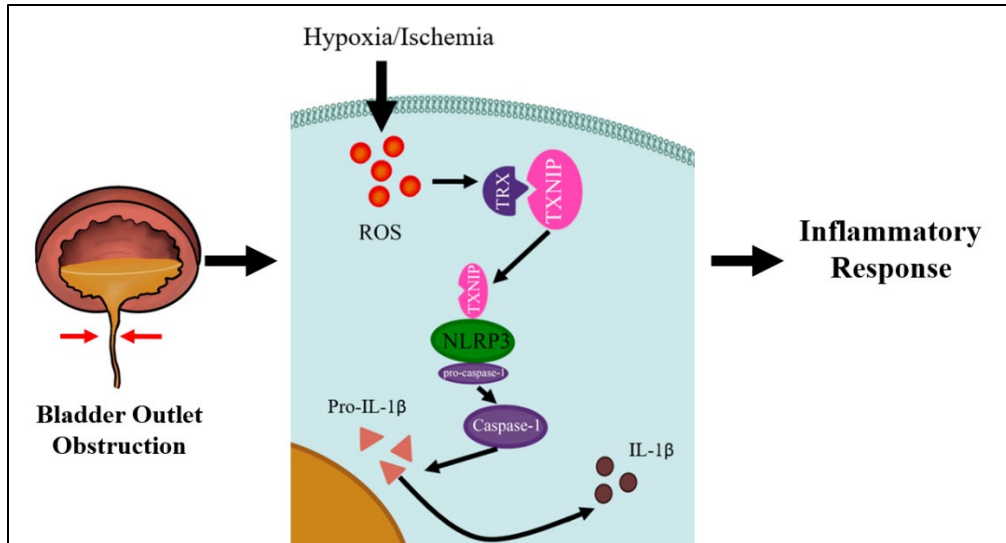
Figure 1.2 Depiction of NLRP3 inflammasome activation in BOO pathology. Hypoxia or tissue ischemia leads to the production of ROS, which separates TRX and TXNIP. TXNIP associates and promotes NLRP3 assembly and activation. NLRP3 activation cleaves pro-caspase-1 to active caspase-1, which cleaves pro-IL-1β to IL-1β. Figure adapted from Minutoli et al. [102] and Kelley et al. [118].

1.6 Effects of Pressure on Urothelial Cells

Mechanical stress has been associated with bladder dysfunction due to BOO; however, there are few studies that investigate the urothelial response to elevated pressure. As previously mentioned, elevated hydrostatic pressure has been linked to ATP-mediated NLRP3 inflammasome activation, EMT, and fibrosis.[17,18] Through an *in vitro* study with rat urothelial cells, Olsen et al. demonstrated that extracellular ATP release in response to various intensities of hydrostatic pressure was magnitude and time dependent.[26] In another study, elevated intravesical pressure along with bladder distention activated the extracellular signal-regulated kinase (ERK) in the urothelium. [55] Expression levels of MMP1 and MMP2 were significantly downregulated in human urothelial cells exposed to 6 hours of 70 cmH$_2$O *in vitro*.[56] These studies show that the urothelium responds to elevated pressures and contribute to inflammation initiation in BOO. Further research is needed to better understand the role of pressure in BOO pathology.

1.6 Extracellular Vesicles

Lipid bound extracellular vesicles (EVs) can be classified into three groups based upon there size and origin: exosomes (30-200 nm), microvesicles (MVs) (100-1000 nm), and apoptotic bodies (> 1000 nm).[57] Exosomes contain various cargo, including peptides, small proteins, and nucleic acids, such as mRNA, and non-coding RNAs (lncRNA, and miRNA). The nanovesicles play a role in cell-to-cell communication, coordinating biological functions, and maintaining homeostasis.[58] Exosomes are formed by an endosomal route through inward budding creating early endosomes. These early endosomes then mature into late endosomes or multivesicular bodies (MVBs), which are rich in intraluminal vesicles (ILVs). MVBs undergo exocytosis and the secreted ILVs become exosomes. Other MVBs are degraded by direct fusion with lysosomes.[57,59] The biogenesis of exosomes is depicted in **Figure 1.3**. Originally thought to be specific markers of exosomes, common exosomal markers are surface proteins in the tetraspanin family: CD81, CD9, and CD63. Exosomes are secreted by all cell types and have been found in almost all bodily fluids including urine.
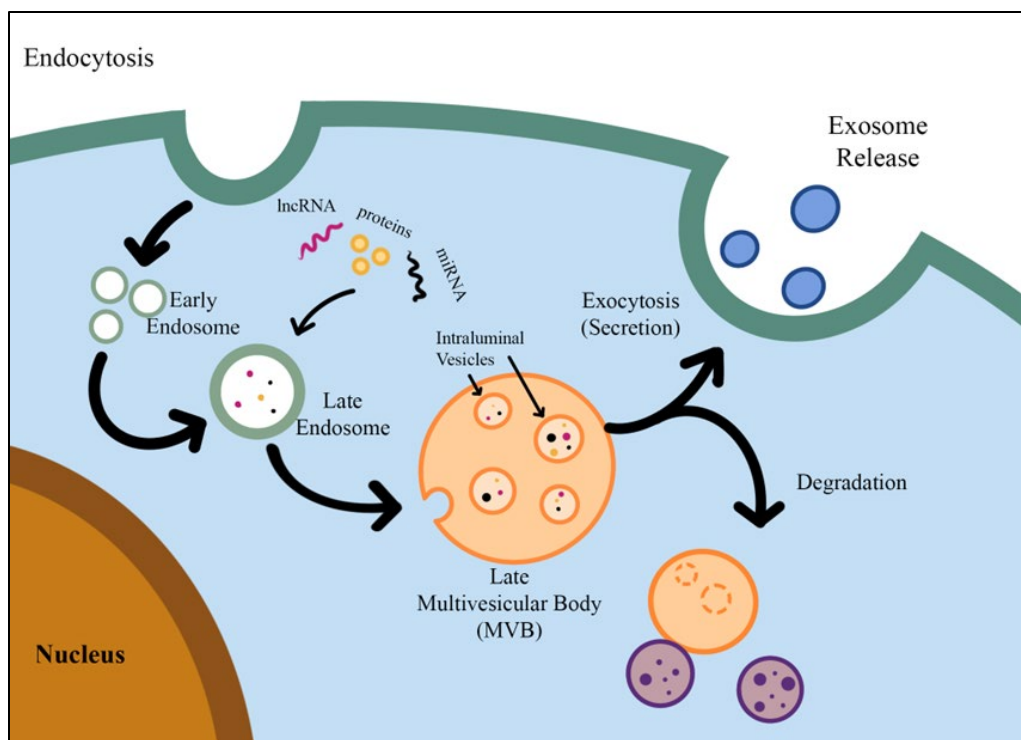
Figure 1.3 The biogenesis of exosomes. Figure adapted from Gurunathan et al. [60] Gurung et al. [57] and Koritzinsky et al. [59]

Methods for Exosome Isolation and Characterization

The gold standard for exosome isolation remains ultracentrifugation-based methods. However, challenges associated with the use of ultracentrifugation have hindered bringing exosomes into the clinical setting. Alternative methods have been developed based upon immunoaffinity, precipitation of exosomes, or size exclusion chromatography.[61] Commercially available kits are able to capture exosomes; however, these kits have high cost and leave significant amounts of impurities.[62] For example, the Invitrogen Total Exosome Isolation Kit works to precipitate exosomes by tying up water molecules, which allows for the less-soluble components such as exosomes to be pelleted with short low-speed centrifugation. However, this reagent also entraps other extracellular vesicles and cellular debris.

Recently a novel method has been developed where exosomes are isolated based upon hydrophobic interaction chromatography (HIC) by Marcus and colleagues using patented

15

capillary-channeled polymer (C-CP) fiber spin down tips. Polyethylene terephthalate (PET) polymer is collinearly aligned and packaged into a column, creating an 8-channeled 1-cm C-CP fiber tip. The tip is then attached to a micropipette tip and inserted into a conical centrifuge tube. Using a benchtop centrifuge, the C-CP tips can rapidly harvest exosomes from a variety of biological fluids.[63–66] A diagram of the C-CP fiber spin down tips is depicted in **Figure 1.4**.[66] This method has been rigorously tested and studied by Marcus and colleagues, demonstrating the technique's effectiveness in capturing exosomes within the fiber as seen in **Figure 1.5**.[67]
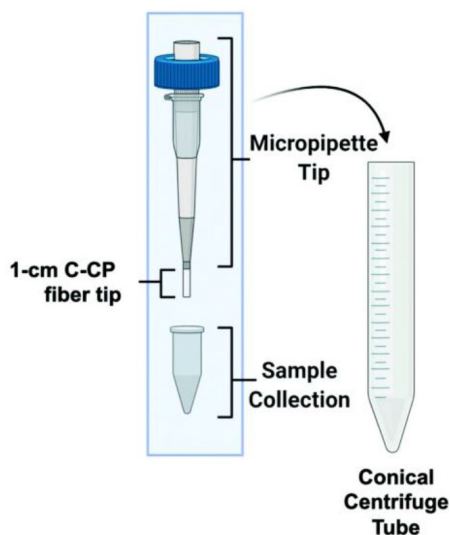
Figure 1.4 Image of the C-CP fiber spin down tips. Image adapted from Jackson et al. Analyst (2021) [66]
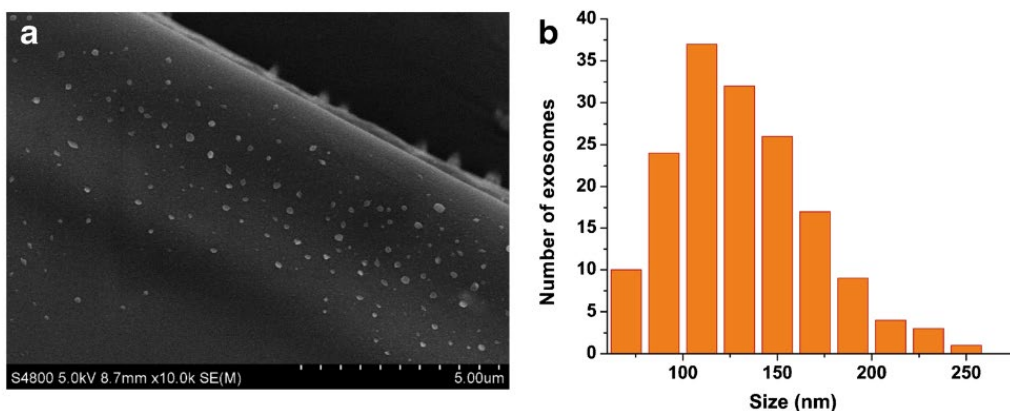
Figure 1.5 SEM image of urinary exosomes immobilized on C-CP fiber (a). Number of exosomes within in exosome size range via ImageJ analysis (b). These images were adapted from Huang et al., *Anal. Bioanal. Chem.* (2019) [67].

Methods to characterize and validate exosomes typically measure properties such as size, membrane surface markers, density, and shape. Characterization of EV size can be achieved through optical nano-particle tracking (NTA), dynamic light scattering (DLS), and transmission electron microscopy (TEM) or scanning electron microscopy (SEM).[60] Membrane protein concentration can be quantified with Bradford assay or BCA assay. Techniques such as western blotting, dot blotting, or enzyme-linked immunosorbent assay (ELISA) are usually employed to validate the presence of tetraspanin proteins (CD81, CD9, CD63).

Exosomes as Biomarkers

Exosomes as a source of biomarkers are ideal since the exosomes are present in nearly all bodily fluids, such as blood and urine. This allows for minimally to completely non-invasive methods to diagnose a disease. In addition, RNAs are stable within exosomes as they are protected from degradation by RNases. Exosomes have been documented to contain non-coding RNAs including long non-coding RNAs (lncRNA) and micro RNAs (miRNA). The cargo of exosomes correlates to the state of a tissue. For instance, exosomes harvested from plasma of patients with early-stage Parkinson's disease (PD) contained higher levels α-synuclein, a marker for PD, when compared to healthy patients.[68] Hypoxic exposure to cells have been able to not only increase the secretion of exosomes but also lead to changes in exosomal cargo. Different studies have shown that cells along the urinary tract can secrete more exosomes in response to hypoxia and have demonstrated changes in exosomal cargo, including an increase in miRNAs (**Table 1.2**).

Table 1.2 *In vitro* hypoxia changes to exosomes in urinary cells

Changes in Exosomal Cargo under hypoxia	Changes in exosome number under hypoxia	Exosome Donor Cell	Ref
TGF-β1 mRNA	Increased exosome secretion	Tubular epithelial cells (*in vitro*) mouse and human)	Borges et al. 2013
Increase miR-20a-5P	N/A	Renal tuber epithelial cells (*in vitro*)	Yu et al. 2020
Increase miR-21	Increased CD63 expression	Mouse renal tubular epithelial cells (*in vitro*)	Liang et al. 2019
Increase miR-150-5p	Increased exosome secretion	Rat renal tubular epithelial tissue (*in vitro*)	Zhou et al. 2021
N/A	Increase in exosome secretion	Kidney cells (HEK293T) *in vitro*	Muñiz-García et al. 2022

There is limited research on the impact of pressure on exosomal cargo and secretion *in vitro*. However, it is hypothesized that pressure fluctuations are reflected in exosomes and act as intercellular messengers.[69] Studies of hypertension demonstrate that elevated pressure can impact exosomal cargo. For instance, exosomes harvested from plasma contained 27 miRNAs that were differentially expressed between hypertensive rats and normotensive rats.[70] Osmotic stress has been found to alter miRNA profiles in exosomes released from Chinese hamster ovary (CHO) cells0.[71] In addition, exosomes are believed to play a role in inflammation by carrying inflammatory mediators.[72] Together these studies support the notion that elevated pressure and hypoxia contributes to exosome secretion and may bring forth changes in exosomal cargo.

CHAPTER TWO

Rationale and Specific Aims

Bladder outlet obstruction (BOO) is caused by a partial urethral blockage that leads to abnormal chemical and mechanical changes such as high-pressure voiding and tissue ischemia. Although the symptoms of BOO can impact a patient's quality of life, patients may delay seeking treatment until BOO progresses. In addition, current methods to diagnose BOO involve invasive methods. It has been established that a BOO bladder experiences inflammation and fibrosis.[73,74] *In vitro* data demonstrates that urothelial cells respond to elevated pressure and hypoxia.[17,18,52] Specifically, elevated hydrostatic pressure can activate ATP-mediated NLRP3 inflammasome.[17] Furthermore, pressure and hypoxia has been linked to inflammation, fibrosis, and EMT gene expression changes. [17,18,52] Though there has been some association between chemical and mechanical stressors and inflammatory pathways in BOO, the exact roles of pressure, and tissue ischemia in BOO pathology are not fully understood. Further research is needed to determine the role of hypoxia and the initiation of NLRP3 inflammasome in urothelial cells.

In addition, recent studies have shown a difference between microRNA profiles in the tissues and cell free urine from patients with BOO experiencing LUTS and healthy patients.[75,76] We hypothesize these changes may be observed in urinary extracellular vesicles released by urothelial cells, more specifically exosomes. Furthermore, hypoxia and pressure may directly influence and change the non-coding RNAs packaged within exosomes and the stimuli may increase the release of exosomes from urothelial cells. Thus, we aim to further knowledge on BOO pathology and characterize extracellular vesicles released after exposure to chemical and mechanical stressors through the following aims.

19

Ch 3: Aim 1: Characterize Two-Enzyme System for Creating an *in vitro* Hypoxic Environment.

Ch 4: Aim 2: Quantify Urothelial Cell Response to Hypoxia and Identify Inflammasome Activation Mechanisms.

Ch 5: Aim 3: Characterize Exosome Release from UCs in Response to Pressure and Hypoxia.

The proposed studies will provide a novel method for investigating the effects of hypoxia *in vitro*. This will further the understanding of how mechanical and chemical stimuli leads to cellular responses (inflammation and extracellular vesicle release and cargo changes) and may offer a new biomarker for BOO.

CHAPTER THREE

Aim 1: Characterize Two-Enzyme System for Creating an *in vitro* Hypoxic Environment

*Parts of this chapter is published in "Enzyme-induced hypoxia leads to inflammation in urothelial cells *in vitro*." [77]*

3.1 Introduction

Hypoxia is a state in which there is an imbalance between oxygen supply and demand within an organism or low oxygen availability. This can occur within the organism as a whole or in specific locations (tissue hypoxia). Additionally, tissue hypoxia can occur in the absence of a decrease in oxygen concentration in the blood.[34] Oxygen concentration can vary between 0 to 19% in different healthy tissues around the body: oxygen concentration of the lungs tends to be around ~19%, ~13% in the alveoli and oxygen tension in the bladder can fluctuate when filling and voiding.[78]

The main regulator of the cellular response to hypoxia is a family of transcription factors called hypoxia inducible factors (HIFs). There are three members of the HIF family (HIF-1, HIF-2, and HIF-3) and the active HIFs are composed of alpha and beta subunits. HIF-1 is ubiquitously expressed in human tissues. The HIF-β subunit is stably expressed in cells unlike the HIF-α subunit, which is degraded under normoxia. Under hypoxia, HIF-α subunits are stabilized, as oxygen dependent degradation via prolyl-4-hydroxylases (PHDs) is inhibited due to the lack of available oxygen.

Nitric oxide (NO) is a signaling molecule that is generated by a family of nitric oxide synthases or NOS. There are three isoforms of NOS: neuronal NOS, inducible NOS and endothelial NOS. NOS enzymes use L-arginine and oxygen as a substrate to generate NO. Under

acute reduction in oxygen, NO concentrations are elevated to increase blood flow and restore

oxygen delivery. [79] Additionally, intracellular NO can destabilize HIF-1α under hypoxia by

preventing mitochondrial cellular respiration by inhibiting mitochondrial cytochrome c oxidase.

This causes a change in intracellular oxygen availability redistributing respiratory oxygen

towards other oxygen-dependent targets such as prolyl hydroxylases.[34,80]

Traditional methods to induce hypoxia for cell culture often require the use of expensive

equipment such as a hypoxia chamber. These gas-controlled devices have been shown to slowly

equilibrate the oxygen partial pressure between the chamber and the culture medium. One study

demonstrated that 3 hours was required for media inside closed dishes with intact lids to reach

the oxygen tension of the flushed gas. However, media oxygen tension was significantly reduced

when the lids of the dishes were perforated.[81] Additionally, chambers also only provide hypoxia

at set oxygen tensions and once the culture plates are removed from the chamber, oxygen quickly

diffuses from the air to the culture medium. Furthermore, hypoxia chambers limit additional

analysis such as real time imaging, as the cells are confined within the chamber.

Another method to induce hypoxia *in vitro* is through chemical stabilization HIF-α with

$CoCl_2$. Along with oxygen, PHDs require iron to hydroxylate HIF-1α. $CoCl_2$ works to inhibit

PHDs by displacing Fe^{2+} with Co^{2+}, leading to stabilization of HIF-1α.[82] Though HIF-1 is

stabilized, not all components of hypoxia are mimicked, as oxygen concentration remains

unchanged and there isn't any generation of reactive oxygen species. Thus, there needs to be an

alternative method to induce hypoxia *in vitro*.

Enzymes have been used in previous research to create *in vitro* hypoxic environments

without the use of additional apparatus.[83,84] Glucose oxidase (GOX) can rapidly reduce oxygen

in cell culture media by catalyzing the oxidation of β-D-glucose to D-glucono-δ-lacotone, which

spontaneously hydrolyzes to D-gluconic acid and hydrogen peroxide (**Figure 3.1**).[85] Two different methods were used to protect cells from cytotoxic hydrogen peroxide generated from GOX. First, glutathione (GSH) was chosen as it can react with hydrogen peroxide resulting in glutathione disulfide and water (**Figure 3.1**). Another enzyme, catalase (CAT) can also be used to breakdown hydrogen peroxide into water and oxygen. Although catalase results in the generation of a half mole of oxygen, the net reaction of the GOX and CAT together results in the depletion of oxygen in solution and has been used to induce hypoxia in cell culture.[86–88] The enzyme method can create a hypoxic environment in solution even with an air/liquid interface and stirring. [89] Additionally, enzymes can create an *in vitro* hypoxic environment while allowing for the use of regular cell culture equipment.

To demonstrate the efficacy of enzyme-induced hypoxia, we will first characterize oxygen depletion at various concentrations of GOX to determine optimal enzyme concentrations. The impact of the enzyme system on cell viability will also be assessed. Secondly, HIF-1α stabilization will be quantified via immunostaining to verify that MYP3 rat urothelial cells are indeed experiencing and responding to an *in vitro* hypoxia environment. Thirdly we will further characterize MYP3 urothelial cellular response by quantifying extracellular nitric oxide (NO). Furthermore, cellular response due to enzyme-induced hypoxia will be compared to a more traditional method using a modular hypoxia chamber flushed with gas containing 5% O_2, 5% CO_2, balanced with nitrogen.

$$\beta\text{-D-glucose} + O_2 \xrightarrow{\text{Glucose Oxidase}} \text{D-glucono-}\delta\text{-lacotone} + H_2O_2 \quad \text{(i)}$$

$$H_2O_2 \xrightarrow{\text{Catalase}} H_2O + \frac{1}{2}O_2 \quad \text{(ii)}$$

$$GSH + H_2O_2 \leftrightarrows 2H_2O + \text{G-S-S-G} \quad \text{(iii)}$$
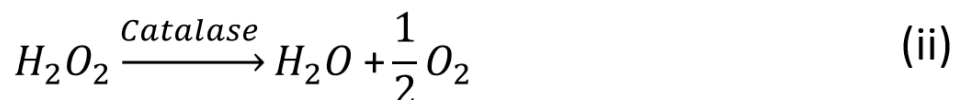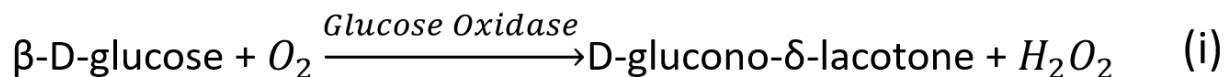
Net Reaction with Catalase

$$2\beta\text{-D-glucose} + O_2 \xrightarrow{GOX/CAT} \text{D-glucono-}\delta\text{-lacotone} + H_2O \quad \text{(iv)}$$

Figure 3.1 Enzyme reaction scheme. (i) Glucose oxidase enzyme reaction. (ii) Catalase enzyme reaction. (iii) Reaction of glutathione and hydrogen peroxide. (iv) Net reaction of glucose oxidase and catalase.

3.2 Materials and Methods

Urothelial Cell Culture

An immortalized rat non-tumorigenic urothelial cell line (MYP3) originally created by Dr. Ryoichi Oyasu (Northwestern University, Chicago, IL, USA) [90] were generously provided to our lab via Samuel M. Cohen through the lab of Lora L. Arnold, both at the University of Nebraska Medical Center, Omaha. The cells were cultured in complete MYP3 media: F-12 Kaighn's modified Ham's F-12 media (HyClone, Logan, UT, USA) supplemented with 10% low endotoxin-dialyzed fetal bovine serum (Gibco, Carlsbad, CA, USA), 10 µM non-essential amino acids (Cytiva, Marlborough, MA, USA), 1.0 µgd/ml hydrocortisone (Sigma, St. Louis, MO, USA), 10 µg/ml insulin, 5 µg/ml transferrin and 6.7 ng/ml selenium (Gibco).[17] All cells were cultured under standard conditions (sterile, humidified, 37°C, 5% CO_2/95% air) before exposure to hypoxic conditions.

Oxygen Concentration measurements

A stock solution at a concentration of 2 mg/mL of GOX was prepared by dissolving dry GOX in sterile PBS. Similarly, a 2 mg/mL stock solution of CAT was prepared. GSH was dissolved in sterile PBS to create a stock solution of 100 mM GSH. A 1 M stock solution was prepared by dissolving HEPES in sterile PBS. All stock solutions were sterilized with a 0.22 µM syringe filter. Initially, to find the optimal concentration of GOX to induce hypoxia, solutions were prepared by diluting stock solutions to a final concentration of various concentrations of GOX and 120 U/mL CAT, and 25 mM HEPES in PBS containing 11 mM of glucose. Normoxic solutions (0 µg/mL GOX, 120 U/mL catalase CAT, and 25 mM HEPES) were also prepared in PBS containing 11 mM of glucose. Oxygen concentrations were measured using a benchtop fermenter and an oxygen probe. Once enough data was obtained, GOX concentrations were narrowed down to 0.15 and 0.5 ug/mL. Oxygen tension in media containing GOX, 120 U/mL CAT, and 25 mM HEPES were measured using an ABL blood gas analyzer (Radiometer, Brea, CA, USA) at 0.5, 1-, and 2-hour time points after the enzymes were added to solutions.

Cell Viability

Cell viability was quantified by following the protocol of the commercially available MTT Cell Viability kit (Invitrogen). MYP3 cells were seeded at a density of 5000 cells per well in a 96 well plate in 100 µL of complete MYP3 media and cultured for 24 hours. After which the plate was exposed to enzyme-induced hypoxia (0.15 or 0.5 µg/mL GOX) or normoxia. Immediately after exposure, supernatant media was aspirated and replaced with fresh 100 µL phenol-red free Ham's F12 media (Sigma) along with 10 µL MTT stock solution for a final concentration of 1.2 mM MTT. The plate was incubated at 37°C for 3 hours and 50 µL of the

supernatant was aspirated and replaced with DMSO. After 10 minutes of incubation with shaking at 37°C, absorbance of the samples was read at 540 nm. Percent cell viability was quantified from the ratio of optical densities of experimental group over the control group.

Immunostaining

MYP3 cells ($4x10^4$ cells/mL) were cultured in ibidi 8 well chamber glass slides (Fisher) for 48 hours before serum starving overnight. After which, the cells were exposed to either normoxia (0 µg/mL GOX), enzyme-induced hypoxia (0.5 µg/mL GOX), gas-induced hypoxia or 100 µM CoCl$_2$. Immediately after hypoxia exposure, media was aspirated, and cells were washed. All washed steps included rocking and washing three times with PBS. Cells were then fixed with enough 4% paraformaldehyde in PBS to cover the cells for 10 minutes at room temperature, followed by another wash. At this point the fixed cells were either stored at 4°C for up to a week or immediately permeabilized with 0.2% Triton X-100 in PBS for 15 minutes and then washed. To prevent non-specific binding, cells were blocked with a solution comprising of 5% BSA and 0.05% Triton in PBS for 1 hour at room temperature. Immediately after blocking, cells were incubated with primary antibody rabbit anti-HIF-1α (Fisher PA1-16601) at a dilution of 1/200 overnight at 4°C in a humidified chamber. After primary antibody incubation, cells were washed and then incubated with Alexa Flour® 488 conjugated goat polyclonal anti-rabbit IgG (Fisher) at concentration of 2 ug/mL at room temperature for 1 hour protected from light. The cells were washed and then counter stained with 0.5 uM DAPI for 5 minutes and washed again before imaging with a Nikon inverted microscope equipped with a Hamamatsu camera. Cells were kept hydrated with PBS for the duration of the imaging process.

Hypoxic Cellular Response Experiments

MYP3 cells were seeded at a density of 10^6 cells per well in 6 well plates and cultured for 24 hours before serum starved overnight. For exposure experiments, the cells were cultured with 1 mL of either normoxic media or hypoxic media for two hours. To ensure that the enzyme system induced the desired hypoxic conditions without unintended side effects, another set of MYP3 cells were exposed to a traditional method of inducing hypoxia via a hypoxia chamber (5% O_2, and 5% CO_2 balanced with N_2) in the presence or absence of CAT in the culture media. In addition, cellular responses to enzyme-induced and gas-induced hypoxia (via hypoxia chamber) were compared with hypoxia mimetic response to 100 µM cobalt chloride ($CoCl_2$) in culture for 2 hours.[91] For these experiments a stock solution of 1 mM $CoCl_2$ was prepared in sterile PBS and diluted to 100 µM in serum free cell culture media for hypoxic mimetic experiments. Cells were exposed to the hypoxic conditions for up to two hours and supernatant was collected at different time points to be used to determine nitric oxide levels by quantifying nitrite concentration using a commercially available Griess reagent kit following the manufacturer's instructions (Invitrogen, Carlsbad, CA, USA). For each group, 150 µL of supernatant media was mixed with 20 µL of the Griess reagent and 130 µL ddH_2O in a 96 well plate and incubated for 30 minutes at room temperature before the absorbance (490 nm) was measured spectrophotometrically (Tecan Genios microplate reader). To convert optical density values to nitrite concentrations, at the time of the assay a standard curve of nitrite concentrations against absorbance was prepared. Data were normalized to the normoxic control for that experiment and reported as fold change.

Statistical Analysis

A minimum of three independent experiments were performed with data presented as the mean ± standard error of the mean (SEM). For time course experiments, the data were analyzed using two-way analysis of variance (ANOVA) with a Bonferroni post-test. One-way ANOVA was used for single timepoint experiments with post-hoc Tukey test. All statistical analyses were performed using GraphPad Prism 5 software for Windows (San Diego, CA) and *p* values less than 0.05 were considered statistically significant.

3.3 Results

Enzymes Rapidly Reduced Oxygen Tension in PBS Solutions and Media

To determine the effectiveness in inducing hypoxic conditions *in vitro*, time-course changes in oxygen tensions of the hypoxic PBS solutions were determined using a benchtop fermenter probe. Initially, concentrations of 150, 100, 50 and 7.5 ug/ml of GOX were chosen based upon concentrations used in literature.[84] These concentrations of GOX were able to reduced oxygen tension to below 5% O_2 and maintain this low oxygen tension for up to 48 hours (**Figure 3.2A**). Although these GOX concentrations were able to reduce oxygen tension, MYP3 cell viability was significantly impacted by these higher GOX concentrations, even with the addition of glutathione. At 30 min, 7.5 µg/ml GOX with 5 mM GSH resulted in cell viability dropping to 15.5% (**Figure 3.2B**).

Thus, lower GOX concentrations were characterized using a blood gas analyzer at 0.5 hr, 1 hr and 2 hr timepoints. The oxygen tension in media that contained 0.15 µg/mL and 120 U/mL CAT of GOX was ~12% after 30 minutes (**Figure 3.3A**). In contrast, the oxygen content in the media that contained 0.5 µg/mL of GOX, and 120 U/mL CAT was right around 5% after 30

minutes and remained low at least for the next 2.5 hours (**Figure 3.3A**). MYP3 cell viability was

maintained around 100% for up to 1 hour under 0.15 μg/mL of GOX (12% O_2) and there was no

difference from normoxia after 2 hours. Under 0.5 μg/mL of GOX (5% O_2) in the presence of

CAT, MYP3 cell viability was stable at 100% up to 1 hour and not statistically different from

normoxia at hour 2 (**Figure 3.3B**). The absence of CAT resulted in a 50% reduction in MYP3

cell viability after 30 minutes of enzyme-induced hypoxic exposure (**Figure 3.3B**). Since GOX

uses glucose as substrate in the reaction to consume oxygen in media, glucose concentrations

were measured (using the blood gas analyzer) after 2 hours. The results demonstrated that

glucose concentration of 0.5 μg/mL GOX in hypoxic media was not statistically different from

the control media, indicating its impact on available glucose for cells was minimal. (**Figure 3.4**)

For the next experiments 0.5 μg/mL GOX was used due to this concentration leading to an

oxygen tension below 5% and minimal impact on cell viability.
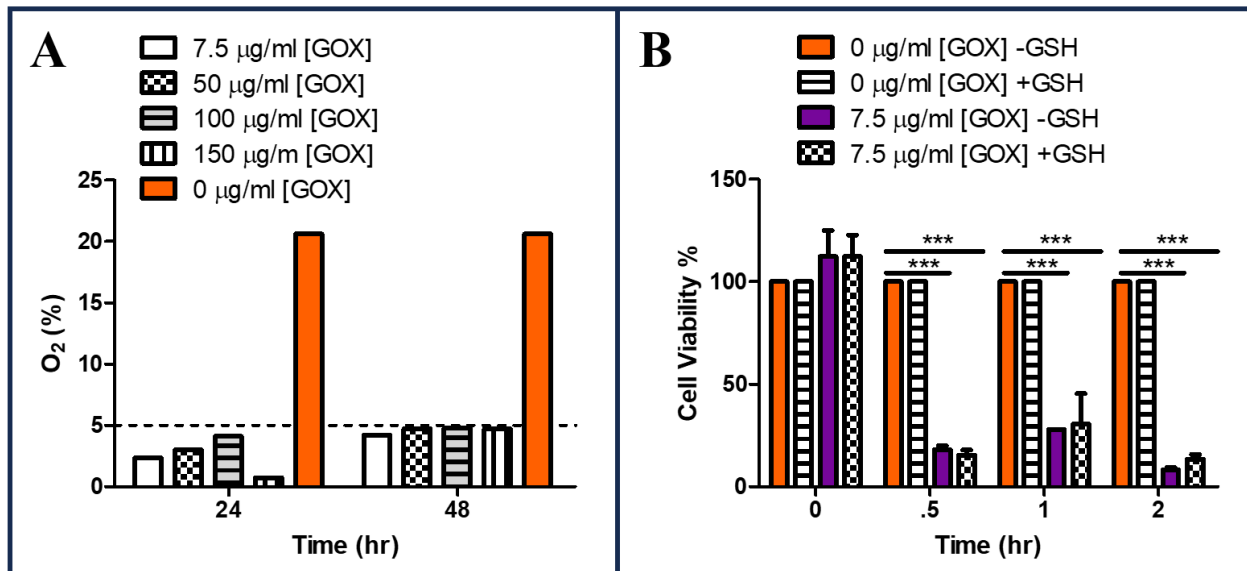
Figure 3.2 Characterization of enzyme-induced hypoxic PBS solution oxygen tension (A) and cell viability (B) with high concentrations of GOX. For all GOX concentrations, 5 mM of GSH was used. All of the high GOX concentrations were able to reduce oxygen for 48 hours. However, even the lowest GOX concentration of 7.5 μg/ml significantly impacted MYP3 cell viability within 30 minutes of exposure. Data are the mean ± SEM analyzed using two-way ANOVA. Each group is compared to the control, *$p < 0.05$, **$p < 0.01$, ***$p < 0.001$. N=1.
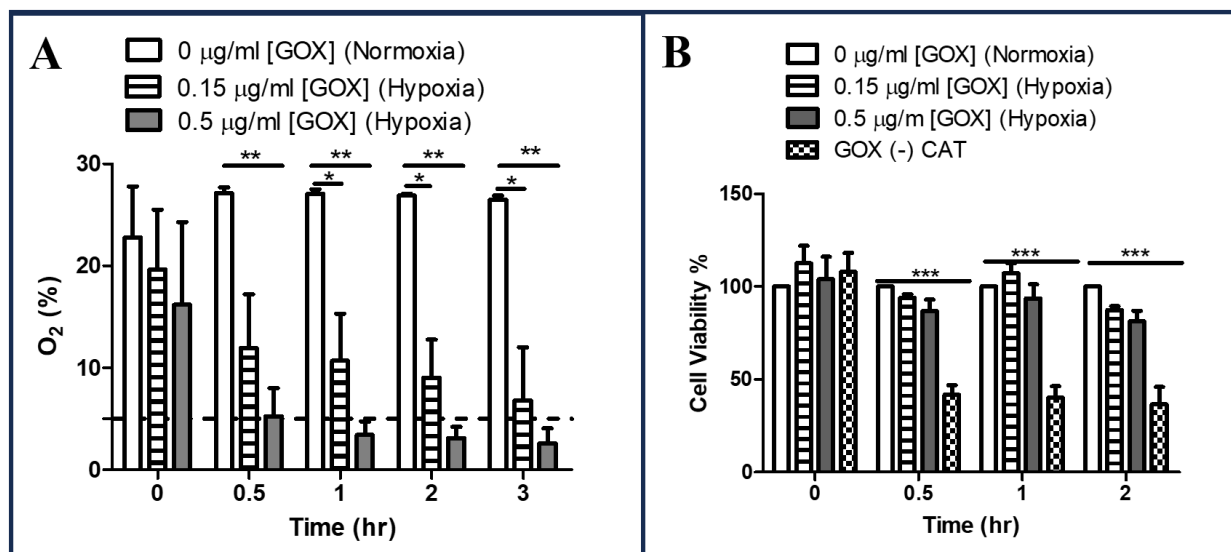
Figure 3.3 Characterization of enzyme-induced hypoxic media oxygen tension (A) and cell viability (B). For all GOX concentrations 120 U/mL of CAT was used. While both GOX concentrations (0.15 and 0.5 mg/mL) lowered oxygen tension rapidly, the higher concentration (0.5 μg/ml) GOX lowered and maintained oxygen tension below 5% for 3 hours. Both GOX concentrations (0.15 and 0.5 μg/mL) maintained cell viability at 1- and 2-hour timepoints. The absence of CAT significantly reduced cell viability. Data are the mean ± SEM analyzed using two-way ANOVA. Each group is compared to the control, **p<0.01, ***p<0.001. N=3. Image adapted from Hudson et al. [77].
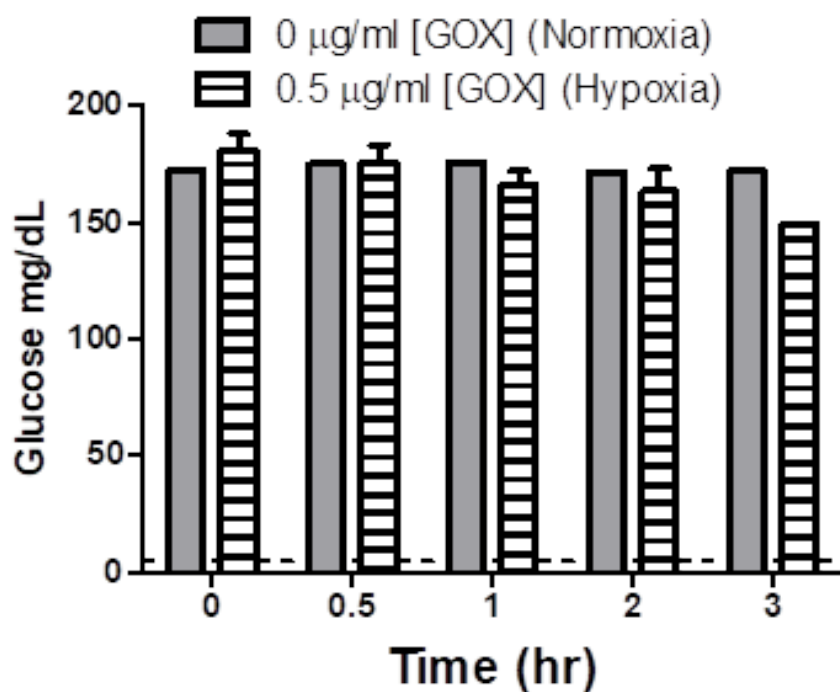
Figure 3.4 Glucose levels of GOX/CAT media. Media solutions with GOX and 120 U/mL of CAT. There was no difference in glucose levels between the 0 and 0.5 μg/ml of GOX. Each group is compared to the control. N=2. Image adapted from Hudson et al. [77].

Enzyme-induced and Gas-Induced Hypoxia Provoke Hypoxic Cellular Response

To ensure that GOX/CAT elicits a hypoxic cell response in MYP3 cells, stabilization of HIF-1α was examined using immunostaining. Under normoxia, there was a faint background signal of Alexa 488; however, this is not an indicator for HIF-1α stabilization. Conversely, MYP3 cells exposed to 0.5 μg/mL of GOX (5% O_2) enzyme-induced hypoxia and gas-induced hypoxia (5% O_2) both contained HIF-1α positive cells. The greatest fluorescent intensity, which is associated with stabilization of HIF-1α, was observed under artificial hypoxia-mimic conditions using cobalt chloride (**Figure 3.5**). Exposure of MYP3 cells to enzyme-induced hypoxia (0.5 μg/mL of GOX/ 5% O_2) created a two-fold increase in extracellular nitric oxide at hour 1 with levels returning to normoxic levels after 2 hours. Similar results were also seen with gas-induced hypoxia and artificial stabilization of HIF-1α under cobalt chloride showing a 5-fold and a 3.7-fold nitric oxide increase at hour 1, respectively. The enzyme catalase also acts as an antioxidant in the body and mitigates oxidative stress by removing cellular hydrogen peroxide. Thus, there is some concern that catalase in the two-enzyme system may impede the MYP3 hypoxic cellular response. Therefore, catalase was added to some cells exposed to gas-induced hypoxia. The presence of catalase did not hinder the hypoxic cellular response under gas-induced hypoxia, with nitric oxide levels reaching a 4-fold increase. At hour 2, nitric oxide concentration returned to that of normoxia for all methods (**Figure 3.6**).
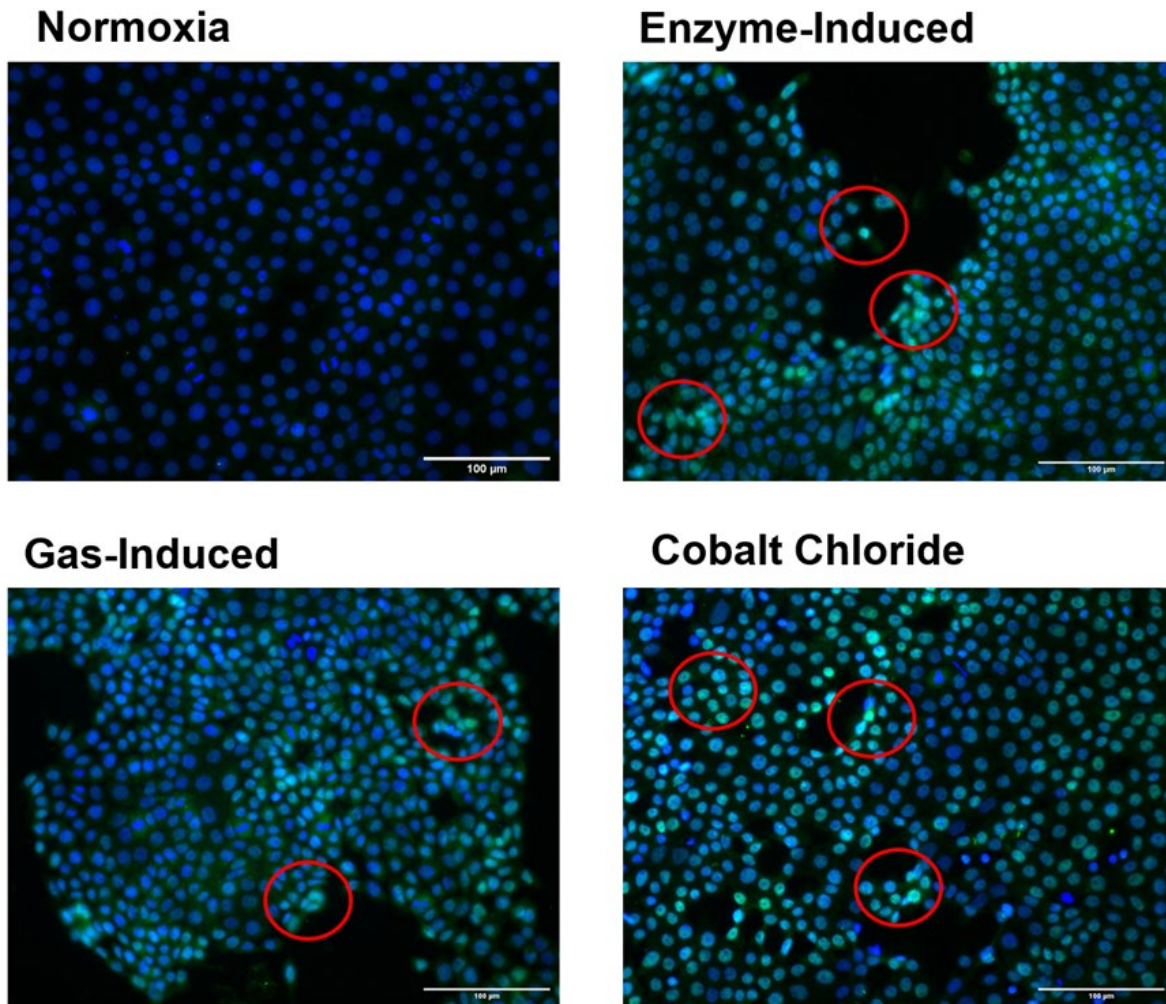
Figure 3.5 Staining of MYP3 cells for HIF-1α. MYP3 cells were maintained under normoxic (control) conditions (A) or exposed to enzyme-induced hypoxia with 0.5 µg/ml of GOX (B), 5% O_2 gas-induced hypoxia (C) or 100 µM $CoCl_2$ (D) for 2 hours and immunostained for HIF-1α (green, Alexa 488) and counterstained for cell nuclei (blue, DAPI). All methods to induce hypoxia resulted in increased HIF-1α stabilization (indicated by higher Alexa 488 fluorescence intensity in cell nuclei) when compared to the normoxic control. Under all of the hypoxic methods, Alexa 488 is present in most cell nuclei. The red circles enclose representative cells. Image adapted from Hudson et al. [77].
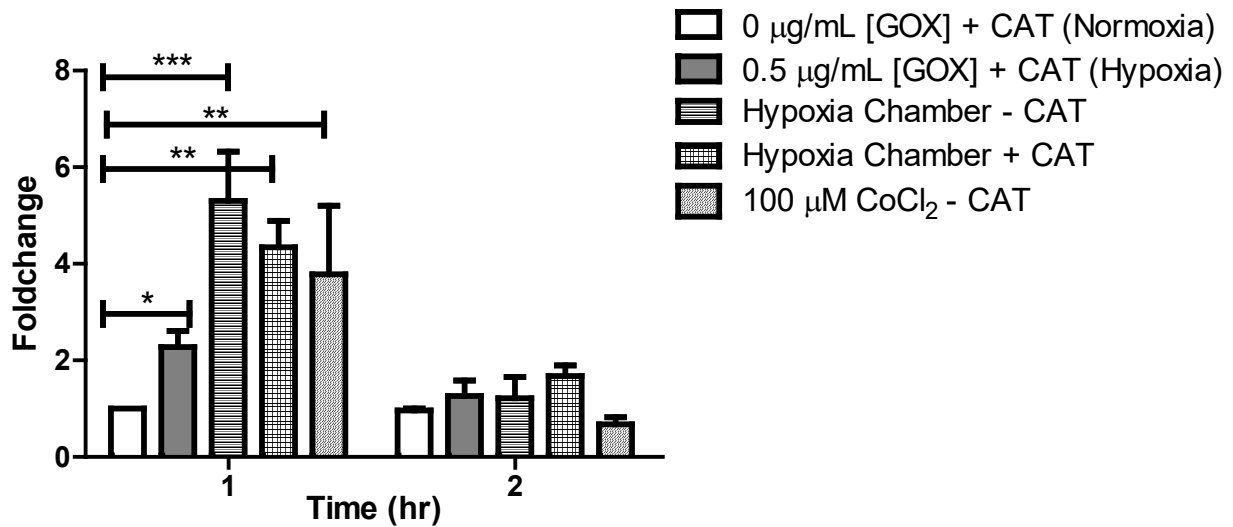
Figure 3.6 Increased nitric oxide release by MYP3 cells in response to short-term hypoxia. MYP3 cells were cultured under normoxic (control) conditions or exposed to enzyme-induced hypoxia (0.5 µg/ml [GOX]), gas-induced hypoxia (~5% O_2), or 100 µM $CoCl_2$ for up to 2 hours. NO levels increased after one hour of hypoxic exposure and returned to the baseline after two hours. Data are mean ± SEM and compared to the normoxic control (one-fold). Data was analyzed using two-way ANOVA followed by a Bonferroni posttest. *$p<0.05$, **$p<0.01$, ***$p<0.001$. N>4. Image adapted from Hudson et al. [77].

3.4 Discussion

The results of the present study demonstrated that different enzyme concentrations (0.15 µg/ml GOX and 0.5 µg/ml GOX) produced rapid reduction in oxygen tension within 30 minutes and sustained the hypoxic condition for up to 3 hours (**Figure 3.3A**). When MYP3 cells were cultured under 0.5 µg/mL GOX media, cell viability was no different than that of normoxia hours (**Figure 3.3B**). Enzymes were chosen as our model, as cultured cells in hypoxia chamber tend to equilibrate slowly to set oxygen tensions. Specifically, media inside dishes with intact lids would take around three hours to reach the oxygen tension of the flushed gas. [81] In contrast, it has been reported that the GOX/CAT enzyme system, like the one employed in the present study, can rapidly reduce oxygen in solution within minutes and can maintain oxygen depletion even with a liquid/air interface and stirring [89]

One of the first cellular responses to hypoxia that are common to various organ systems is stabilization and accumulation of HIF-1α, which degrades under normal oxygen conditions.[35] In the present study, MYP3 cells were exposed to low oxygen (<5%) through 0.5 µg/ml GOX media, gas-induced hypoxia, and a known HIF stabilizer $CoCl_2$ for two hours and all methods exhibited accumulation of HIF-1α as shown via immunostaining (**Figure 3.5**). These results are in agreement with a previous study that showed HIF-1α stabilization in Huh7 cells after 2 hours of hypoxia exposure via GOX/CAT.[86] In contrast, another study demonstrated that cells exposed to hypoxia via a chamber stabilized HIF-1α after 6 hours, further demonstrating how slowly chambers equilibrate to set oxygen tension. [86] Another typical cellular response to hypoxia in many organ systems is the release of nitric oxide because of its role in vasodilation to increase blood flow and oxygen supply to the affected tissue.[92] In the present study, MYP3 cells demonstrated a time-dependent NO response under the different methods of hypoxia exposure tested. Enzyme-induced hypoxia led to a significant increase in exogenous NO after 1 hour of exposure. Likewise, gas-induced hypoxia with or without the addition of antioxidant catalase also demonstrated an increase in NO at hour 1, indicating that the addition of catalase to our enzyme system had minimal impact on our results. In addition, artificial hypoxia via $CoCl_2$ resulted in higher NO at hour 1. For all methods to induce hypoxia, NO levels returned to that of normoxia at hour 2. This early response was similar to the results of a study where a short-term hypoxic exposure led to an increase in NO and nitrites by endothelial cells in as little as 15 minutes.[93] Taken together, the results of HIF-1α stabilization and NO release clearly demonstrated that cell culture media containing GOX/CAT provides hypoxic conditions that elicit typical cellular responses to low oxygen without the use of other devices, which in turn allow for the easy combination of hypoxia to bioreactors. For instance, Dunton et al. used a

custom hydrostatic pressure chamber to expose urothelial cells to elevated hydrostatic pressure, linking elevated pressure to ATP mediated NLRP3 inflammasome activation.[17] However, elevated pressure is only one component of the *in vitro* bladder outlet obstruction disease environment. As mentioned in chapter 1, elevated pressure can causes pinching of the bladder tissue vasculature which creates an ischemic environment. Thus, to get a full understanding of how pressure (mechanical) and hypoxia (chemical) initiate inflammation, these two stimuli should be combined. However, a hypoxia chamber and pressure chamber cannot be used in conjunction. Enzymes offer the opportunity to combine hypoxia with pressure or any other stimuli.

In the present study, we demonstrated that the two-enzyme system is suitable for inducing solution hypoxia *in vitro*. The GOX/CAT system was able to trigger an appropriate hypoxic response in urothelial and is a potential tool that can be used to investigate the role of hypoxia in various disease models.

CHAPTER FOUR

Aim 2: Quantify Urothelial Cell Response to Hypoxia and Identify Inflammasome Activation
Mechanisms

*Parts of this chapter is published in "Enzyme-induced hypoxia leads to inflammation in
urothelial cells *in vitro*." [77]*

4.1 Introduction

Bladder outlet obstruction is a prevalent urological condition that affects around 21.8% of

adults over the age of 20 and is a major cause of lower urinary tract symptoms (LUTS) such as

weak stream, incontinence, and noctoria.[1] The obstructions is usually caused by an enlarged

prostate that narrows the urethra, resulting in high pressure voiding,[94] excessive stretch, and

tissue ischemia caused by blood flow disruption. As a result of the obstruction, the bladder

becomes inflamed, which eventually leads to chronic inflammation and tissue fibrosis and

ultimately bladder decompensation if the obstruction is not resolved. BOO-induced inflammation

and fibrosis of the bladder has been linked to NLRP3 inflammasome/IL-1β pathway as found by

Hughes et al. via a rat model of BOO. This inflammasome can be activated through either

pathogen-associated molecular patterns (PAMPs) or damage-associated molecular patterns

(DAMPS) such as ATP and reactive oxygen species (ROS) and leads to release of pro-

inflammatory cytokine release. Furthermore, in this rat model, inhibition of NLRP3 via

glyburide blocked NLRP3-induced collaged deposition in rat bladder tissues. Previous in vitro

studies from our lab have shown that elevated hydrostatic pressure associated with BOO can

trigger ATP-mediated NLRP3 inflammasome activation in urothelial cells[17] and BOO-specific

pressure cycles trigger fibrosis and epithelial to mesenchymal transition (EMT) in the

urothelium, which was demonstrated through changes in genes related to fibrosis (collagen I,

collagen III, and lysyl oxidase) and EMT (NCAD, ECAD, MMP9 and αSMA).[18] However, the

urothelium is not only exposed to elevated voiding pressures but also hypoxia as well, which can play a role in BOO-induced inflammation; however, the exact contribution of hypoxia to inflammation in the urothelium has yet to be expounded.

Several studies have aimed to characterize the bladder blood flow of a normal and obstructed bladder. In one study, the detrusor oxygen tension of an obstructed pig bladder decreased by 42% when compared to the sham-operated bladders after 12 weeks of obstruction.[95] In normal human bladders, Batista et al. reported a decrease in bladder flood flow as the vesicle filled, with blood flow reduction being the greatest at the bladder dome.[96] In contrast, another study found blood flow increased with bladder distention in normal human bladders.[97] The discrepancies between whether blood flow increases or decreases during filling could partially be due to the lack of doppler laser methodology standardization and difference in patient bladder wall thickness.[98] Nevertheless, there is general agreement that bladder blood flow is reduced at capacity, and that obstruction exacerbates this reduction.[96,99,100] Furthermore, hypoxic response have been observed in the BOO bladder tissues, specifically the hypoxic response progression was seen in a BOO rat model, where HIF-1α reactivity was initially seen in the urothelium and mucosa 3 days post obstruction, and moved to the detrusor after two weeks.[36] Similarly, a hypoxic response was expressed in the stromal cells of bladder tissues biopsied from male BOO patients.[101] An in vitro study by Wiafe et al. demonstrated that human bladder smooth muscle cells cultured under low oxygen tension (~3%, using a hypoxia incubator) lead to the stabilization of HIF-1α in as early as 2 hours. Moreover, an increase in inflammatory cytokine gene expression such as IL-1β and IL-6 was observed under prolonged and continuous exposure to hypoxic conditions.[52] These studies clearly indicate that BOO not only creates a hypoxic environment in the urothelium and bladder wall tissue, but also these hypoxic conditions can

illicit an inflammatory response in bladder smooth muscle cells. However, the role of hypoxia in BOO pathology in the urothelium is not well understood. Several studies have linked hypoxia with NLRP3 inflammasome activation in other organ systems (e.g. brain, heart).[102–105] In addition, hypoxia has been shown to induce EMT in other organs, specifically in cases related to cancer.[106–108] Thus, we hypothesize that hypoxia may induce ATP-mediated NLRP3 inflammasome activation in bladder urothelial cells, similar to elevated hydrostatic pressure. Additionally, we hypothesize that multiple intermittent hypoxic insults may lead to EMT gene changes similar to elevated pressure cycles.

To the best of our knowledge, no other study examined the effect of hypoxia on bladder urothelial cells in vitro as it relates to bladder outlet obstruction. As discussed in chapter three, we found enzyme-induced hypoxia to be a cheap and convenient way to induce hypoxia in vitro and that the GOX/CAT system was able to illicit a hypoxic response in urothelial cells with the use of normal cell culture equipment. In this study, enzyme-induced hypoxia was used to create short and long durations of hypoxia and also to expose urothelial cells to 6 hours of intermittent hypoxia over the course of 3 days. Following exposure to enzyme-induced hypoxic conditions, intracellular caspase-1 as well as extracellular ATP release by a urothelial cell line (MYP3 cells) were measured. EMT gene related changes were measured in MYP3 cells exposed to 6 hours of intermittent hypoxia for 3 days.

4.2 Materials and Methods

Cell Culture

MYP3 cells were originally created by Dr. Ryoichi Oyasu (Northwestern University, Chicago, IL, USA) and are an immortalized rat non-tumorigenic urothelial cell line.[90] Samuel M.

Cohen, through the lab of Lora L. Arnold, both at the University of Nebraska Medical Center, Omaha, NE kindly provided the cells to us. The cells were cultured in complete MYP3 media: F-12 Kaighn's modified Ham's media (HyClone, Logan, UT, USA) supplemented with 10% low endotoxin-dialyzed fetal bovine serum (Gibco, Carlsbad, CA, USA), 10 µM non-essential amino acids (Cytiva, Marlborough, MA, USA), 1.0 µg/ml hydrocortisone (Sigma, St. Louis, MO, USA), 10 µg/ml insulin, 5 µg/ml transferrin and 6.7 ng/ml selenium (Gibco). [17] All cells were cultured under standard conditions (sterile, humidified, 37°C, 5% CO_2/95% air) before exposure to hypoxic conditions. MYP3 cells were chosen as our model.[109] In addition, these cells have been previously used by our lab.[17,18]

Hypoxia Experiments

Stock solutions of 2 mg/mL of glucose oxidase (GOX) and 2 mg/mL catalase (CAT) were prepared by dissolving dry GOX or CAT in sterile PBS. A 1 M stock solution of HEPES was prepared by dissolving dry HEPES in sterile PBS. All stock solutions were filtered with a 0.22 µM syringe filter. A stock solution of 1 mM $CoCl_2$ was prepared in sterile PBS and diluted to 100 µM in serum free cell culture media. MYP3 cells were seeded at a density of 10^6 cells/well in a sterile 6 well culture plate and incubated for 24 to 48 hours until cells reached 90% confluency. At the beginning of each experiment, enzymatically induced hypoxic media [89] were prepared by diluting stock solutions to a final concentration of 0.15 or 0.5 µg/mL GOX, 120 U/mL CAT, and 25 mM HEPES in sterile phenol-red free Dulbecco's Modified Eagle Media (DMEM, Sigma). The solutions were allowed to equilibrate to below 5% oxygen content for 30 minutes before exposure to cells. Cell culture media was replaced with 1 mL of either normoxic (5% CO_2/95% air, 0 µg/mL GOX, 120 U/mL CAT, and 25 mM HEPES) media or hypoxic (~5% O_2, 0.5 µg/mL GOX, 120 U/mL CAT, and 25 mM HEPES) media for two to six hours. To extend hypoxic

conditions to 6 hours, the media was replaced at hour 3 with fresh GOX/CAT hypoxic media. A control experiment was conducted with MYP3 cells using a hypoxia chamber (5% O_2, and 5% CO_2 balanced with N_2) in the presence or absence of CAT in the culture media, to ensure that the enzyme system induced the desired hypoxic conditions without unintended side effects. In addition, cellular responses to enzyme-induced and gas-induced hypoxia were compared chemical hypoxia which was induced with 100 µM cobalt chloride ($CoCl_2$) in culture for 2 hours. [91]

To inhibit nitric oxide, some cells were pre-treated with 16 mM NG-Nitroarginine methyl ester, N-Nitro-L-arginine methylester (L-NAME), a non-specific NOS inhibitor, one hour before and during shorter duration of enzyme-induced hypoxia. Cells were treated with 5 mM glutathione (GSH) (Fisher, Waltham, MA, USA) during exposure to enzyme-induced hypoxia to inhibit ROS. To inhibit TXNIP, another group of cells were pre-treated with 100 µM verapamil (ApexBio, Houston, TX, USA), a calcium channel blocker, for 1 hour prior to enzyme-induced hypoxia. Verapamil remained in the culture medium for the duration of the 6-hour hypoxic exposure. In addition, Intracellular caspase-1 concentrations were obtained from these groups.

Some groups of cells were exposed to 6 hours of enzyme-induced hypoxia over the course of 3 days. MYP3 cells were cultured at 10^6 cells/well in a sterile 6 well plate and allowed to incubate overnight in complete MYP3 media. At the beginning of the experiment, standard culture media was replaced with either enzyme induced low serum (5% FBS) hypoxic media (0.5 µg/mL GOX, 120 U/mL CAT, and 25 mM HEPES in sterile F-12K media) or low serum normoxic media (0 µg/mL GOX, 120 U/mL CAT, and 25 mM HEPES in sterile F-12K media). To extend hypoxic conditions to 6 hours, the media was replaced at hour 3 with fresh enzyme hypoxic media. After 6 hours of hypoxia, enzyme media was replaced with low serum F-12K

media overnight. The following day, the cells were exposed to enzyme-induced hypoxia for 6 hours again. After day 3 of this hypoxic exposure (**Figure 4.1**), cells were trypsinized and stored in 500 µl RNAlater (Fisher, Waltham, MA, USA).

Extracellular ATP Quantification

Extracellular ATP in supernatant media was quantified using a commercially available luciferin-luciferase assay kit according to the manufacturer's protocol (Molecular Probes, Eugene, OR, USA). Briefly, 10 µL of supernatant media was mixed with 90 µL of the standard reaction solution in a 96 well plate. Luminesce values were converted to ATP concentration using a standard curve prepared at the time of the assay. ATP concentration was only obtained from shorter duration experiments. Data were normalized to the normoxic control for that experiment and reported as fold change.

Quantification of Caspase-1 Activation

At the end of each experiment, intracellular caspase-1 activation levels were determined using a previously established method. [110] Supernatant media was removed, and cells were lysed with 500 µL of a buffer containing 10 mM $MgCl_2$ and 0.25% Igepal CA-630 (Sigma). Cell lysates were combined with 500 µL of a storage buffer that consisted of 40 mM HEPES, 20 mM NaCl, 2 mM EDTA and 20% glycerol, and stored at -80°C degrees until ready for use in the assay. In a black-walled 96 well plate, 100 µL of stored cell lysates were combined with 10 µL of 100 µM DTT, 20 µL of 100 mM stock Z-YVAD-AFC substrate (VWR, Radnor, PA, USA) and 50 µL of caspase assay buffer (50 mM HEPES, 10% sucrose and 0.1% CHAPS) and incubated at 37°C with shaking for 24 hours. Fluorescence intensity was measured at 340 nm excitation and 535 nm emissions. Data were normalized to the control for each group.

Quantitative RT-PCR

Total RNA was isolated from MYP3 cells exposed to 6 hours of intermittent enzyme-induced hypoxia for 3 days via the commercially available RNeasy spin column kit according to manufacturer's protocol (Qiagen, Germantown, MD, USA). Quantitative reverse transcription-polymerase chain reaction (qRT-PCR) was conducted on RNA following the established protocol of a commercially available Luna Universal Probe One-Step qRT-PCR kit (New England Biolabs, Ipswich, MA, USA) with primers designed to amplify a region of mRNA of target genes (**Table 4.1**). The comparative threshold cycle method ($\Delta\Delta C_t$) normalized to the C_t values of GAPDH (housekeeping gene) was used to calculate relative differences in the groups.

Statistical Analysis

A minimum of three independent experiments were performed with data presented as the mean ± standard error of the mean (SEM). For time course experiments, the data were analyzed using two-way analysis of variance (ANOVA) with a Bonferroni post-test. One-way ANOVA was used for single timepoint experiments with post-hoc Tukey test. All statistical analyses were performed using GraphPad Prism 5 software for Windows (San Diego, CA) and *p* values less than 0.05 were considered statistically significant.
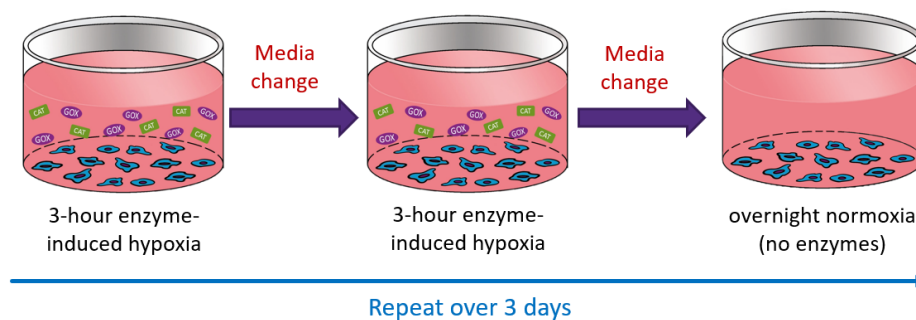
Figure 4.1 Illustration of the protocol for intermittent hypoxic exposure for 3 days. Urothelial cells were exposed to longer duration of hypoxia over a course of 3 days. All experiments were done in low serum media.

Table 4.1 PCR primer list for pro-EMT genes

Gene	GenBankID	Sequence (5'-3')
α Smooth Muscle Actin (αSMA)	NM_031004.2	F-GAGCGTGGCTATTCCTTCGTG R-CAGTGGCCATCTCATTTTCAAAG
Matrix Metallopeptidase 9 (MMP-9)	NM_031055.1	F-GAGCGTGGCTATTCCTTCGTG R-CAGTGGCCATCTCATTTTCAAAG
Neuronal Cadherin (N-CAD)	NM_031333.1	F-ACTGCACCGACGTAGACAGG R-CTTTATCCCGGCGTTTCATC
Endothelial Cadherin (E-CAD)	NM_031334.1	F-AGACCAACGAGGGCATTCTG R-GGCTGTGGAAGGGACAAGAG
Cytokeratin 20 (CK20)	NM_173128.1	F-TGAGACGCAGCTACCAGACC R-CAACTGGCTGGCATAACGAG
GAPDH	NC_086022.1	F-ACC ACA GTC CAT GCC ATC AC R-TCC ACC ACC CTG TTG CTG TA

4.3 Results

Longer Duration of Hypoxia Leads to NLRP3 Activation

To investigate whether hypoxia would facilitate a purinergic-dependent inflammatory response in cells, ATP release (purinergic pathway indicator) and intracellular caspase-1 (indicator of NLRP3 activation) were quantified. Under short durations of enzyme-induced hypoxia (0.5 ug/mL of GOX/ 5% O_2), or gas-induced hypoxia (5% O_2) there was no difference in ATP release compared to the normoxic control at after 1 or 2 hours. The presence of CAT had no impact on these and artificial HIF-1α stabilization had very little impact on extracellular ATP in 2 hours (**Figure 4.2**).
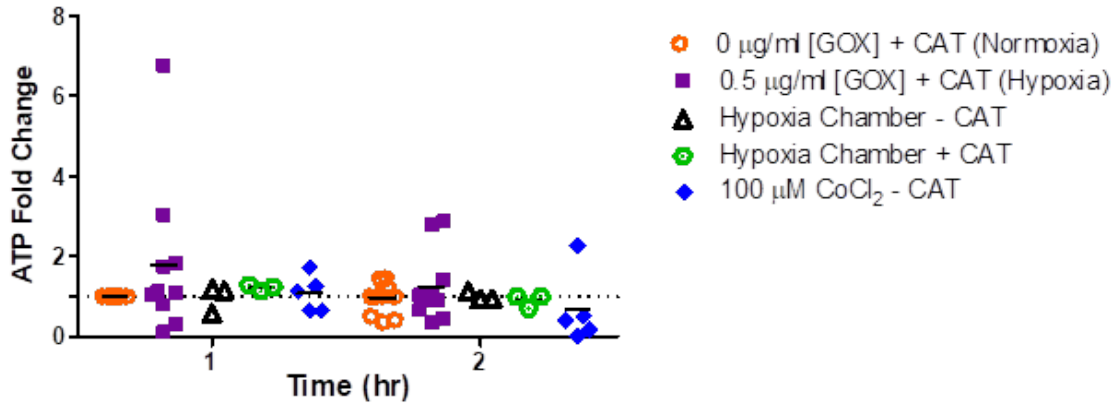
Figure 4.2 Extracellular ATP release by MYP3 cells under short-term hypoxia. MYP3 cells were maintained under normoxic (control) conditions, or exposed to enzyme-induced hypoxia, gas-induced hypoxia, or 100 μM CoCl$_2$ for up to 2 Hours. Average ATP releases were similar under all the conditions tested. Data are mean ± SEM and compared to the normoxic control (one-fold). Data was analyzed using two-way ANOVA followed by a Bonferroni post hoc test. N>4. Image adapted from Hudson et al. [77].

Likewise, MYP3 cells demonstrated no change in caspase-1 under short durations of enzyme-induced or gas-induced hypoxia in the presence or absence of CAT. Even with artificial HIF-1α stabilization, caspase-1 levels remained unchanged when compared to normoxic (**Figure 4.3**). Nitric oxide may play a protective role for urothelial cells during hypoxic insults. Treatment with L-NAME during shorter durations of hypoxia was able to attenuate enzyme-induced hypoxia increases in NO levels at hour 1. However, inhibiting hypoxia induced NO increase didn't lead to any changes in caspase-1 levels (**Figure 4.4**).
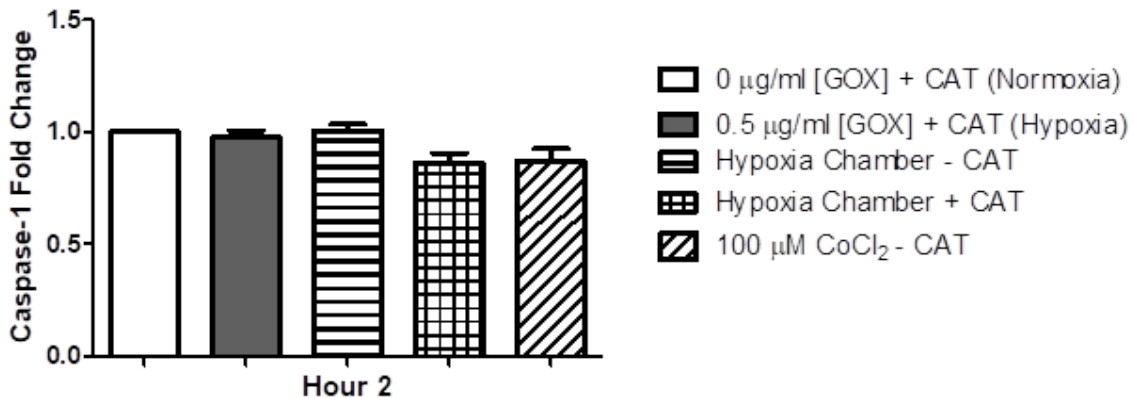
Figure 4.3 Intracellular caspase-1 activity unaffected under short-term hypoxia. MYP3 cells were maintained under normoxic (control) conditions, or exposed to enzyme-induced hypoxia, gas-induced hypoxia, or 100 μM CoCl$_2$ for up to 2 Hours. Caspase-1 activity was similar under all the conditions tested. Data are mean ± SEM and compared to the normoxic control (one-fold). Data was analyzed using one-way ANOVA. N>4. Graph taken from Hudson et al. [77].
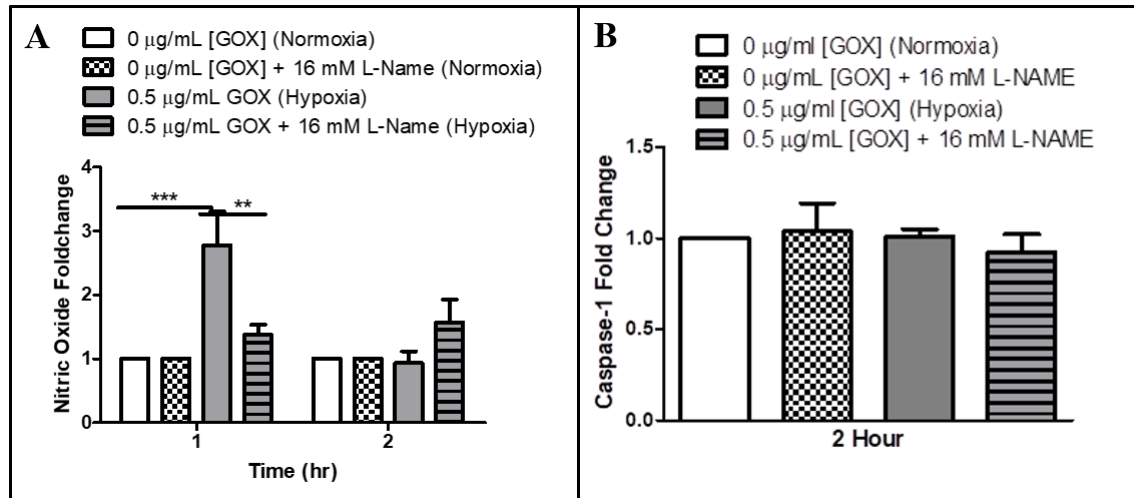
Figure 4.4 Nitric oxide levels after treatment with L-NAME (A). Caspase-1 levels after treatment with L-NAME (B). Treatment with L-NAME was able to attenuate the hypoxia induced increase in NO levels at hour 1. However, attenuating NO levels had no impact on intracellular caspase-1 activity. Data are mean ± SEM and compared to the normoxic control (one-fold). Data was analyzed using one-way ANOVA. N>4. Graph taken from Hudson et al. [77].

Previous research has shown that longer instances of hypoxia lead to inflammatory response in smooth muscle bladder cells.[52] Therefore, we exposed our MYP3 cells to six hours of enzyme induced hypoxia and found a 1.6-fold increase in intracellular caspase-1 when compared to the normoxic control. To determine the pathway involved, verapamil was employed to inhibit TXNIP and GSH to inhibit ROS. Verapamil treatment lowered the hypoxic-induced increase in caspase-1 levels similar to the normoxic control (**Figure 4.5**). Further, inhibiting ROS with glutathione also reduced caspase-1 levels to those of normoxia (**Figure 4.5**).
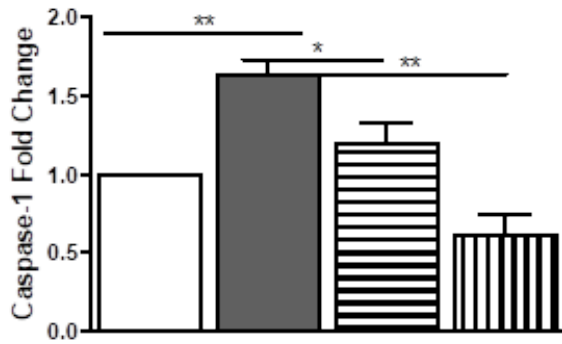
Figure 4.5 Intracellular caspase-1 increased under longer duration of Hypoxia. MYP3 cells were maintained under normoxic (control) conditions or exposed to enzyme-induced hypoxia for 6 hours. At the end of the 6-hour exposure to caspase-1 activity was significantly increased compared to control. Treatment with TXNIP inhibitor verapamil and antioxidant GSH both attenuated the hypoxia induced caspase-1 increase. Data are mean ± SEM and compared to the normoxic control (one-fold). Data was analyzed using one-way ANOVA followed by Tukey post-hoc test. N=4. *$p<0.05$, **$p<0.01$, ***$p<0.001$. Image adapted from Hudson et al. [77].

Intermittent Hypoxia Didn't Initiate EMT

A previous study from our lab has demonstrated that exposure of MYP3 cells to 72 hours of high pressure cycling mimicking chronic BOO was able to illicit EMT gene related changes.[18] Thus, MYP3 were exposed to 6 hours of intermittent hypoxia for 3 days, as we found that the 6 hour duration of hypoxia led to the activation of NLRP3 inflammasome. There was a trend of higher expression of CK20 (epithelial marker) and NCAD (mesenchymal marker) compared to the normoxic control, with ECAD and MMP9 expression levels remaining close to the normoxic levels. There was a slight reduction in αSMA in cells exposed to hypoxia than those exposed to normoxia (**Figure 4.6**).
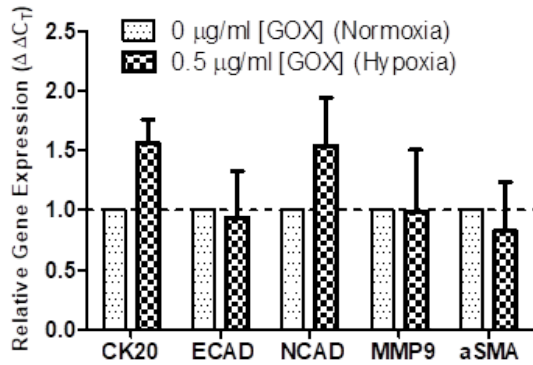
Figure 4.6 Gene expression changes after exposure to 6 Hours of Intermittent Hypoxia. After a 3-day exposure to intermittent hypoxia there was no observable trend in EMT gene expression changes under exposure to repeated instances of 6 hours of hypoxia. Data are the mean $\pm$ SEM analyzed using one-way ANOVA followed by a post-hoc Tukey-test. N=3.

4.4 Discussion

Although some observations of bladder tissue ischemia and inflammation associated with BOO are reported in literature,[36,111,112] the exact relationship between hypoxia and inflammation in bladder urothelial cells is not well expounded. We hypothesized that hypoxia experienced by urothelial cells would lead to activation of NLRP3 inflammasome and intermittent hypoxia would initiate EMT gene related changes. To assess the hypothesis that hypoxia leads to inflammation through NLRP3 activation, we exposed MYP3 urothelial cells to hypoxic conditions using an enzyme (GOX/CAT) system and quantified cellular responses. Based upon the results of chapter 3, the GOX concentration of 0.5 ug/ml was selected for its ability to rapidly decrease oxygen within culture dishes and minimal effect on cell viability.

Previous studies conducted by our lab demonstrated that BOO-associated inflammation and fibrosis were mediated, at least in part, by the NLRP3 inflammasome activation [73,113] and involved hydrostatic pressure-induced extracellular ATP amplification and activation of P_2X_4 in urothelial cells.[17] Moreover, previous research by other groups demonstrated a link between BOO-induced hypoxia and bladder inflammation.[102,111] For this reason, we initially hypothesized that oxidative stress on urothelial cells might also trigger an increase in extracellular ATP and lead to NLRP3 activation. Although we found that urothelial cells respond to a hypoxic

environment as seen through cellular responses such as HIF-1α stabilization and NO release, there were no changes detected in extracellular ATP or intracellular caspase-1 under any of the hypoxic conditions that were tested (enzyme-induced, gas-induced, or with cobalt chloride) within the two-hour period. In contrast, when MYP3 cells were exposed to enzyme-induced hypoxia for a longer duration of 6 hours, there was a significant ($p<0.05$) increase in caspase-1 activity compared to control (**Figure 4.5**) indicating NLRP3 inflammasome activation. We speculated that NO may have played some protective role for urothelial cells from hypoxia in the early time points (1-2 hours) as previously reported that treatment with L-NAME led to higher instances of ischemic damage in rabbit bladders.[45,54] Therefore, MYP3 cells were pre-treated with 16 mM L-NAME, which led to a reduction in NO after 1 hour exposure to hypoxia (**Figure 4.4**), but caspase-1 activity remained unchanged (**Figure 4.4**). This further supports our hypothesis hypoxia driven inflammation requires longer durations of low oxygen. Since urothelial cells are regularly exposed to short durations of hypoxic conditions during voiding, even in healthy individuals,[114] perhaps a urothelial inflammatory response to hypoxia is specific to prolonged insults.

Low oxygen can stimulate the production of reactive oxygen species (ROS) and mitochondrial ROS (mtROS) in various cells.[115,116] NLRP3 inflammasome may be activated via ROS and mtROS through TXNIP/NLRP3 signaling, which can be independent of the ATP-mediated pathway.[117–119] For instance, in an in vitro study, gas-induced hypoxia induced increased levels of NLRP3 and TXNIP proteins in mice insulinoma MIN6 cells. In addition, the researchers were able to attenuate this increase by inhibiting elevated ROS levels caused by hypoxia via treatment with antioxidant N-acetylcysteine (NAC).[51] Moreover, in rat primary urothelial cells, caspase-1 activation caused by 24 hour exposure to calcium pyrophosphate

(CPPD) was inhibited by 150 µM of verapamil, TXNIP inhibitor, and 2.5 mM of NAC, demonstrating that NLRP3 inflammation is through a ROS/TXNIP pathway.[30] Therefore, in the present study MYP3 cells were exposed to longer duration of hypoxia following treatment with verapamil, and ROS reducer, GSH, to test the hypothesis that this pathway was involved in hypoxia-induced inflammasome activation. The results of the present study provide evidence that treatment with verapamil and GSH both attenuated hypoxia-induced NLRP3 activation in MYP3 cells (**Figure 4.5**). This indicated that an increase in ROS production resulted from exposure to longer duration of hypoxia and led to TXNIP mediating NLRP3 inflammasome activation in urothelial cells, similar to the study on the effect of CPPD.[30] The hypoxia-induced NLRP3 activation observed in the present study may lead to subsequent IL-1b-dependent bladder tissue fibrosis as shown in our previous study.[113] Moreover, activation of caspases has been shown to play a role in mediating programmed cell death such as apoptosis and pyroptosis.[120,121] Therefore, in future studies, impacts of long-term hypoxia on urothelial cells need to be carefully examined from multiple aspects.

Intermittent hypoxia didn't initiate EMT gene related changes. This could be due to the duration of hypoxia chosen for this study. For example, an in vitro study of lung adenocarcinoma cells saw reduction of epithelial marker ECAD and an upregulation of mesenchymal markers NCAD and Vimentin in a time-dependent manner under exposure to 1% gas induced hypoxia. The greatest increase in EMT markers was seen at 24 hours.[122] Likewise, the urothelial cells may not illicit changes in EMT under our experimental set-up because for the majority of the study, normal oxygen levels were maintained, which may allow for some repair to the oxidative stress.

Our results have clinical relevance regarding the debate over the importance of high voiding pressures versus high storage pressures as the source of bladder damage in obstructed

patients. Based on urodynamic studies and long-term monitoring of patients with BOO, clinicians have raised the dangers of elevated storage pressures over elevated voiding pressures and this study further supports that conclusion. Compression of blood vessels occurs during voiding and with high pressure storage, which results in a hypoxic environment. However, our data shows that 2 hours of hypoxia is insufficient to activate NLRP3 to produce inflammation, it would be highly unlikely that short bursts of pressure/hypoxia would illicit an inflammatory response if normal pressures and oxygen levels are maintained during the much longer storage phase. On the other hand, in the later stages of BOO where bladder compliance is decreased and the storage pressures rise, our 6-hour data suggests that this is the time when patients would be most at risk for bladder damage. Thus, our data supports the conclusion from clinical data that maintaining a lower storage pressure via frequent voiding, catheterization, or use of bladder relaxing medications may prevent inflammation, fibrosis, and long-term bladder damage.

The results of this study indicated that short-term exposure to hypoxia didn't lead to inflammatory response, although a hypoxic response was observed (chapter 3). Furthermore, the results provide evidence that longer duration of hypoxia activates NLRP3 in urothelial cells through ROS and TXNIP. Thus, antioxidants and TXNIP inhibitors may have some potential in mitigating inflammation and subsequent risk of fibrosis in later stages of BOO that involve prolonged tissue ischemia and other bladder pathologies such as acute urinary retention. Further studies are needed, however, to investigate the effects of hypoxia on the events downstream of NLRP3 activation such as changes in fibrosis-related gene expression and decreases in cell viability due to programmed cell death to better understand bladder pathologies involving inflammation and thus provide better treatment.[77]

CHAPTER FIVE

Aim 3: Characterize Exosome Release from Urothelial Cells in Response to

Pressure and Hypoxia

5.1 Introduction

Occasionally, patients experiencing lower urinary tract symptoms (LUTS) delay

treatment seeking until symptoms worsen and bladder remodeling has already occurred. One

assessment reported only a third of participants with voiding, storage, and postmicturition LUTS

sought treatment.[123] In addition, tools for bladder outlet obstruction (BOO) diagnosis are

invasive and often times involves the use of catheters to determine the pressure of the detrusor

(Pdet). Standard urodynamic testing is associated with pain and embarrassment, and carries the

risks associated with catheter insertion.[9,124] On another note, invasive methods are required to

investigate tissue changes caused by BOO such as, fibrosis, and epithelial mesenchymal

transition (EMT), which has been shown to be initiated in urothelial cells exposed to BOO

specific pressure profiling.[18] Thus, there is a need for the development of a non-invasive

diagnostic tool for BOO. Urine testing is an attractive alternative as urine is comprised of

proteins and exosomes that contain biomolecular cargo, including lipids and non-coding nucleic

acids, such as long non-coding RNAs (lncRNAs) and micro RNAs (miRNAs). Exosomes are a

class of extracellular vesicles (EVs) and can be distinguished from other EVs based upon size

and the expression of tetraspanin CD81, CD9, and CD63. These phospholipid bilayer vesicles

are thought to be released to mediate cell-to-cell communication processes through the delivery

of cargo. In addition, stressors has been found to stimulate the release of EVs.[125–127] Exosomes

also have potential as biomarkers for diseases since these vesicles are secreted into virtually

every bodily fluid and contain cargo that may mirror the physiological state of the donor cell.

51

Previous research has indicated hypoxia can stimulate the release of exosomes and alter exosomal cargo.[128–132] However, little research has been conducted on the effects of elevated pressure on exosome release and the alterations in exosomal cargo. A few studies have applied pressure to cells to stimulate exosome release and changes in the cargo; however, the content of the exosomes wasn't investigated. Instead, the impacts of the pressure-derived exosomes were researched by exposing different cells to these pressure-derived exosomes. More specifically, the researchers found that exposing naïve microglia cells to exosomes secreted from microglia cells subjected to elevated hydrostatic pressure led to an increase pro-inflammatory cytokines in the naïve microglia cells.[133]

In the tissues of rat bladders, different miRNA expression profiles were identified in obstructed bladders and with some variation depending on the duration of obstruction.[134] In patients experiencing LUTS due to bladder obstruction there was a distinct profile of miRNAs in the tissues of obstructed bladders and normal bladders.[76] In addition, cell free urine from obstructed patients had three differentially expressed miRNAs compared to cell free urine from normal healthy bladders. More specifically, bladders with BOO induced LUTS demonstrated an up-regulation of miR-301b-3p and a down-regulation of miR-363-3p and miR-10a-5p.[75] Furthermore, the miRNA profiles of bladders experiencing BOO induced LUTS vs neurogenic LUTS were different.[75] Together these studies demonstrate that the chemical and mechanical changes of BOO may lead to changes in the miRNAs expressed in bladder tissues and urine. However, effects of BOO on urinary exosomes have not been investigated. Furthermore, the direct effects of pressure and hypoxia on urothelial exosome secretion and cargo have not yet been explored. Identifying the differences lncRNAs observed in exosomes released from pressurized cells can aid in the development of a non-invasive BOO diagnostic. We hypothesize

that pressure can stimulate the release of exosomes from urothelial cells. A graphical depiction of this hypothesis is shown in **Figure 5.1**. Thus, in the present study, human and rat urothelial cells were exposed to either an elevated pressure cycling profile mimicking late-stage BOO or 6 hours of enzyme-induced hypoxia. Extracellular vesicles were harvested from the conditioned media and characterized. RNA in EVs collected from conditioned media supernatant of human urothelial cells exposed to pressure conditions were investigated using Oxford Nanopore Technologies (ONT) direct RNAsequencing.
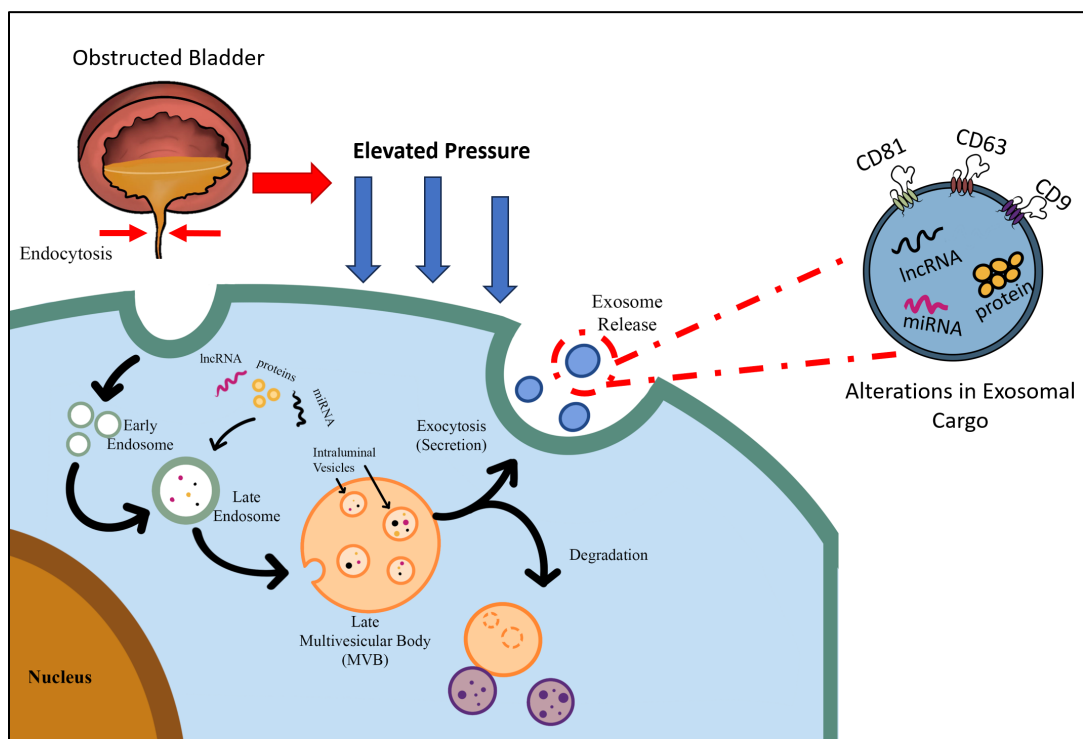
Figure 5.1 Depiction of elevated pressure proposed mechanism for elevated pressure leading to changes in the cargo from exosomes released from urothelial cells.

5.2 Materials and Methods

Urothelial cell culture

MYP3 cells are an immortalized rat non-tumorigenic urothelial cell line, originally created by Dr. Ryoichi Oyasu (Northwestern University, Chicago, IL, USA).[90] Samuel M. Cohen, through the lab of Lora L. Arnold, both at the University of Nebraska Medical Center,

Omaha, NE kindly provided the cells to us. The cells were cultured in complete MYP3 media: F-12 Kaighn's modified Ham's F-12 media (HyClone, Logan, UT, USA) supplemented with 10% low endotoxin-dialyzed fetal bovine serum (Gibco, Carlsbad, CA, USA), 10 µM non-essential amino acids (Cytiva, Marlborough, MA, USA), 1.0 µg/mL hydrocortisone (Sigma, St. Louis, MO, USA), 10 µg/mL insulin, 5 µg/mL transferrin and 6.7 ng/mL selenium (Gibco).[17] Primary bladder epithelial cells (BDeC) were obtained from American Type Culture Collection (ATCC). The cells were grown in bladder epithelial cell basal medium (ATCC) supplemented with bladder epithelial growth kit with the final concentration for each component being as follows: 6 mM L-glutamine, 0.4% Extract P, 1.0 µM epinephrine, 5 ng/mL rh EGF (epidermal growth factor), 100 ng/mL hydrocortisone, 5 µg/mL insulin, 5 µg/mL Apo-transferrin, 0.5 ng/mL rh TGF-α (transforming growth factor), and 5 ng/mL rh KGF (keratinocyte growth factor). All cells were cultured under standard conditions (sterile, humidified, 37°C, 5% CO_2/95% air) before exposure to pressure conditions.

Pressure Response Experiments

Cells were exposed to a pressure cycling profile using a custom pressure bioreactor. Either MYP3 or BDeC cells were seeded at 2.2 million cells in a 100 mm dish and incubated for 48 hours until cells reached 70% confluency in regular culture media. Both BDeC and MYP3 cells were briefly rinsed 3x with sterile PBS to remove any residual serum in the culture dish. Afterwards, the PBS was replaced with basal cell culture media containing 25 mM HEPES without serum prior to pressure experiments for MYP3 cells. Because BDeC cells are conventionally cultured in serum free media, normal BDeC culture media with the addition of 25 mM HEPES was used during pressure cycling experiments. Both BDeC and MYP3 cells were

exposed to either atmospheric or pressure cycles consisting of a storage pressure of 15 cmH$_2$O

for 175 minutes and a voiding pressure of 75 cmH$_2$O for 5 minutes for 24 or 72 hours.

Immediately following pressure exposure, media supernatant was collected and filtered with a

0.22 µM syringe filter. Filtered media was stored at 4°C before exosome isolation for up to a

week. Experimental conditions are depicted in **Figure 5.2**.
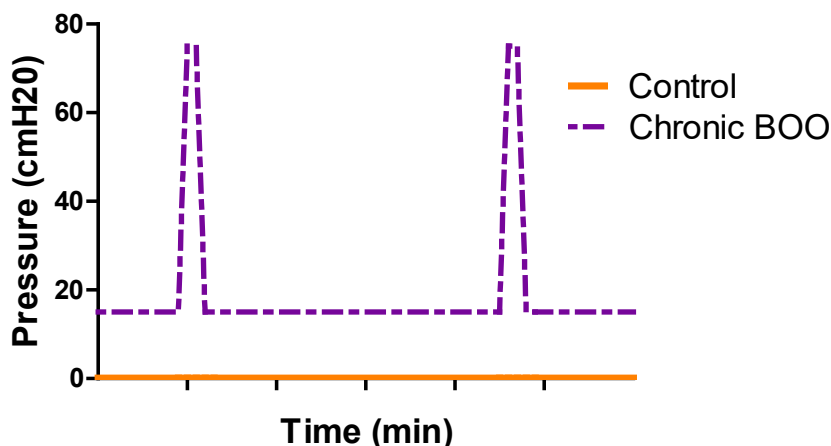
Figure 5.2 Graphical depiction of pressure cycling profile. Late-stage pressure conditions consisted of a storage pressure of 15 cmH$_2$O for 175 minutes and a voiding pressure of 75 cmH$_2$0 for 5 minutes.

Hypoxic Exposure Experiments

Stock solutions of 2 mg/mL of glucose oxidase (GOX) and 2 mg/mL catalase (CAT) were

prepared by dissolving dry GOX or CAT in sterile PBS. The stock solutions were stored at -20°C

until ready for use. A 1 M stock solution of HEPES was prepared by dissolving dry HEPES in

sterile PBS and stored at 4°C until use. All stock solutions were filtered with a 0.22 µM syringe

filter. MYP3 or BDeC cells were seeded at a density of 2.2 million cells in a 100 mm cell culture

dish and incubated for 24 to 48 hours until cells reached 90% confluency. At the beginning of

each experiment, enzymatically induced hypoxic media [89] were prepared by diluting stock

solutions to a final concentration of 0.5 µg/mL GOX, 120 U/mL CAT, and 25 mM HEPES in

sterile serum free F-12K modified media (Sigma) for MYP3 cells. For BDeC cells, enzyme

hypoxic media was prepared by diluting stock solutions to a final concentration of 0.5 µg/mL

GOX, 120 U/mL CAT, and 25 mM HEPES in sterile BDeC culture media. The solutions were

allowed to equilibrate to below 5% oxygen content for 30 minutes before exposure to cells.

Before replacing culture media with hypoxic media, the cells were washed 3x with sterile PBS.

To extend hypoxic conditions to 6 hours, the hypoxic media was replaced at hour 3 with fresh

GOX/CAT hypoxic media. Immediately following hypoxic exposure, media supernatant was

collected and filtered with a 0.22 µM syringe filter. Filtered media was stored at 4°C before

exosome isolation.

Exosome Isolation

EVs were harvested from filtered conditioned media and either stored or immediately

used for various assays within one week of the experiment. Three different methods were used to

extract EVs from the culture media: ultracentrifugation, Invitrogen Total Exosome Isolation kit,

and capillary-channeled fiber spin down tips (C-CP) (**Figure 5.3**). Ultracentrifugation was

performed using the protocol depicted in **Figure 5.3.**[135] Initially, serial centrifugation was used to

remove cell and cell debris: 1000 x g for 10 min and 17,000 x g. Then supernatant was

centrifuged at 200,00 x g for 60 min to pellet EVs. The EV pellet was gently resuspended in

sterile PBS before centrifuging again at 200,000 x g for 60 min. Another method used to isolate

EVs was the Invitrogen Total Exosome Isolation kit following the manufacturer's protocol. The

Invitrogen reagent was added to the conditioned media at a volume of 0.5 x the total amount of

conditioned media and left to incubate overnight at 4°C. Afterwards, the mixtures were spun

down to pellet EVs at 10,000 x g for 1 hour at 4°C. Two different solvents can be used for the C-

CP exosome isolation method: glycerol or acetonitrile (ACN). Because ACN can react with the

polymethyl methacrylate (PMMA) cuvettes of the Malvern zetasizer, the solvent glycerol was used for size characterization. The protocol for use of the C-CP fiber spin down tips are as follows: 100 µL of conditioned media was directly added to the fiber spin down tip reservoir along with 100 µL of the loading solution (2M ammonium sulfate in PBS) and mixed before spinning at 300 x g for 3 minutes. Once the EVs were loaded onto the fiber, proteins were eluted by adding 200 µL of the protein elution solution (1M ammonium sulfate and 25% glycerol or ACN in PBS) and spun down for 300 x g for 3 minutes. A clean 1.5 ml microcentrifuge tube was added to the bottom of the C-CP tip and EVs were collected by adding 200 µL of the exosome isolation solution (50% glycerol or ACN in PBS) and spun down at 300 x g for 3 minutes. For EVs harvested using glycerol as the solvent, they were either stored at -80°C or the solvent was removed using 100 kDa Amicon™ Ultra Centrifuge tubes (Sigma). For EVs harvested using ACN as the solvent, ACN was immediately off-gassed overnight at 4°C or under a low vacuum at 4°C for at least 1-3 hours. Samples of EVs harvested with both solvents were used for the following assays: Bradford reagent assay for protein quantification, enzyme-linked immunosorbent assay (ELISA) for exosome marker, and RNA isolation. EVs were stored for a maximum of 1 week after conditioned media collection at 4°C.
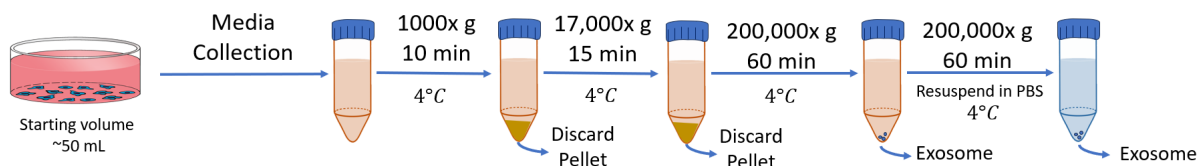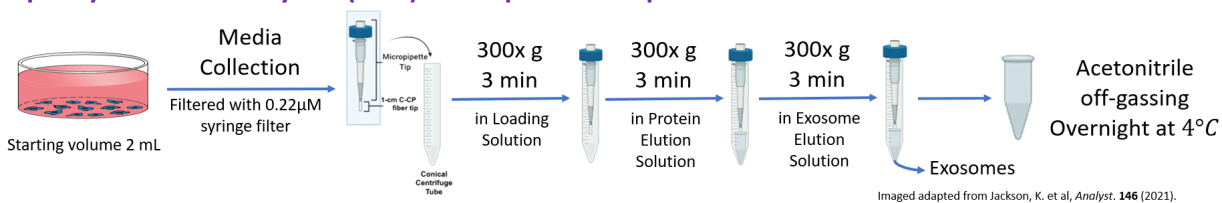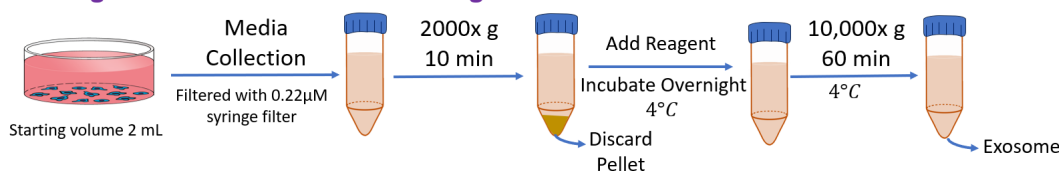
Figure 5.3 Graphic depiction of the different methods used to harvest EVs. Parts of image adapted from Jackson et al. *Analyst.* 2021 [66]. Ultracentrifugation protocol adapted from Huang et al. *J. Pers. Med*. 2022 [135].

Size Characterization

Once isolated, dynamic light scattering (DLS) via a Malvern Zetasizer Nano ZS (Malvern Panalytical Ltd, Malvern, UK) was used for size characterization efforts. Only EVs isolated with glycerol as the solvent were used to characterize size as acetonitrile is incompatible with PMMA cuvettes. Glycerol was not removed from the EV preps and was diluted 1:1 with sterile DNase/RNase free water. To prevent the formation of aggregates the diluted EV preps were sonicated for 5 minutes immediately before adding the EV solutions to the cuvettes.

Protein Quantification

The protein concentration in the EV solutions were measured via the commercially available Pierce Bradford Reagent assay (Fisher) following the manufacturer's microplate procedure. A standard curve of albumin was prepared at the time of each assay. In the appropriate well of a clear microplate, 150 µL of either standard or EV samples were pipetted into the

microplate along with 150 µL of room temperature Bradford reagent. The solutions in the microplate were mixed for 30 secs via a VWR mini shaker and incubated for 10 minutes at room temperature. The absorbance was measured at 595 nm using a BioTek Synergy 4 plate reader (Agilent Technologies, Santa Clara, CA, USA). The protein concentration of the EV samples was measured using the standard curve determined by the average blanked absorbance of albumin standard vs its concentration.

Exosome Marker Quantification

The Stamatikos lab at Clemson University used a western blot to confirm expression of exosome marker CD81 from EVs harvested using ultracentrifugation as described in [135]. A commercially available Exo-ELISA kit (System BioSciences, Palo Alto, CA, USA), following the manufacturer's protocol was used to detect exosome marker CD63 in EVs harvested using either the C-CP method or Invitrogen kit from MYP3 conditioned media. Samples or standards were added to the ELISA plate, covered with the sealing film, and incubated overnight at 37°C. After incubation, the plate was washed 3X for 5 minutes using the 1X wash buffer with shaking. Immediately after washing, the plate was incubated with 1:100 primary CD63 goat antibody for 1 hour with shaking at room temperature. The plate was again washed and then incubated with 1:5000 anti-goat HRP secondary antibody for 1 hour with shaking at room temperature. After which, the plate was washed and then incubated with the super-sensitive TMB ELISA substrate for 45 minutes at room temperature with shaking. A stop buffer was added to each well and immediately measured at 450 nm using a BioTek Synergy 4 plate reader. The RayBiotech kit quantified the presence of CD63 for EV preps harvested with the C-CP from BDeC conditioned media, following the manufacturer's protocol. Samples and standard were added to appropriate

well and incubated at room temperature with gentle shaking for 2.5 hours. The plate was washed 4 times using the inversion method by blotting the plate against a Kim wipe on top of clean paper towels. Next, 1:80 fold diluted biotinylated primary CD63 antibody was added to each well and incubated for 1 hour at room temperature with gentle shaking. The plate was again washed and then incubated with 1:900 horse radish peroxidase conjugated streptavidin for 45 minutes with gentle shaking at room temperature. The plate was washed again and then the TMB One-Step Substrate Reagent was added to the plate and incubated for 30 minutes in the dark with gentle shaking. Afterwards, a stop solution was added to each well and the plate was immediately read at 450 nm using a BioTek Synergy 4 plate reader.

RNA Isolation and Library Prep

RNA of EV samples obtained from the conditioned media of BDeC cells was extracted using a commercially available ZYMO Quick-*cf*RNA Serum and Plasma kit (ZYMO Research, Irvine, CA, USA) following the manufacturer's protocol. An equal volume of digestion buffer was added to the EV preps along with 10 µL of Proteinase K per 200 µL of sample. Sample mixtures were vortexed and incubated at 37°C degrees for two hours. After digestion, 1 volume of a binding buffer was added, and the samples were thoroughly mixed by vortexing. Then 1.5 volume of 100% isopropanol was added to the mixture and vortexed. The samples were passed through the Spin-Away™ Filter and immediately afterwards the RNA Prep buffer was passed through the filter. RNA was recovered by adding the RNA Recovery Buffer to the Spin-Away™ Filter and centrifuged at 12,000 x g for 30 secs, collecting the flow through in a clean RNase free microcentrifuge tube. To the recovered RNA, 100% of ethanol was added to the flow through, mixed via pipetting, and transferred to the Zymo-Spin™ IC Column. Afterwards the RNA Prep

Buffer was passed through the column via centrifugation at 12,000 x g for 30 secs. Then the RNA was washed 2X using the RNA Wash Buffer and centrifugation at 12,000 x g for 30 secs and then 2 minutes. RNA was eluted with 15 µl of DNase/RNase-free water. A nanodrop (Thermo Fisher) was used to quantify the amount of RNA captured from EVs. Afterwards, the EV RNA was prepared for sequencing using the Oxford Nanopore direct RNA sequencing kit (SQK-RNA002). To improve the number of reads obtained from the EV RNA, a poly-A-tail was added following NEB poly(A) tailing of RNA using E. coli poly(A) polymerase kit (New England Biolabs, Ipswich, MA) and was either stored at -80°C or used immediately in the library prep. 50 ng of the A-tailed EV RNA was used for the Oxford Nanopore library prep, following the manufacturer's protocol. Once prepared, the library was loaded into the minION flow cell (FLO-MIN106D) via the flow cell priming kit. The sequencing experiment ran for 48 to 72 hours and stopped when the read quality or read speed declined. Every 24 hours, the flow cell refueled with the flush buffer, following the manufacturer's protocol. Detailed experimental protocols are in Appendix A.

RNAseq Data Analysis

Reads were aligned and processed using the Clemson Palmetto Cluster and scripts for analysis are available in Appendix B. The quality of the reads was determined using fastQC. Reads were trimmed and filtered using fastp and quality post trim was determined using fastQC. Different software aligner tools were used to analyze the RNAseq data: STAR, EPI2ME and GMAP/GSNAP. Indexes were compiled using GENCODE primary human reference (GRCh38.p13) and reads were aligned to the index using the respective program. Prominent features were found using featureCounts. Further quality of the data was determined using

RStudio. To visualize the variation in the expression of features between the samples, a relative log expression plot was generated. In addition, a Q-Q (quantile-quantile) residuals plot was generated to assess whether the data followed a normal distribution. A principal component analysis (PCA) plot was generated. Differential gene expressions were calculated using DESeq2 in RStudio using the likelihood ratio test (LRT). The results of differential gene expression were represented using an enhanced volcano plot with a $\lvert \text{Log}_2\text{FC} \rvert > 0.5$ and p values less than 0.05. A list of reads with a $\lvert \text{Log}_2\text{FC} \rvert > 0.6$ was obtained and further researched to determine changes in the gene expression of the data.

Statistical Analysis

For experiments with replicates data are presented as the mean ± standard error of the mean (SEM). One-way ANOVA was used for single timepoint experiments with post-hoc Tukey test. All statistical analyses for non-RNAseq data were performed using GraphPad Prism 5 software for Windows (San Diego, CA) and p values less than 0.05 were considered statistically significant. Analysis of RNAseq data was performed using RStudio and DESeq2.

5.3 Results

Comparison of EV isolation methods

Though ultracentrifugation is a well-established and researched method for EV isolation; this method proved to be inconsistent. Specifically, only a single EV pellet was obtained after multiple attempts (**Figure 5.4A**). Additionally, this method required approximately 50 mL of media which exceeded the volume of a typical experiment. In contrast, both the Invitrogen kit and C-CP EV isolation methods required about 2 mL of media and could be scaled up and down

to match typical culture volumes. Nevertheless, this one pellet obtained was found to be CD81 positive via a western blot (**Figure 5.4B**). The size distribution from EV preps harvested via the Invitrogen kit size were within exosome range (30 – 200 nm)[57] (**Figure 5.5A**). Furthermore, the Invitrogen method also results in an EV prep that was positive for exosome marker CD63. Pressure induced an increase in CD63 expression when compared to the control (**Figure 5.5B**). Also, EVs harvested from both rat and human urothelial cell conditioned media via C-CP method were within exosome size range (**Figure 5.6**). EVs harvested from MYP3 cell conditioned media via C-CP method were also CD63 positive. In addition, a trend of higher CD63 secretion was observed in both the pressure and hypoxic groups (**Figure 5.7**). EVs obtained from the conditioned media of BDeC cells were positive for exosome marker CD63 (**Figure 5.8**). Although the Invitrogen kit was scalable to the size of our sample, use of the kit was too expensive. The C-CP method was chosen for additional experiments as it was cheaper, required low medium volume, and proved to produce EVs that were characteristic of exosomes.
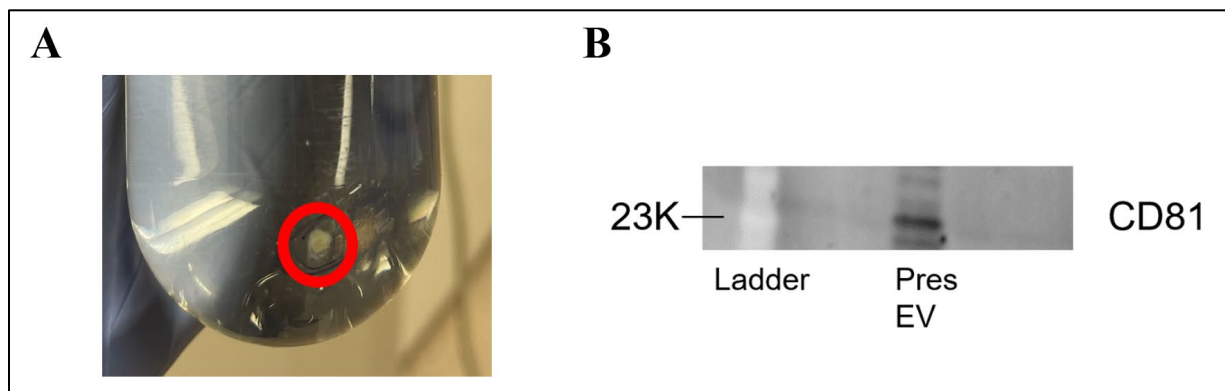
Figure 5.4 Image of EV pellet from pressure group (A) and western blot for exosome marker CD81 (B). The red circle encloses an EV pellet obtained from conditioned media of rat MYP3 cells exposed to pressure. The pellet was positive for exosome marker CD81.

A

B
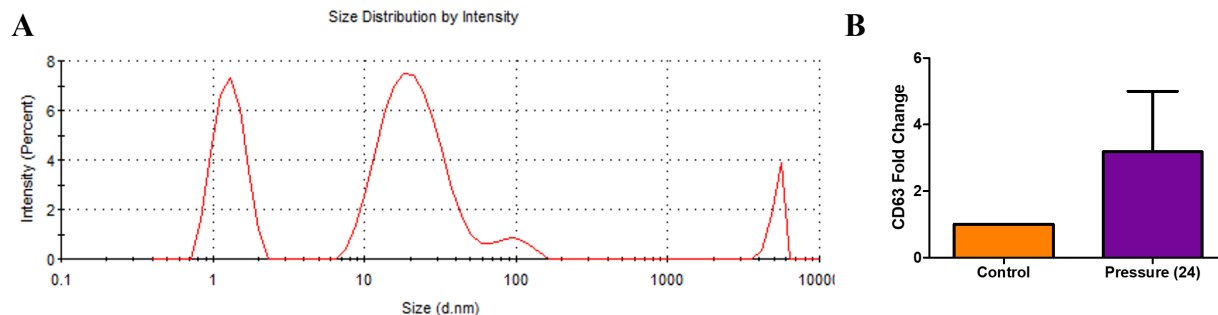
Figure 5.5 Size (A) and CD63 expression of exosomes harvested using the Invitrogen Kit from MYP3 conditioned media (B). (A) Representative image of DLS measurements. In general, the two most prominent peaks were less than 200 nm and within exosome size range. There was a 3rd peak that was greater than 200 nm; however, this peak was generated by the EVs pelleting and creating aggregates. (B) CD63 expression was greater in EVs harvested under pressure conditions. Pressure increased CD63 expression. N=2.

(A) 24 hr Atmospheric Pressure (BDeC)

(B) 24 hr High Pressure (BDeC)

(C) 24 hr Atmospheric Pressure (MYP3)

(D) 24 hr High Pressure (MYP3)
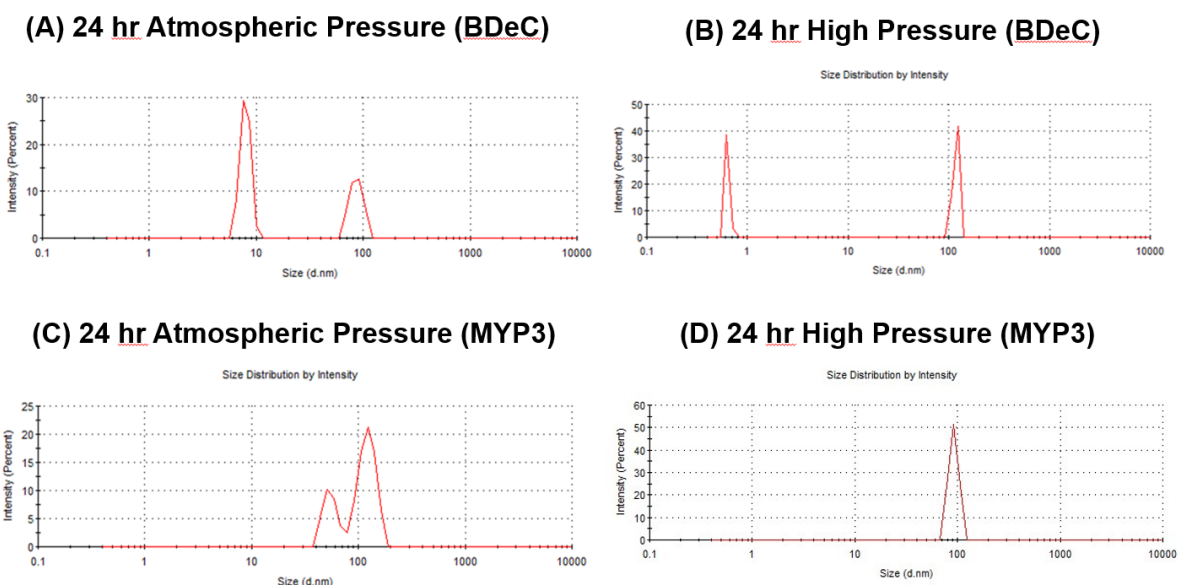
Figure 5.6 DLS size distribution of exosomes harvested using C-CP fiber spin-down tips. (A-B) Representative images from DLS measurements. Human (BDeCs) EVs from the control and high pressure groups were less than 200 nm and within exosome size range. (C-D) Rat (MYP3) EVs size range was also less than 200 nm and within exosome size range.

RNAseq Reads and Aligner Comparison

For RNAseq analysis, EV RNA obtained from BDeC conditioned media under 72 hours of exposure was used. Biological replicates were used for each condition (atmospheric (control) and high pressure). The number of reads obtained differed between the control and pressure

64

group, with pressure resulting in more reads (Appendix C **Table C.1**). In addition, the quality of the reads from the runs were in an acceptable range except for the first replicate of the control group (Appendix C **Figure C.1**).

EVs preps from human BDeC cells were aligned using three different software aligner tools: STAR, EPI2ME, and GMAP/GSNAP. Initially, STAR was chosen as an aligner as it incorporates annotations when building the index, which has been considered helpful in improving the accuracy of alignment, especially when the end goal is to determine non-coding RNAs present in the reads. However, STAR was eliminated as a possible alignment tool as STAR is intended for use with shorter reads obtained from sequencing tools like Illumina. ONT produces long single strand reads which resulted in errors relating to the length of reads. Another contender was the EPI2ME software provided by ONT; however, the EPI2ME software was not able to provide further analysis (differential expression) of the aligned reads. Additionally, the EPI2ME software provided its own reference index; therefore, obtaining an annotation file that matched the format of the reference index proved difficult when counting the features of the aligned data. Therefore, for further analysis, GSNAP was used for ease of index creation and alignment.
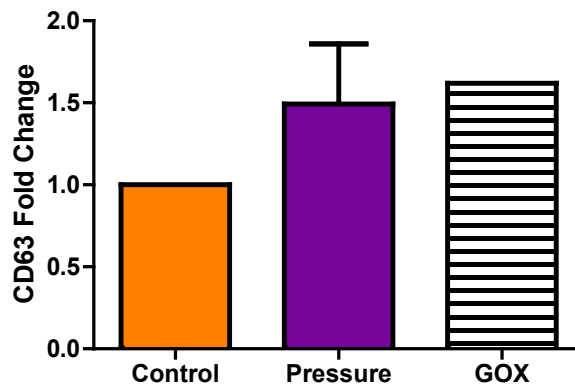
Figure 5.7 CD63 Expression of exosomes harvested from MYP3 using C-CP method. Higher CD63 expression was noted in EVs harvested from rat urothelial cells exposed to elevated pressure cycles for 48 hours and hypoxia for 6 hours. N=3 for pressure group. N=1 for GOX group.
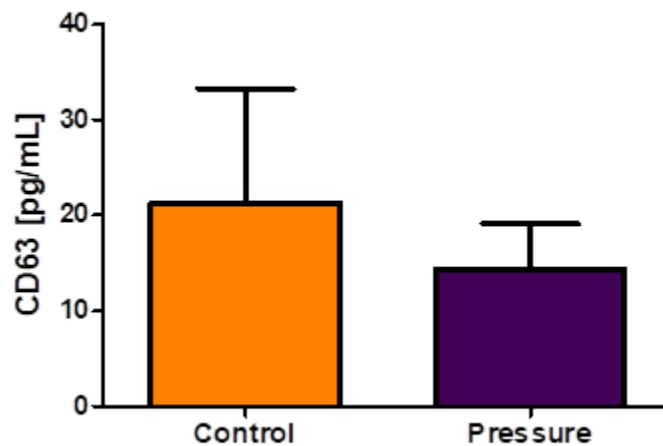
Figure 5.8 CD63 Expression of exosomes harvested from BDeC Conditioned media using C-CP method. CD63 was present in the EV preps from both control and conditioned media. N=2.

Several novel transcripts upregulated in pressure group

To assess the normality of the data, the expression levels and Q-Q residuals were visually represented. The expression levels from the different BDeC groups were relatively equal (**Figure 5.9**). In addition, the Q-Q residuals followed the horizontal line with the tails sloping down-ward or up-ward, indicating some gene expressions that may differ between the two groups (**Figure 5.10**). A principal component analysis (PCA) plot shows the similarities between different groups of a data set. The PCA plot generated from our data demonstrates that there is not much similarity between the control and pressure groups. Additionally, replicates within their respective groups were not closely related to each other (**Figure 5.11**). Due to the low expression level and low read quality of the first replicate from the control group, this set was removed from further analysis.

No genes were found to be differentially expressed in the data (**Figure 5.12**). Thus, the Log_2FC of genes greater than 0.6 was investigated to capture slightly meaningful changes in gene expression of the data. Genes from exosomes harvested under pressure were correlated with

genes related to cancer and EMT (**Table 5.1**). Long intergenic non-coding RNA 01391 (LINC01391), cell adhesion molecule 2 (CADM2), diacylglycerol kinase alpha (DGKA), SEL1L adaptor subunit of ERAD E3 ubiquitin ligase (SEL1L) and straw berry notch homolog 2 (SBNO2) were upregulated in the pressure group. Whereas, phosphatidylinositol-4-phosphate 5-kinase type 1 gamma (PIP5K1C), and 5'-nucleotidase domain containing 3 (NT5DC3) were upregulated in the control group. Three novel lncRNA transcripts were upregulated in the pressure group (**Table 5.2**). A complete list of genes can be found in appendix C2.
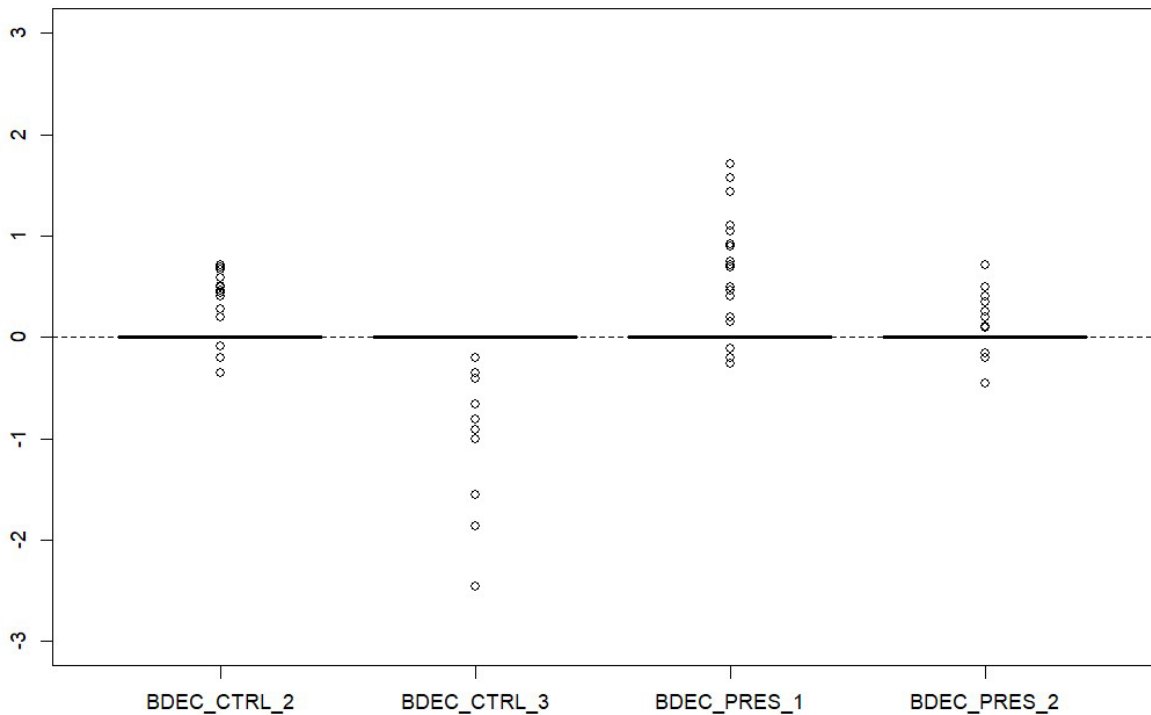
Figure 5.9 Relative log expression plot. The dark line represents the mean expression level for each group. Expression levels of the different groups were relatively similar as they aligned with the dotted line.
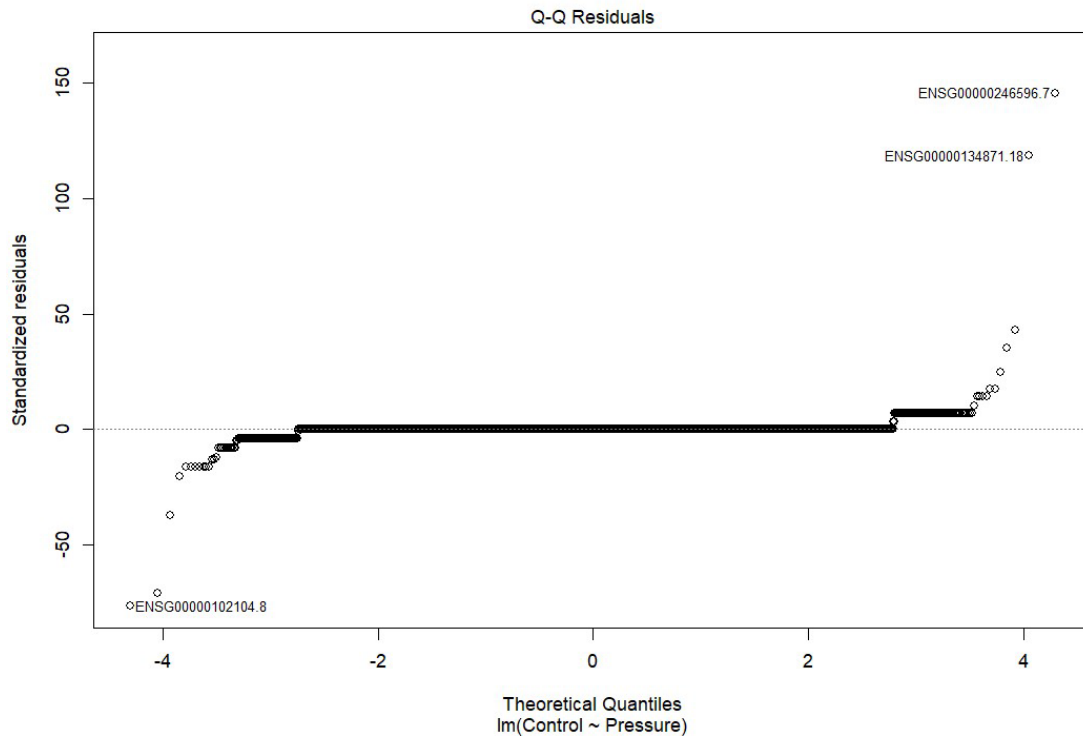
Figure 5.10 Quantile-Quantile plot of residuals. The Q-Q residuals followed the horizontal line closely indicating the data follow a normal trend.
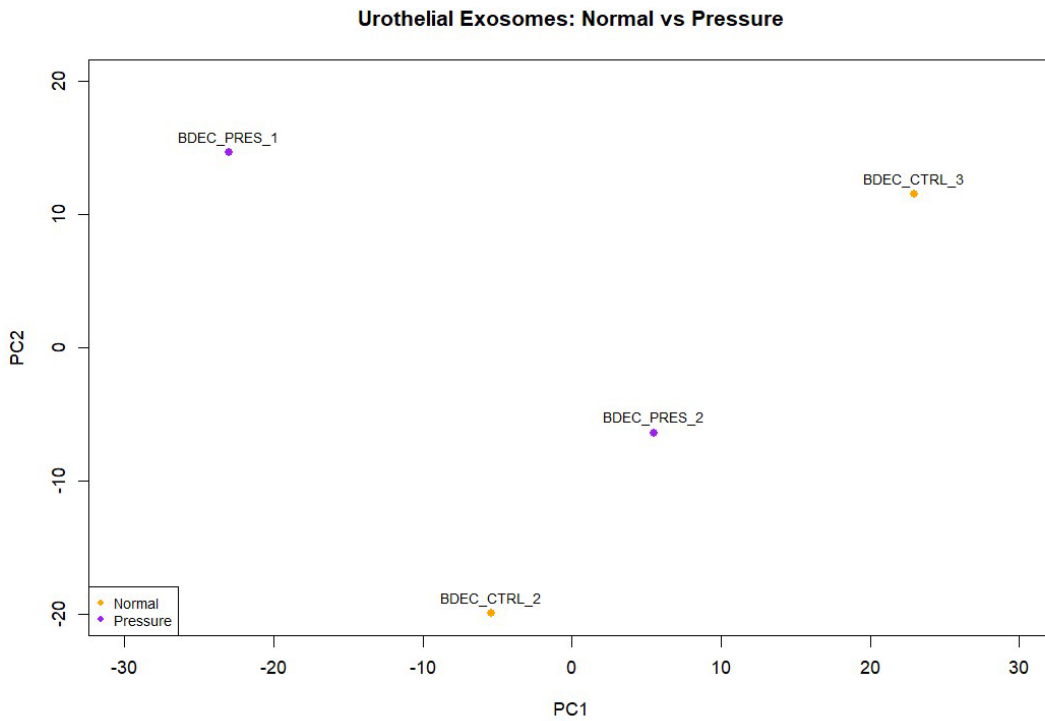
Figure 5.11 PCA plot of the different groups. There was little similarity between the different groups. The principal components of each replicate were also dissimilar.
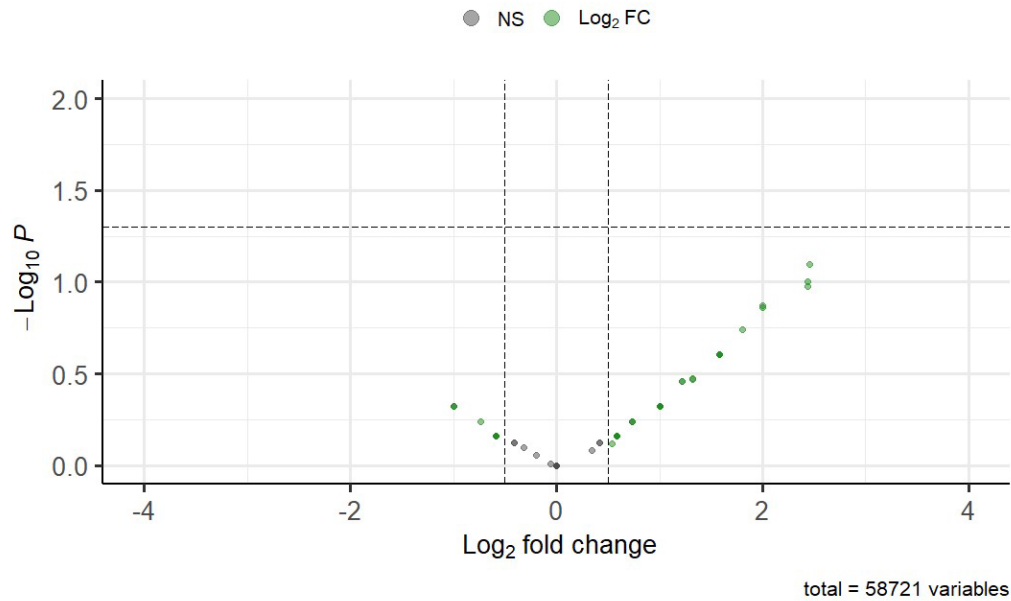
Figure 5.12 Volcano plot of differential gene expression analysis. Genes within the vertical dotted lines are not significant. Genes outside the vertical dotted lines have some changes in expression level between control and high pressure. Genes above the horizontal dotted line would be significantly differentially expressed. No genes were differentially expressed from the data.

Table 5.1 EMT and Cancer Related Expression from human bladder exosome

Gene	Log₂FC	Function	REF
CADM2	1.0	Downregulation related to invasion and migration in tumors.	Yu Wang et al. 2023
LINC01391	2.0	Associated with gastric cancer. Over expression prevent cancer cell migration.	Qian et al. 2020
DGKA	0.74	Involved in promoting cancer cell metastasis.	Fu L. et al. 2022
SEL1L	1.0	Expressed in various cancer tissues.	Mellai et al. 2020
SBNO2	1.6	Expressed in human glioblastoma. Involved in inflammation in the central nervous system.	Coppieters et al. 2023 and Glia et al. 2015
PIP5K1C	-1.0	involved in focal adhesion formation and disassembly. Suppression inhibits tumor growth (breast cancer).	Jonas et al. 2023
NT5DC3	-1.0	Reduced expression in pancreatic cancer.	T. Yatsuoka et al. 2004

Table 5.2 List of novel transcripts upregulated in the pressure group

Ensembl ID	Type	Log₂FC
ENSG00000236676	lncRNA	2.4
ENSG00000243243	lncRNA	1.8
ENSG00000272305	lncRNA	1.2

69

5.4 Discussion

Due to difficulties with obtaining an EV pellet with ultracentrifugation, different methods for EV isolation were used. Although ultracentrifugation resulted in one CD81 pellet from the pressure group, this method was scrapped due to the large volume of media required and the inconsistency of results. EVs from both the Invitrogen kit and the C-CP method captured vesicles that were less than 200 nm and within size range. The Invitrogen Total Exosome Isolation kit was scalable and easily allowed for isolation of EVs from conditioned media. However, the kit was expensive and still required a centrifuge with refrigeration, and could reach a speed of 10,000 x g. The C-CP method allowed for easy, and cheap isolation of exosomes using a benchtop centrifuge at low speeds (300 x g) for shorter time periods. Additionally, the solvent versatility allowed for easy storage of EVs at -80°C with cryoprotectant glycerol or immediate characterization and further processing with solvent ACN.

Pressure and hypoxia were able to lead to changes in exosome secretion in MYP3 cells. A higher fold expression of CD63 was observed in the pressure group of EVs harvested using the Invitrogen kit. Similarly, higher CD63 expression was demonstrated from EVs harvested from conditioned media from rat urothelial cells using the C-CP method exposed to pressure (48 hours) and hypoxia (6 hours). For EVs harvested from both control and pressure BDeC conditioned media, the particle sizes were below 200 nm and positive for CD63, indicating the EVs could be characterized as exosomes.

No genes were differentially expressed between the group control and pressure group of EVs from BDeC conditioned media (p-value < 0.05). The lack of differential gene expression may be due to the short duration of exposure of urothelial cells to high-pressure as compared to *in vivo* conditions, where urothelial cells are exposed to elevated pressures for longer periods of

time. Thus, trends in the data were explored through Log$_2$FC instead. Although this method does not show significance in the data, using the Log$_2$FC can highlight valuable changes in the gene expression between high pressure and control. The standard Log$_2$FC is typically a value of 0.5; however, a value of 0.6 for this data was used.[136,137] For this study, a slightly higher Log$_2$FC was chosen to look for potential trends in the data. Several genes that met this threshold correlated with cancer cell EMT and tumorigenesis (**Table 5.1**). Three genes (DKGA, SEL1L, and SBNO2) were upregulated in the pressure group, whose upregulation has been found to promote EMT and tumorigenesis. DGKA has been linked to promotion of non-small cell lung cancer EMT and metastasis.[138] Additionally, the expression of DGKA was elevated in metastatic lesions of lung cancer. In that same *in vitro* study, artificial overexpression of DGKA promoted EMT and its knockdown inhibited this invasive phenotype.[139] Expression of SEL1L was correlated with cell proliferation and tumor progression in gliomas.[140] SBNO2 expression was increased in the tissues of glioblastomas.[141]In addition, SBNO2 is hypothesized to play a role in inflammation, as treatment with hyper-IL-6 upregulated SBNO2 mRNA.[142]

Inversely, the downregulation of PIP5K1C and upregulation of LINC01391 and CADM2 has been linked to suppressing EMT and tumorigenesis. PIP5K1C expression was downregulated in the pressure group. The suppression of PIP5K1C has been linked with inhibition of tumor growth in breast cancer.[143] Conversely, LINC01391 and CADM2 was upregulated in the pressure group. LINC01391 is a non-coding RNA that expression has been found to be restrained in gastric cancer.[144] The overexpression of LINC01391 has been linked to delaying of tumor growth progression by suppressing cell proliferation, migration, and invasion.[144,145] Similarly CADM2 has been associated with tumor suppression.[146] In human glioma cells, inducing the overexpression of CADM2 inhibited proliferation and altered genes related to EMT, including a

slight upregulation in epithelial marker ECAD.[147] The highest Log_2FC was seen with the novel lncRNAs. These three lncRNAs could be potential biomarkers of elevated bladder pressure.

Located in appendix C, **Figure C.2** shows the reads per gene for the genes listed in **Table 5.1.** Also located in appendix C, **Figure C.3** displays the reads per novel transcripts (lncRNAs) in **Table 5.2**. From these figures, further examination of the trends in Log_2FC can be examined. LINC01391 shows a clear increase of the gene in pressure compared to the control. For the other genes in **Table 5.1**, it appears as if the trend was only prevalent in one of the pressure replicates. This could be due to activation occurring in only one of the replicates and not the other.

There seems to be conflicting signaling within the exosomal cargo because of pressure. Upregulation of genes associated with EMT correlates with previous research from our lab that demonstrated the same pressure cycles led to EMT gene expression changes in urothelial cells.[18] As this study is one of the first to investigate the impacts of elevated pressure *in vitro* on urothelial cells, this may be a novel result. However, a limitation of this study is the low number of replicates. Nevertheless, the data from this study provide evidence that pressure does indeed lead to changes in exosomal cargo and provides insight on the possible genes associated with pressure fluctuations.

In summary, these results indicate that high pressure cycling, and hypoxia can stimulate the secretion of exosomes from urothelial cells as indicated by increased CD63 in MYP3 cells. Furthermore, exosomes released from human urothelial BDeC cells exposed to elevated pressure cycling led to changes in the exosomal cargo, which can aid in the development of a non-invasive tool for BOO detection. Although these genes were not differentially expressed, the trends in genes expressed due to elevated pressure should be further investigated as a urinary exosome marker for BOO.

CHAPTER SIX

Conclusions and Future Directions

One aspect of this project was to develop an enzyme system for creating *in vitro* hypoxia without the use of complex devices or additional instruments. Thus, the ability of GOX and CAT to lower oxygen tension in media using normal cell culture equipment was characterized. The two-enzyme system successfully stabilized HIF-1α without significantly lowering cell viability. Extracellular nitric oxide levels increased, demonstrating a hypoxic response in urothelial cells in response to enzyme-induced hypoxia. Enzyme-induced hypoxia led to an appropriate cell response and was comparable to different techniques for creating a hypoxic environment *in vitro*. Further characterization of the enzyme system should include expanding the time periods for which oxygen tension was measured and creating different oxygen tension profiles based upon enzyme concentration. Another avenue for future work should investigate alternative oxygen consuming enzymes that do not produce cytotoxic byproducts, such as laccase or bilirubin oxidase.

The urothelium experiences hypoxia during BOO; however, the urothelial cellular response and role in initiation of inflammation due to hypoxia has not been established. Based upon the data from Aim 1 (chapter 3), a glucose oxidase concentration of 0.5µg/ml was used to create an *in vit*ro hypoxic environment and investigate the role of hypoxia in BOO-induced inflammation. The results from the study demonstrated that UCs exposed to hypoxia led to inflammation in a time-dependent manner. Furthermore, short time periods of hypoxic exposure (2 hours) didn't change extracellular ATP levels or activate the NLRP3 inflammasome. However, a longer insult of hypoxia (6 hours) did initiate inflammation through the ROS/TXNIP/NLRP3 pathway. In addition, unlike pressure cycling, repeated instances of

intermittent hypoxia didn't promote EMT. Further work should include combining different stimuli with hypoxia. Specifically, combine pressure and hypoxia to observe the impacts on BOO-induced inflammation or epithelial-mesenchymal transition (EMT).

A non-invasive diagnostic tool for BOO is necessary as patients may not seek treatment for LUTS until they worsen, and current methods are invasive. In addition, research has shown that the experience of cells is reflected in the extracellular vesicles they release. Thus, the mechanical (pressure) and chemical (hypoxia) changes experienced by urothelial cells due to BOO might be expressed in urinary exosomes. We have shown that hypoxia and pressure can stimulate EV release in rat urothelial cells. In addition, pressure induced gene expression changes in exosomes released from human urothelial cells, which was found through RNAseq analysis. The gene expression changes were related to EMT and tumorigenesis. In addition, three novel lncRNAs were upregulated in EVs exposed to elevated pressure cycling. These results support the hypothesis that pressure changes experienced by the bladder could be reflected in urinary exosomes. However, one limitation of this work is the low number of replicates for each group. Therefore, the number of RNAseq runs for each group should be increased. In addition, future work should include characterizing EV cargo under various degrees of elevated pressure. EV cargo should be investigated under hypoxic conditions and under a combination of hypoxia and pressure. Furthering the knowledge of pressure and hypoxia can lead to changes in EV cargo can aid in not only a non-invasive method to diagnose BOO but an early BOO diagnostic.

APPENDICES

Appendix A

RNAseq Library Preparation

A-1 Poly(A) Tailing of RNA (NEB M0276)

1. The following components were added to a nuclease free tube
    a. Max amount of exosomal RNA with volume adjusted to 15 μL in nuclease free water.
    b. 2 μL of 10x *E. coli* Poly(A) Polymerase Reaction Buffer
    c. 2 μL ATP (10 mM)
    d. 1 μL of *E. coli* Poly(A) Polymerase
2. Incubate reaction at 37°C for 30 minutes.
3. Stop the reaction by adding EDTA to a final concentration of 10mM or by freezing the sample at -80°C.

A-2 Library Prep Protocol (Direct RNA Sequencing Protocol SQK-RNA002)

1. Prepare the RNA in nuclease-free water with the following steps.
    a. Transfer 50 ng of poly(A)-tailed RNA to a nuclease free tube.
    b. Adjust the volume to 9 μL with nuclease-free water.
    c. Mix by flicking the tube and spin down briefly.

2. To prepare the RT adapter-ligated RNA, the following components were added to a nuclease free Eppendorf tube:
    a. 3 μL of NEBNext Quick Ligation Reaction Buffer
    b. 9 μL of the prepared RNA
    c. 0.5 μL of RNA CS (RCS), 110 nM
    d. 1 μL RT Adapter (RTA)
    e. 1.5 μL T4 DNA Ligase
3. Mix by pipette mixing.
4. Incubate the reaction for 10 min at room temp.
5. Prepare the reverse transcription master mix by adding the following reagents to a separate clean nuclease-free Eppendorf tube:
    a. 9 μL of Nuclease free water
    b. 2 μL of 10 mM dNTPs
    c. 8 μL of 5x First-Strand Buffer
    d. 4 μL of 0.1 M DTT
6. Add the master mix to the RT adapter-ligated RNA and mix by pipetting.
7. Add 2 μl of SuperScript III reverse transcriptase to the reaction and mix by pipetting.
8. Incubate the tube at 50°C for 50 min, then 70°C for 10 min, and bring the sample to 4°C by placing in fridge before proceeding to the next step.
9. Transfer the sample to a clean nuclease free tube.
10. Resuspend the stock of Agencourt RNAClean XP beads by vortexing.

11. Add 72 µL of resuspended beads to the reverse transcription reaction and mix by pipetting.
12. Incubate in the Hula mixer or shaker for 5 min at room temperature.
13. Prepare 200 µL of fresh 70% ethanol in nuclease-free water (140 µL ethanol, 60 µL water).
14. Spin down the sample and pellet on a magnet. Keep the tube on the magnet, and pipette off the supernatant without disturbing the pellet.
15. Keep the tube on the magnet and wash the beads with 150 µL of freshly prepared 70% ethanol without disturbing the pellet.
    a. Keeping the magnetic rack on the benchtop, rotate the bead-containing tube by 180°. Wait for the beads to migrate towards the magnet and form a pellet.
    b. Rotate the tube 180° again (back to the starting position) and wait for the beads to pellet on the magnet.
16. Carefully remove the ethanol using a pipette and discard.
17. Spin down the tube and place the tube back on the magnet. Pipette off any residual 70% ethanol.
18. Remove the tube from the magnetic rack and resuspend pellet in 20 µl nuclease-free water. Incubate for 5 minutes at room temperature.
19. Pellet the beads on a magnet until the eluate is clear and colorless.
20. Pipette 20 µL of eluate into a clean Eppendorf tube.
21. In the same tube, mix the reagents in the following order:
    a. 8 µL of NEBNext Quick Ligation Reaction Buffer
    b. 6 µL of RNA adapter (RMX)
    c. 3 µL of Nuclease-free water
    d. 4 µL of T4 DNA Ligase
22. Mix by pipetting.
23. Incubate the reaction for 10 min at room temperature.
24. Resuspend the stock of Agencourt RNAClean XP beads by vortexing.
25. Add 16 µL of resuspended RNAClean XP beads to the adapter ligation reaction and mix by pipetting.
26. Incubate on a Hula mixer for 5 min at room temp.
27. Spin down the sample and pellet on a magnet. Keep the tube on the magnet and pipette off supernatant.
28. Add 150 µL of the Wash Buffer (WSB) to the beads. Close the tube lid and resuspend the beads by flicking the tube. Return the tube to the magnetic rack, allow beads to pellet and pipette off the supernatant.
29. Repeat the previous step.
30. Remove the tube from the magnetic rack and resuspend the pellet in 21 µL Elution Buffer. Incubate for 10 min at room temp.
31. Pellet the beads on a magnet until the eluate is clear and colorless.
32. Remove and retain 21 µL of eluate into a clean Eppendorf tube.
33. Quantify 1 µL of adapted RNA using the nanodrop (recovery aim ~20 ng)

A-3 Priming and loading the SpotOn flow cell

1. Thaw the RNA running buffer (RRB), Flush Tether (FLT), and one tube of Flush Buffer (FB) at room temp.
2. Mix the RRB, FB, and FLT tubes thoroughly by vortexing each tube and spin down at room temp.
3. Prepare the flow cell priming mix by adding 30 μL of FLT directly to the tube of t FB, and mix by vortexing at room temp.
4. Connect the MinION device to the computer. Open the MinION device lid and slide the flow cell under the clip. Press down firmly to ensure correct contact.
5. Complete a flow cell check to assess the number of pores available before loading the library.
6. Slide the priming port cover clockwise to open the priming port.
7. After opening the priming port, check for a small air bubble under the cover with the following steps.
   1. Obtain a p1000 pipette and set it to 200 μL.
   2. Place the tip of the pipette into the priming port.
   3. To draw back a small volume, slowly increase the set volume until you see some liquid in the pipette tip. (This should happen around ~220-230 μL)
8. Load 800 μl of the priming mix into the flow cell via the priming port, avoiding the introduction of air bubbles. Wait 5 minutes.
9. Mix 17.5 μL of nuclease-free water with 20 μL of the prepared RNA library by gently pipette mixing.
10. In a new tube, prepare the library for loading by combining the following reagents:
    1. 37.5 μL of RNA Running Buffer (RRB)
    2. 37.5 μL of RNA library in nuclease-free water
11. Complete the flow cell priming with the following steps:
    1. Gently lift the SpotON sample port cover to make the SpotON sample port visible and accessible.
    2. Load 200 μL of the priming mix into the flow cell priming port (NOT the SpotON sample port), avoiding the introduction of air bubbles
12. Mix the prepared library gently by pipette mixing just prior to loading.
13. Add 75 μL of sample to the Flow Cell via the SpotON sample port in a dropwise fashion.
14. Gently replace the SpotON sample port cover, making sure the bung enters the SpotON port, close the priming port, and replace the MinION device lid.

A-4 Refueling of Flowcell

1. The tube of Flush Buffer (FB) designated for refueling was thawed and brought to room temperature.
2. Pause the experiment on the MinKnow software by clicking Pause.
3. Open the priming port, and check for a small bubble by drawing back a small volume.
   a. Set a P1000 pipette to 200 μL
   b. Insert the pipette tip into the priming port

     c. Slowly turn the wheel until you see a small volume entering the pipette tip or until the dial shows 220-230 µL.
4. Refuel the flow cell by loading 250 µL of the FB into the flow cell priming port without introducing any air bubbles.
5. Close the priming port and replace the MinION lid.
6. Unpause the experiment by clicking Resume on the MinKnow software.

Appendix B

Scripts Used for RNAseq Analysis

B-1 fastQC script

```
#!/bin/bash

#PBS -N fastqc
#PBS -l select=1:ncpus=16:mem=40gb
#PBS -l walltime=24:00:00
#PBS -j oe
#PBS -m abe

# load biocontainer

module load biocontainers
module load fastqc/0.12.1

## Program command line
mkdir -p /yourpath/1_fastQC

while read line; do
  echo "Running FastQC on sample ${line}";

  ${APP} fastqc -t 2 /yourpath/fastq_location/${line}.fastq.gz \
-o /yourpath/1_fastQC;

done < "/yourpath/filenames.txt"
```

B-2 fastp script

```
#!/bin/bash

#PBS -N fastp
#PBS -l select=1:ncpus=8:mem=40gb
#PBS -l walltime=24:00:00
#PBS -j oe
#PBS -m abe

#Variable for the Singularity shell for access to the FastQC program
APP="singularity exec \
-B /scratch/$USER/:/scratch1/$USER \
/zfs/gcl/software/gbf/CUCHG-GSL/rnaseq_tools_refbased.sif"

## Program command line
mkdir -p /scratch1/yourpath/2_fastp


  ${APP} fastp \
  -i  / yourpath/location_of_fastq_files/${line}.fastq.gz \
  -o /yourpath/2_fastp/${line}_trimmed.fastq.gz \
  -h /yourpath/2_fastp/${line}.html \
  -j /yourpath/2_fastp/${line}.json;

  ${APP} fastqc -t 2 /yourpath/2_fastp/${line}_trimmed.fastq.gz \
    -o /yourpath/2_fastp;
done < " /yourpath/filenames.txt"
```

B-3 MultiQC script

```
#!/bin/bash
#PBS -N multiQC
#PBS -l select=1:ncpus=8:mem=40gb
#PBS -l walltime=24:00:00
#PBS -j oe
#PBS -m abe

#Variable for the Singularity shell for access to the FastQC program

APP="singularity exec \
-B /scratch1/$USER/:/scratch1/$USER/zfs/gcl/software/gbf/CUCHG-GSL/rnaseq_tools_refbased.sif"

##Program command line

${APP} multiqc /yourpath/1_fastQC \
-o /yourpath/1_fastQC
```

B-4 MultiQC_post script

```
#!/bin/bash

#PBS -N multiQC_post
#PBS -l select=1:ncpus=8:mem=40gb
#PBS -l walltime=24:00:00
#PBS -j oe
#PBS -m abe

#Variable for the Singularity shell for access to the multiQC program
APP="singularity exec \
-B /scratch1/$USER/:/scratch1/$USER/zfs/gcl/software/gbf/CUCHG-GSL/rnaseq_tools_refbased.sif"

## Program command line
${APP} multiqc /yourpath/2_fastp
 -o /yourpath/2_fastp
```

B-5 Gmap script

```
#!/bin/bash

#PBS -N gsnapref
#PBS -l select=1:ncpus=16:mem=40gb:interconnect=10ge
#PBS -l walltime=72:00:00
#PBS -j oe
#PBS -m abe

#Variable for the Singularity shell for access to the gsnap program

APP="singularity exec \
-B /scratch1/$USER/:/scratch1/$USER/zfs/gcl/software/gbf/CUCHG-GSL/rnaseq_tools_refbased.sif"

## Program command line

${APP} gmap_build -D /yourpath/index -d name_of_index \
/your_path_to_reference/GRCh38.primary_assembly.genom
```

B-6 Gsnap script

```
#!/bin/bash

#PBS -N gsnap
#PBS -l select=1:ncpus=8:mem=40gb
#PBS -l walltime=24:00:00
#PBS -j oe
#PBS -m abe

#Variable for the Singularity shell for access to the gsnap program
APP="singularity exec \
-B /scratch1/$USER/:/scratch1/$USER /zfs/gcl/software/gbf/CUCHG-GSL/rnaseq_tools_refbased.sif"

## Program command line
mkdir -p /yourpath/3_gsnap

while read line; do
  echo "Running gsnap on sample ${line}";

  ${APP} gsnap \
  -D /your_patH_to_the_index \
  -d name_of_the_index \
  "/your_path_to_the_trimmed_fastqfiles /${line}_trimmed_nonrRNA.fastq" \
  -t 7 \
  -N 1 \
  -A sam \
  -o "/yourpath/3_gsnap/${line}.sam";

done < "/yourpath/filenames.txt"
```

B-7 Feature Counts script

```
#!/bin/bash

#PBS -N FeatureCounts
#PBS -l select=1:ncpus=16:mem=75gb
#PBS -l walltime=12:00:00
#PBS -j oe
#PBS -m abe

#Loading biocontainers to use featureCounts

module load biocontainers
module load subread/2.0.6

#Specify the output directory and make the output directory

output_dir= "/yourpath/4_featurecounts"
mkdir -p $output_dir


#Program command line with loop for each sample listed in the sample_filenames.txt


${APP} featureCounts -a /your_path_to_reference/gencode.v29.annotation.gtf \
    -Q 0 -d 50 \
    -o  /your_path/4_featurecounts/name_of_file.txt -T 15 -s 0 \
    $Readfilename
```

Supplementary RNAseq Data

Table C.1: Number of Reads generated from ONT RNAseq

	Control	Pressure
Average number of reads generated	272.6 k	728 k
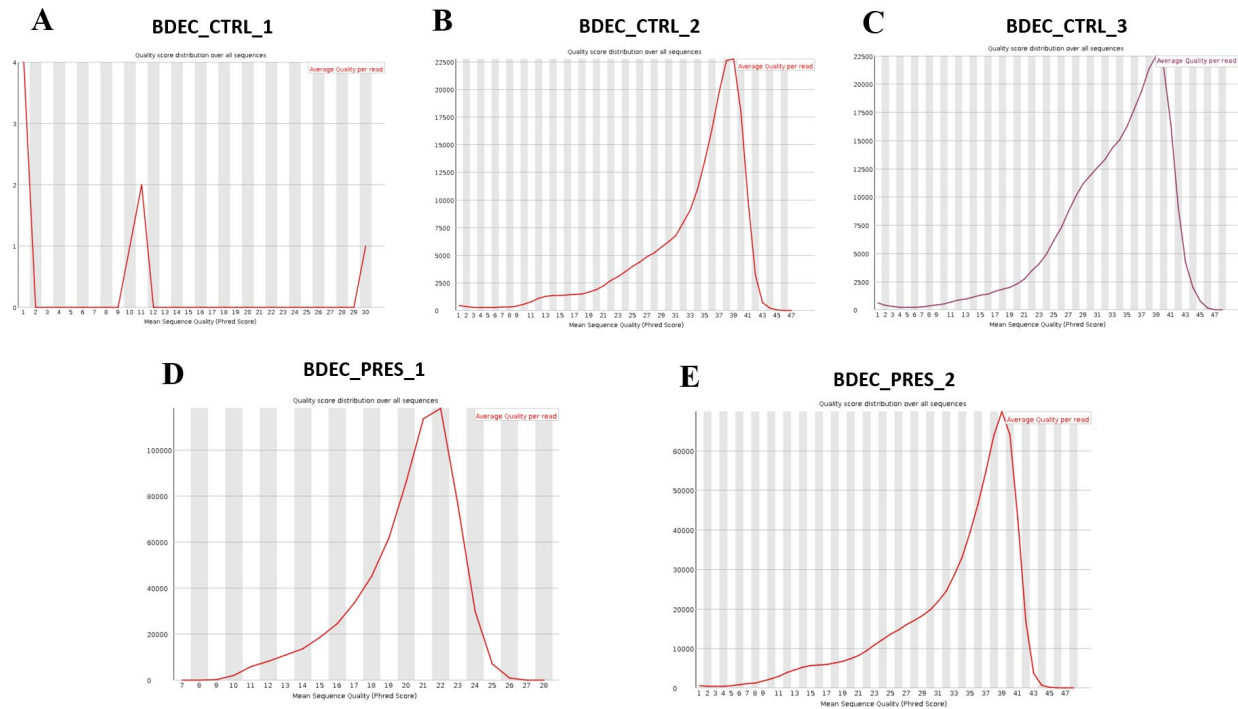
Figure C.1. Quality of reads before trimming. Quality of Reads from First Control run (A), Quality of Reads from Second Control Run (B), Quality of Reads from Third Control Run (C), Quality of Reads from First Pressure Run (D), Quality of Reads from Second Pressure Run (E). All reads used exosomal RNA harvested from conditioned supernatant of BDeC human urothelial cells exposed to pressure or atmospheric control for 72 hours.
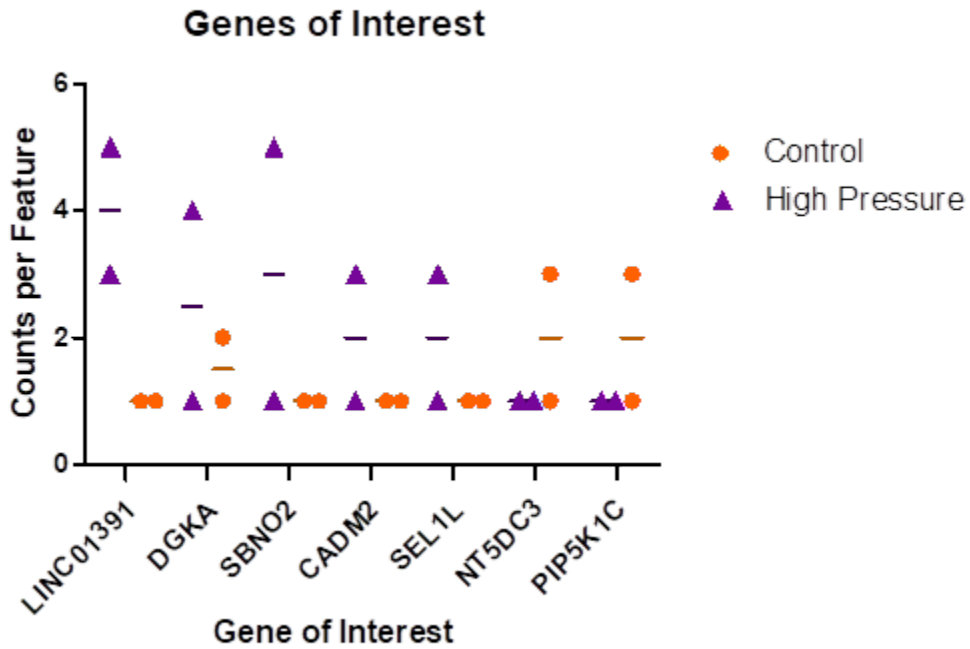
Figure C.2. Counts per Gene of Interest from the EVs Obtained from BDeC Conditioned Media. This shows the counts per gene of interest in the control and high-pressure groups. The graph demonstrates the similarity in the expression level of the gene between the control and high pressure. Solid line represents the average number of counts.
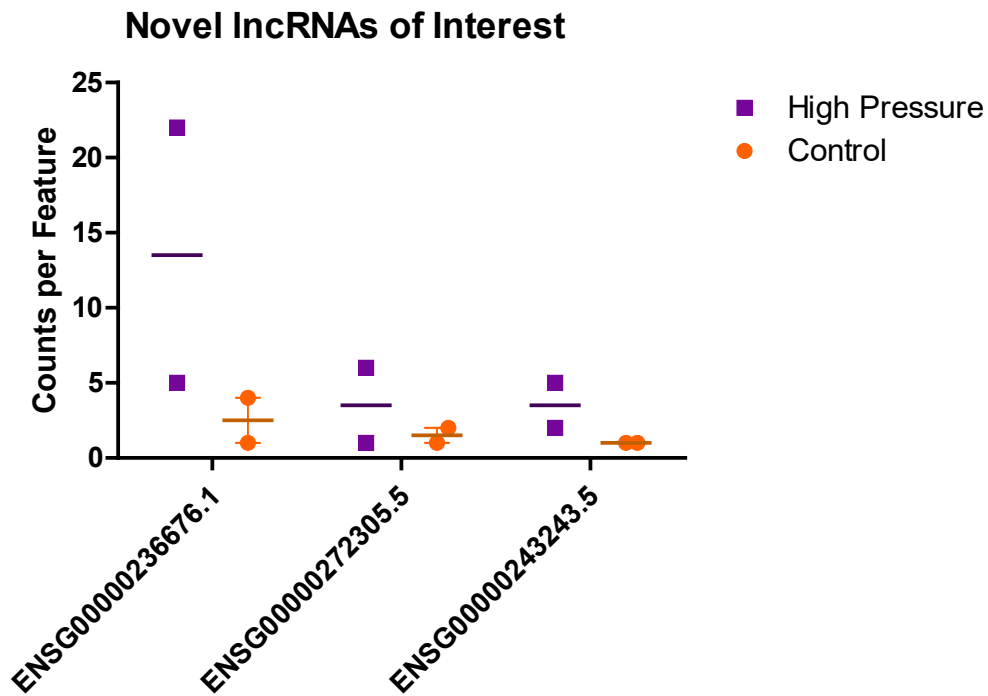
Figure C.3. Counts per Novel lncRNAs of Interest from the EVs Obtained from BDeC Conditioned Media. The graph demonstrates the similarity in the expression level of the lncRNAs between the control and high pressure. Solid line represents the average number of counts.

All Genes with │Log₂FC│ > 0.6

Table C.2: Reads with Log₂FC > 0.6

Gene	Log₂FoldChange
PPIE (peptidylprolyl isomerase E)	1.2
novel lncRNA ENSEMBL	2.4
PGBD5 (PiggyBac transposable element derived 5)	1.0
LINC01876	1.0
STK25 (Serine/threonine kinase 25)	1.0
novel lncRNA ENSEMBL	1.2
CADM2 (cell adhesion molecule 2)	1.0
LINC01391	2
IGSF10 (Immunoglobulin Superfamily Member 10)	1.0
LPP (LIM domain containing preferred translocation partner in lipoma)	1.0
C2H2 zinc finger protein pseudogene	-0.74
RHOBTB3 (Rho related BTB domain containing 3)	1.6
WDR36 (WD repeat domain 36)	1.3
NIPAL4 (NIPA like domain containing 4)	2.0
ABCF1 (ATP binding cassette subfamily F member 1)	1.0
PRIM2 (DNA primase subunit 2)	0.74
TTC4P (tetratricopeptide repeat domain 4 pseudogene 1)	1.6
lncRNA novel transcript ENSEMBL	1.8
WASHC2C (WASH complex subunit 2C)	1.0
WASHC2A (WASH complex subunit 2A)	2.5
ANKRD1 (ankyrin repeat domain 1)	1.0
INTS4 (integrator complex subunit 4)	1.0
DDX25 (DEAD-box helicase 25)	1.0
DGKA (diacylglycerol kinase alpha)	0.74
NT5DC3 (5'-nucleotidase domain containing 3)	-1.0
RPH3A (rapbhilin 3A)	-1.0
SEL1L (SEL1L adaptor subunit of ERAD E3 ubiquitin ligase)	1.0
GSG1L (Germ Cell-Specific Gene 1 Like)	0.74
RN7SL601P (RNA, 7SL, cytoplasmic 601, pseudogene)	1.6
ANKRD20A5P (ankyrin repeat domain 20 family member A5, pseudogene)	1.0
ATP8B1 (ATPase phospholipid transporting 8B1)	1.3
SBNO2 (strawberry notch homolog 2)	1.6
PIP5K1C (phosphatidylinositol-4-phosphate 5-kinase type 1 gamma)	-1.0
RS1 (retinoschisin 1)	2.4
COPS8P1 (COP9 Constitutive Photomorphogenic Homolog Subunit 8 Pseudogene)	1.0
ALG13 (Asparagine-linked glycosylation 13)	1.6

REFERENCES

1. Irwin, D. E., Kopp, Z. S., Agatep, B., Milsom, I. & Abrams, P. Worldwide prevalence estimates of lower urinary tract symptoms, overactive bladder, urinary incontinence and bladder outlet obstruction. *BJU Int.* **108**, 1132–1138 (2011).

2. Dmochowski, R. R. Bladder Outlet Obstruction: Etiology and Evaluation. *Rev. Urol.* **7**, S3–S13 (2005).

3. Abrams, P. *et al.* The standardisation of terminology in lower urinary tract function: report from the standardisation sub-committee of the International Continence Society. *Urology* **61**, 37–49 (2003).

4. Andersson, K.-E., Boedtkjer, D. B. & Forman, A. The link between vascular dysfunction, bladder ischemia, and aging bladder dysfunction. *Ther. Adv. Urol.* **9**, 11–27 (2017).

5. Yao, M. & Simoes, A. Urodynamic Testing and Interpretation. in *StatPearls* (StatPearls Publishing, Treasure Island (FL), 2024).

6. Lose, G. *et al.* Standardisation of urethral pressure measurement: Report from the standardisation sub-committee of the International Continence Society. *Neurourol. Urodyn.* **21**, 258–260 (2002).

7. Klausner, A. P., Galea, J. & Vapnek, J. M. Effect of catheter size on urodynamic assessment of bladder outlet obstruction. *Urology* **60**, 875–880 (2002).

8. Rosier, P. F. W. M. *et al.* International Continence Society Good Urodynamic Practices and Terms 2016: Urodynamics, uroflowmetry, cystometry, and pressure-flow study. *Neurourol. Urodyn.* **36**, 1243–1260 (2017).

9. Yiou, R. *et al.* Comprehensive evaluation of embarrassment and pain associated with invasive urodynamics. *Neurourol. Urodyn.* **34**, 156–160 (2015).

10. Abreu-Mendes, P., Silva, J. & Cruz, F. Pharmacology of the lower urinary tract: update on LUTS treatment. *Ther. Adv. Urol.* **12**, 1756287220922425 (2020).

11. Andersson, K.-E. & Gratzke, C. Pharmacology of α1-adrenoceptor antagonists in the lower urinary tract and central nervous system. *Nat. Clin. Pract. Urol.* **4**, 368–378 (2007).

12. Lepor, H. Alpha Blockers for the Treatment of Benign Prostatic Hyperplasia. *Rev. Urol.* **9**, 181–190 (2007).

13. Lerner, L. B. *et al.* Management of Lower Urinary Tract Symptoms Attributed to Benign Prostatic Hyperplasia: AUA GUIDELINE PART II—Surgical Evaluation and Treatment. *J. Urol.* **206**, 818–826 (2021).

14. Jin, L.-H. *et al.* Persistent detrusor overactivity in rats after relief of partial urethral obstruction. *Am. J. Physiol.-Regul. Integr. Comp. Physiol.* **301**, R896–R904 (2011).

15. Akshay, A. *et al.* De-obstruction of bladder outlet in humans reverses organ remodelling by normalizing the expression of key transcription factors. *BMC Urol.* **24**, 33 (2024).

16. Chai, T. C., Gemalmaz, H., Andersson, K. E., Tuttle, J. B. & Steers, W. D. Persistently increased voiding frequency despite relief of bladder outlet obstruction. *J. Urol.* **161**, 1689–1693 (1999).

17. Dunton, C. L., Purves, J. T., Hughes, F. M., Jin, H. & Nagatomi, J. Elevated hydrostatic pressure stimulates ATP release which mediates activation of the NLRP3 inflammasome via P2X4 in rat urothelial cells. *Int. Urol. Nephrol.* **50**, 1607–1617 (2018).

18. Dunton, C. L., Purves, J. T., Hughes, F. M. & Nagatomi, J. BOO induces fibrosis and EMT in urothelial cells which can be recapitulated in vitro through elevated storage and voiding pressure cycles. *Int. Urol. Nephrol.* **53**, 2007–2018 (2021).

19. HICKLING, D. R., SUN, T.-T. & WU, X.-R. Anatomy and Physiology of the Urinary Tract: Relation to Host Defense and Microbial Infection. *Microbiol. Spectr.* **3**, 10.1128/microbiolspec.UTI-0016–2012 (2015).

20. Birder, L. A. *et al.* How does the urothelium affect bladder function in health and disease? *Neurourol. Urodyn.* **31**, 293–299 (2012).

21. Birder, L. & Andersson, K.-E. Urothelial Signaling. *Physiol. Rev.* **93**, 653–680 (2013).

22. Lewis, S. A. Everything you wanted to know about the bladder epithelium but were afraid to ask. *Am. J. Physiol.-Ren. Physiol.* **278**, F867–F874 (2000).

23. Khandelwal, P., Abraham, S. N. & Apodaca, G. Cell biology and physiology of the uroepithelium. *Am. J. Physiol. - Ren. Physiol.* **297**, F1477–F1501 (2009).

24. Bolla, S. R., Odeluga, N., Amraei, R. & Jetti, R. Histology, Bladder. in *StatPearls* (StatPearls Publishing, Treasure Island (FL), 2024).

25. Flores, J. L., Cortes, G. A. & Leslie, S. W. Physiology, Urination. in *StatPearls* (StatPearls Publishing, Treasure Island (FL), 2024).

26. Olsen, S. M., Stover, J. D. & Nagatomi, J. Examining the Role of Mechanosensitive Ion Channels in Pressure Mechanotransduction in Rat Bladder Urothelial Cells. *Ann. Biomed. Eng.* **39**, 688–697 (2011).

27. Sharma, J. N., Al-Omran, A. & Parvathy, S. S. Role of nitric oxide in inflammatory diseases. *Inflammopharmacology* **15**, 252–259 (2007).

28. Fusco, F. *et al.* Progressive bladder remodeling due to bladder outlet obstruction: a systematic review of morphological and molecular evidences in humans. *BMC Urol.* **18**, 15 (2018).

29. Davis, B. K. & Ting, J. P.-Y. NLRP3 has a sweet tooth. *Nat. Immunol.* **11**, 105–106 (2010).

30. Harper, S. N., Leidig, P. D., Hughes, F. M., Jin, H. & Purves, J. T. Calcium Pyrophosphate And Monosodium Urate Activate The NLRP3 Inflammasome Within Bladder Urothelium Via Reactive Oxygen Species And TXNIP. *Res. Rep. Urol.* **11**, 319–325 (2019).

31. Zhang, Z. *et al.* The PI3K-AKT-mTOR signaling pathway mediates the cytoskeletal remodeling and epithelial-mesenchymal transition in bladder outlet obstruction. *Heliyon* **9**, e21281 (2023).

32. Geng, J. *et al.* TGFβ2 mediates oxidative stress-induced epithelial-to-mesenchymal transition of bladder smooth muscle. *In Vitro Cell. Dev. Biol. Anim.* (2024) doi:10.1007/s11626-024-00864-9.

33. Chee, N. T., Lohse, I. & Brothers, S. P. mRNA-to-protein translation in hypoxia. *Mol. Cancer* **18**, 49 (2019).

34. Jeffrey Man, H. S., Tsui, A. K. Y. & Marsden, P. A. Chapter Seven - Nitric Oxide and Hypoxia Signaling. in *Vitamins & Hormones* (ed. Litwack, G.) vol. 96 161–192 (Academic Press, 2014).

35. Fabian, Z. The Signaling Nature of Cellular Metabolism: The Hypoxia Signaling. *Cell Signal.* (2018) doi:10.5772/intechopen.79952.

36. Ghafar, M. A. *et al.* Hypoxia and an Angiogenic Response in the Partially Obstructed Rat Bladder. *Lab. Invest.* **82**, 903–909 (2002).

37. Radford, A., Hinley, J., Pilborough, A., Southgate, J. & Subramaniam, R. Hypoxic changes to the urothelium as a bystander of end-stage bladder disease. *J. Pediatr. Urol.* **15**, 158.e1-158.e10 (2019).

38. Azadzoi, K. M., Heim, V. K., Tarcan, T. & Siroky, M. B. Alteration of urothelial-mediated tone in the ischemic bladder: Role of eicosanoids. *Neurourol. Urodyn.* **23**, 258–264 (2004).

39. Sunagawa, M. *et al.* Urinary Bladder Mucosal Responses to Ischemia. *World J. Urol.* **33**, 275–280 (2015).

40. Azadzoi, K. M., Chen, B.-G., Radisavljevic, Z. M. & Siroky, M. B. Molecular Reactions and Ultrastructural Damage in the Chronically Ischemic Bladder. *J. Urol.* **186**, 2115–2122 (2011).

41. Chabaud, S. *et al.* Urothelial cell expansion and differentiation are improved by exposure to hypoxia. *J. Tissue Eng. Regen. Med.* **11**, 3090–3099 (2017).

42. Lin, A. E. *et al.* Role of Hypoxia Inducible Factor-1α (HIF-1α) in Innate Defense against Uropathogenic Escherichia coli Infection. *PLoS Pathog.* **11**, e1004818 (2015).

43. Mohanty, S. *et al.* HIF-1 mediated activation of antimicrobial peptide LL-37 in type 2 diabetic patients. *J. Mol. Med. Berl. Ger.* **100**, 101–113 (2022).

44. Lundberg, J. O., Weitzberg, E. & Gladwin, M. T. The nitrate–nitrite–nitric oxide pathway in physiology and therapeutics. *Nat. Rev. Drug Discov.* **7**, 156–167 (2008).

45. Conners, W. *et al.* l-NAME, a nitric oxide synthase inhibitor, diminishes oxidative damage in urinary bladder partial outlet obstruction. *Am. J. Physiol.-Ren. Physiol.* **290**, F357–F363 (2006).

46. Noguchi, K. *et al.* Evaluation of a rat model of functional urinary bladder outlet obstruction produced by chronic inhibition of nitric oxide synthase. *Life Sci.* **234**, 116772 (2019).

47. Pereira, M. L. *et al.* Effects of nitric oxide inhibitors in mice with bladder outlet obstruction. *Int. Braz J Urol Off. J. Braz. Soc. Urol.* **43**, 356–366 (2017).

48. Jiang, Q., Stone, C. R., Geng, X. & Ding, Y. Hypoxia-inducible factor-1 α and RIP3 triggers NLRP3 inflammasome in ischemic stroke. *Brain Circ.* **4**, 191–192 (2018).

49. Lavallard, V. *et al.* NLRP3 Inflammasome is Activated in Rat Pancreatic Islets by Transplantation and Hypoxia. *Sci. Rep.* **10**, 7011 (2020).

50. Yan, Y. R. *et al.* Chronic intermittent hypoxia-induced mitochondrial dysfunction mediates endothelial injury via the TXNIP/NLRP3/IL-1β signaling pathway. *Free Radic. Biol. Med.* **165**, 401–410 (2021).

51. Chen, C. *et al.* Hypoxia potentiates LPS-induced inflammatory response and increases cell death by promoting NLRP3 inflammasome activation in pancreatic β cells. *Biochem. Biophys. Res. Commun.* **495**, 2512–2518 (2018).

52. Wiafe, B. *et al.* Hypoxia-increased expression of genes involved in inflammation, dedifferentiation, pro-fibrosis, and extracellular matrix remodeling of human bladder smooth muscle cells. *In Vitro Cell. Dev. Biol. Anim.* **53**, 58–66 (2017).

53. Mishra, B. B. *et al.* Nitric oxide controls the immunopathology of tuberculosis by inhibiting NLRP3 inflammasome–dependent processing of IL-1β. *Nat. Immunol.* **14**, 52–60 (2013).

54. Mao, K. *et al.* Nitric oxide suppresses NLRP3 inflammasome activation and protects against LPS-induced septic shock. *Cell Res.* **23**, 201–212 (2013).

55. Sano, T. *et al.* Intravital imaging of mouse urothelium reveals activation of extracellular signal-regulated kinase by stretch-induced intravesical release of ATP. *Physiol. Rep.* **4**, e13033 (2016).

56. Lan, J. *et al.* β-Adrenoceptors regulate matrix metalloproteinase expression in human urothelial cells under hydrostatic pressure. *Neurourol. Urodyn.* **39**, 1292–1303 (2020).

57. Gurung, S., Perocheau, D., Touramanidou, L. & Baruteau, J. The exosome journey: from biogenesis to uptake and intracellular signalling. *Cell Commun. Signal.* **19**, 47 (2021).

58. Donoso-Quezada, J., Ayala-Mar, S. & González-Valdez, J. The role of lipids in exosome biology and intercellular communication: Function, analytics and applications. *Traffic Cph. Den.* **22**, 204–220 (2021).

59. Koritzinsky, E. H., Street, J. M., Star, R. A. & Yuen, P. S. T. Quantification of Exosomes. *J. Cell. Physiol.* **232**, 1587–1590 (2017).

60. Gurunathan, S., Kang, M.-H., Jeyaraj, M., Qasim, M. & Kim, J.-H. Review of the Isolation, Characterization, Biological Function, and Multifarious Therapeutic Approaches of Exosomes. *Cells* **8**, (2019).

61. Doyle, L. M. & Wang, M. Z. Overview of Extracellular Vesicles, Their Origin, Composition, Purpose, and Methods for Exosome Isolation and Analysis. *Cells* **8**, 727 (2019).

62. Patel, G. K. *et al.* Comparative analysis of exosome isolation methods using culture supernatant for optimum yield, purity and downstream applications. *Sci. Rep.* **9**, 5335 (2019).

63. Jackson, K. Isolation and Characterization of Extracellular Vesicles from Various Biological Matrices using Capillary-Channeled Polymer (C-CP) Fiber Solid-Phase Extraction Spin-Down Tips. *Diss.* (2022).

64. Jackson, K. K. & Marcus, R. K. Rapid isolation and quantification of extracellular vesicles from suspension-adapted human embryonic kidney cells using capillary-channeled polymer fiber spin-down tips. *ELECTROPHORESIS* **n/a**,.

65. Jackson, K. K., Powell, R. R., Marcus, R. K. & Bruce, T. F. Comparison of the capillary-channeled polymer (C-CP) fiber spin-down tip approach to traditional methods for the

isolation of extracellular vesicles from human urine. *Anal. Bioanal. Chem.* **414**, 3813–3825 (2022).

66. Jackson, K. K., Powell, R. R., Bruce, T. F. & Marcus, R. K. Rapid isolation of extracellular vesicles from diverse biofluid matrices via capillary-channeled polymer fiber solid-phase extraction micropipette tips. *Analyst* **146**, 4314–4325 (2021).

67. Huang, S., Wang, L., Bruce, T. F. & Marcus, R. K. Isolation and quantification of human urinary exosomes by hydrophobic interaction chromatography on a polyester capillary-channeled polymer fiber stationary phase. *Anal. Bioanal. Chem.* **411**, 6591–6601 (2019).

68. Niu, M. *et al.* A longitudinal study on α-synuclein in plasma neuronal exosomes as a biomarker for Parkinson's disease development and progression. *Eur. J. Neurol.* **27**, 967–974 (2020).

69. Arishe, O. O., Priviero, F., Wilczynski, S. A. & Webb, R. C. Exosomes as Intercellular Messengers in Hypertension. *Int. J. Mol. Sci.* **22**, 11685 (2021).

70. Liu, X., Yuan, W., Yang, L., Li, J. & Cai, J. miRNA Profiling of Exosomes from Spontaneous Hypertensive Rats Using Next-Generation Sequencing. *J Cardiovasc. Transl. Res.* **12**, 75–83 (2019).

71. Belliveau, J. & Papoutsakis, E. T. The microRNomes of Chinese hamster ovary (CHO) cells and their extracellular vesicles, and how they respond to osmotic and ammonia stress. *Biotechnol. Bioeng.* **120**, 2700–2716 (2023).

72. Console, L., Scalise, M. & Indiveri, C. Exosomes in inflammation and role as biomarkers. *Clin. Chim. Acta* **488**, 165–171 (2019).

73. Hughes, F. M. *et al.* The NLRP3 Inflammasome Mediates Inflammation Produced by Bladder Outlet Obstruction. *J. Urol.* **195**, 1598–1605 (2016).

74. Metcalfe, P. D. *et al.* Bladder outlet obstruction: progression from inflammation to fibrosis. *BJU Int.* **106**, 1686–1694 (2010).

75. von Siebenthal, M. *et al.* Urinary miRNA profiles discriminate between obstruction-induced bladder dysfunction and healthy controls. *Sci. Rep.* **11**, 10204 (2021).

76. Gheinani, A. H. *et al.* Characterization of miRNA-regulated networks, hubs of signaling, and biomarkers in obstruction-induced bladder dysfunction. *JCI Insight* **2**, e89560 (2017).

77. Hudson, B. N., Purves, J. T., Hughes, F. M. & Nagatomi, J. Enzyme-induced hypoxia leads to inflammation in urothelial cells in vitro. *Int. Urol. Nephrol.* (2023) doi:10.1007/s11255-023-03900-x.

78. Zenewicz, L. A. Oxygen Levels and Immunological Studies. *Front. Immunol.* **8**, 324 (2017).

79. Umbrello, M., Dyson, A., Feelisch, M. & Singer, M. The Key Role of Nitric Oxide in Hypoxia: Hypoxic Vasodilation and Energy Supply–Demand Matching. *Antioxid. Redox Signal.* **19**, 1690–1710 (2013).

80. Hagen, T., Taylor, C. T., Lam, F. & Moncada, S. Redistribution of Intracellular Oxygen in Hypoxia by Nitric Oxide: Effect on HIF1α. *Science* **302**, 1975–1978 (2003).

81. Allen, C. B., Schneider, B. K. & White, C. W. Limitations to oxygen diffusion and equilibration in in vitro cell exposure systems in hyperoxia and hypoxia. *Am. J. Physiol.-Lung Cell. Mol. Physiol.* **281**, L1021–L1027 (2001).

82. Muñoz-Sánchez, J. & Chánez-Cárdenas, M. E. The use of cobalt chloride as a chemical hypoxia model. *J. Appl. Toxicol.* **39**, 556–570 (2019).

83. Dawes, C. S., Konig, H. & Lin, C.-C. Enzyme-immobilized hydrogels to create hypoxia for in vitro cancer cell culture. *J. Biotechnol.* **248**, 25–34 (2017).

84. Hudson, B. N. *et al.* Stabilization of enzyme-immobilized hydrogels for extended hypoxic cell culture. *Emergent Mater.* (2019) doi:10.1007/s42247-019-00038-4.

85. Bauer, J. A., Zámocká, M., Majtán, J. & Bauerová-Hlinková, V. Glucose Oxidase, an Enzyme "Ferrari": Its Structure, Function, Production and Properties in the Light of Various Industrial and Biotechnological Applications. *Biomolecules* **12**, 472 (2022).

86. Millonig, G. *et al.* Hypoxia-inducible factor 1α under rapid enzymatic hypoxia: Cells sense decrements of oxygen but not hypoxia per se. *Free Radic. Biol. Med.* **46**, 182–191 (2009).

87. Mueller, S., Millonig, G. & Waite, G. N. The GOX/CAT system: A novel enzymatic method to independently control hydrogen peroxide and hypoxia in cell culture. *Adv. Med. Sci. Gruyter Open* **54**, 121–135 (2009).

88. Askoxylakis, V. *et al.* Investigation of tumor hypoxia using a two-enzyme system for in vitro generation of oxygen deficiency. *Radiat. Oncol. Lond. Engl.* **6**, 35 (2011).

89. Baumann, R. P., Penketh, P. G., Seow, H. A., Shyam, K. & Sartorelli, A. C. Generation of oxygen deficiency in cell culture using a two-enzyme system to evaluate agents targeting hypoxic tumor cells. *Radiat. Res.* **170**, 651–660 (2008).

90. Kawamata, H., Kameyama, S., Nan, L., Kawai, K. & Oyasu, R. Effect of epidermal growth factor and transforming growth factor beta 1 on growth and invasive potentials of newly established rat bladder carcinoma cell lines. *Int. J. Cancer* **55**, 968–973 (1993).

91. Yuan, Y., Hilliard, G., Ferguson, T. & Millhorn, D. E. Cobalt Inhibits the Interaction between Hypoxia-inducible Factor-α and von Hippel-Lindau Protein by Direct Binding to Hypoxia-inducible Factor-α. *J. Biol. Chem.* **278**, 15911–15916 (2003).

92. Galkin, A., Higgs, A. & Moncada, S. Nitric oxide and hypoxia. *Essays Biochem.* **43**, 29–42 (2007).

93. Hampl, V., Cornfield, D. N., Cowan, N. J. & Archer, S. L. Hypoxia potentiates nitric oxide synthesis and transiently increases cytosolic calcium levels in pulmonary artery endothelial cells. *Eur. Respir. J.* **8**, 515–522 (1995).

94. Nitti, V. W. Pressure Flow Urodynamic Studies: The Gold Standard for Diagnosing Bladder Outlet Obstruction. *Rev. Urol.* **7**, S14–S21 (2005).

95. Greenland, J. e. *et al.* The effect of bladder outlet obstruction on tissue oxygen tension and blood flow in the pig bladder. *BJU Int.* **85**, 1109–1114 (2000).

96. Batista, J. E., Wagner, J. R., Azadzoi, K. M., Krane, R. J. & Siroky, M. B. Direct Measurement of Blood Flow in the Human Bladder. *J. Urol.* **155**, 630–633 (1996).

97. Hohlbrugger, G., Frauscher, F., Strasser, H., Stenzl, A. & Bartsch, G. Evidence for the autoregulation of vesical circulation by intravesical potassium chloride and distension in the normal human bladder. *BJU Int.* **85**, 412–415 (2000).

98. Volikova, A. I. *et al.* Structural, biomechanical and hemodynamic assessment of the bladder wall in healthy subjects. *Res. Rep. Urol.* **11**, 233–245 (2019).

99. Belenky, A. *et al.* Detrusor resistive index evaluated by doppler ultrasonography as a potential indicator of bladder outlet obstruction. *Urology* **62**, 647–650 (2003).

100. Kershen, R. T., Azadzoi, K. M. & Siroky, M. B. Blood Flow, Pressure and Compliance in the Male Human Bladder. *J. Urol.* **168**, 121–125 (2002).

101. Koritsiadis, G. *et al.* Immunohistochemical estimation of hypoxia in human obstructed bladder and correlation with clinical variables. *BJU Int.* **102**, 328–332 (2008).

102. Jiang, Q. *et al.* Hypoxia Inducible Factor-1α (HIF-1α) Mediates NLRP3 Inflammasome-Dependent-Pyroptotic and Apoptotic Cell Death Following Ischemic Stroke. *Neuroscience* **448**, 126–139 (2020).

103. Minutoli, L. *et al.* ROS-Mediated NLRP3 Inflammasome Activation in Brain, Heart, Kidney, and Testis Ischemia/Reperfusion Injury. *Oxid. Med. Cell. Longev.* **2016**, 2183026 (2016).

104. Xin, X., Yang, K., Liu, H. & Li, Y. Hypobaric hypoxia triggers pyroptosis in the retina via NLRP3 inflammasome activation. *Apoptosis* (2022) doi:10.1007/s10495-022-01710-7.

105. Watanabe, S. *et al.* Glucose regulates hypoxia-induced NLRP3 inflammasome activation in macrophages. *J. Cell. Physiol.* **n/a**, (2020).

106. Choi, B.-J., Park, S.-A., Lee, S.-Y., Cha, Y. N. & Surh, Y.-J. Hypoxia induces epithelial-mesenchymal transition in colorectal cancer cells through ubiquitin-specific protease 47-mediated stabilization of Snail: A potential role of Sox9. *Sci. Rep.* **7**, 15918 (2017).

107. Joseph, J. P., Harishankar, M. K., Pillai, A. A. & Devi, A. Hypoxia induced EMT: A review on the mechanism of tumor progression and metastasis in OSCC. *Oral Oncol.* **80**, 23–32 (2018).

108. Zhu, J. *et al.* HIF-1α promotes ZEB1 expression and EMT in a human bladder cancer lung metastasis animal model. *Oncol. Lett.* **15**, 3482–3489 (2018).

109. Hughes, F. M., Turner, D. P. & Todd Purves, J. The potential repertoire of the innate immune system in the bladder: expression of pattern recognition receptors in the rat bladder and a rat urothelial cell line (MYP3 cells). *Int. Urol. Nephrol.* **47**, 1953–1964 (2015).

110. Hughes, F. M. *et al.* Inflammasomes are important mediators of cyclophosphamide-induced bladder inflammation. *Am. J. Physiol. - Ren. Physiol.* **306**, F299–F308 (2014).

111. Lin, A. T. L. & Juan, Y.-S. Ischemia, Hypoxia and Oxidative Stress in Bladder Outlet Obstruction and Bladder Overdistention Injury. *LUTS Low. Urin. Tract Symptoms* **4**, 27–31.

112. Ghafar, M. A. *et al.* Effects of chronic partial outlet obstruction on blood flow and oxygenation of the rat bladder. *J. Urol.* **167**, 1508–1512 (2002).

113. Hughes, F. M., Sexton, S. J., Jin, H., Govada, V. & Purves, J. T. Bladder fibrosis during outlet obstruction is triggered through the NLRP3 inflammasome and the production of IL-1β. *Am. J. Physiol. Renal Physiol.* **313**, F603–F610 (2017).

114. Azadzoi, K. M., Pontari, M., Vlachiotis, J. & Siroky, M. B. Canine Bladder Blood Flow and Oxygenation: Changes Induced by Filling, Contraction and Outlet Obstruction. *J. Urol.* **155**, 1459–1465 (1996).

115. Chandel, N. S. *et al.* Mitochondrial reactive oxygen species trigger hypoxia-induced transcription. *Proc. Natl. Acad. Sci. U. S. A.* **95**, 11715–11720 (1998).

116. Guzy, R. D. *et al.* Mitochondrial complex III is required for hypoxia-induced ROS production and cellular oxygen sensing. *Cell Metab.* **1**, 401–408 (2005).

117. Jo, E.-K., Kim, J. K., Shin, D.-M. & Sasakawa, C. Molecular mechanisms regulating NLRP3 inflammasome activation. *Cell. Mol. Immunol.* **13**, 148–159 (2016).

118. Abais, J. M., Xia, M., Zhang, Y., Boini, K. M. & Li, P.-L. Redox Regulation of NLRP3 Inflammasomes: ROS as Trigger or Effector? *Antioxid. Redox Signal.* **22**, 1111–1129 (2015).

119. Kelley, N., Jeltema, D., Duan, Y. & He, Y. The NLRP3 Inflammasome: An Overview of Mechanisms of Activation and Regulation. *Int. J. Mol. Sci.* **20**, (2019).

120. McIlwain, D. R., Berger, T. & Mak, T. W. Caspase Functions in Cell Death and Disease. *Cold Spring Harb. Perspect. Biol.* **5**, a008656 (2013).

121. Molla, M. D., Ayelign, B., Dessie, G., Geto, Z. & Admasu, T. D. Caspase-1 as a regulatory molecule of lipid metabolism. *Lipids Health Dis.* **19**, 34 (2020).

122. Liu, K.-H. *et al.* Hypoxia Stimulates the Epithelial–to–Mesenchymal Transition in Lung Cancer Cells Through Accumulation of Nuclear β-Catenin. *Anticancer Res.* **38**, 6299–6308 (2018).

123. Sexton, C. C. *et al.* The overlap of storage, voiding and postmicturition symptoms and implications for treatment seeking in the USA, UK and Sweden: EpiLUTS. *BJU Int.* **103**, 12–23 (2009).

124. Yeung, J. Y., Eschenbacher, M. A. & Pauls, R. N. Pain and embarrassment associated with urodynamic testing in women. *Int. Urogynecology J.* **25**, 645–650 (2014).

125. Abramowicz, A., Widłak, P. & Pietrowska, M. Different Types of Cellular Stress Affect the Proteome Composition of Small Extracellular Vesicles: A Mini Review. *Proteomes* **7**, 23 (2019).

126. Parolini, I. *et al.* Microenvironmental pH is a key factor for exosome traffic in tumor cells. *J. Biol. Chem.* **284**, 34211–34222 (2009).

127. Crewe, C. Energetic Stress-induced Metabolic Regulation by Extracellular Vesicles. *Compr. Physiol.* **13**, 5051–5068 (2023).

128. Borges, F. T. *et al.* TGF-β1–Containing Exosomes from Injured Epithelial Cells Activate Fibroblasts to Initiate Tissue Regenerative Responses and Fibrosis. *J. Am. Soc. Nephrol. JASN* **24**, 385–392 (2013).

129. Yu, W. *et al.* miR-20a-5p is enriched in hypoxia-derived tubular exosomes and protects against acute tubular injury. *Clin. Sci.* **134**, 2223–2234 (2020).

130. Zhou, X. *et al.* Tubular cell-derived exosomal miR-150-5p contributes to renal fibrosis following unilateral ischemia-reperfusion injury by activating fibroblast *in vitro* and *in vivo*. *Int. J. Biol. Sci.* **17**, 4021–4033 (2021).

131. de Jong, O. G., van Balkom, B. W. M., Gremmels, H. & Verhaar, M. C. Exosomes from hypoxic endothelial cells have increased collagen crosslinking activity through up-regulation of lysyl oxidase-like 2. *J. Cell. Mol. Med.* **20**, 342–350 (2016).

132. Liang YR, Zhang T, Jia P, Xu XL, Fang Y, Ding XQ. Interaction between bone marrow-derived dendritic cells and miR-21 of tubular renal epithelial cells under hypoxia. *European Review* https://www.europeanreview.org/article/17124 (2019).

133. Aires, I. D. *et al.* Exosomes derived from microglia exposed to elevated pressure amplify the neuroinflammatory response in retinal cells. *Glia* **68**, 2705–2724 (2020).

134. Gheinani, A. H. *et al.* Concordant miRNA and mRNA expression profiles in humans and mice with bladder outlet obstruction. *Am. J. Clin. Exp. Urol.* **6**, 219–233 (2018).

135. Huang, K. *et al.* Comparison of Human Urinary Exosomes Isolated via Ultracentrifugation Alone versus Ultracentrifugation Followed by SEC Column-Purification. *J. Pers. Med.* **12**, 340 (2022).

136. Dewenter, M. *et al.* Chronic isoprenaline/phenylephrine vs. exclusive isoprenaline stimulation in mice: critical contribution of alpha1-adrenoceptors to early cardiac stress responses. *Basic Res. Cardiol.* **117**, 15 (2022).

137. Gómez, I. *et al.* Differential expression profile of genes involved in the immune response associated to progression of chronic Chagas disease. *PLoS Negl. Trop. Dis.* **17**, e0011474 (2023).

138. Fu, L. *et al.* DGKA Mediates Resistance to PD-1 Blockade. *Cancer Immunol. Res.* **9**, 371–385 (2021).

139. Fu, L. *et al.* DGKA interacts with SRC/FAK to promote the metastasis of non-small cell lung cancer. *Cancer Lett.* **532**, 215585 (2022).

140. Mellai, M. *et al.* SEL1L plays a major role in human malignant gliomas. *J. Pathol. Clin. Res.* **6**, 17–29 (2020).

141. Coppieters, N. *et al.* Study of Strawberry Notch homolog 1 and 2 expression in human glioblastoma. *J. Neurooncol.* **161**, 515–523 (2023).

142. Grill, M. *et al.* Strawberry notch homolog 2 is a novel inflammatory response factor predominantly but not exclusively expressed by astrocytes in the central nervous system. *Glia* **63**, 1738–1752 (2015).

143. Jonas, K. *et al.* MiR-4649-5p acts as a tumor-suppressive microRNA in triple negative breast cancer by direct interaction with PIP5K1C, thereby potentiating growth-inhibitory effects of the AKT inhibitor capivasertib. *Breast Cancer Res.* **25**, 119 (2023).

144. Qian, C., Xu, Z., Chen, L., Wang, Y. & Yao, J. Long noncoding RNA LINC01391 restrained gastric cancer aerobic glycolysis and tumorigenesis via targeting miR-12116/CMTM2 axis. *J. Cancer* **11**, 6264–6276 (2020).

145. Fan, X. *et al.* Piplartine suppresses proliferation and invasion of hepatocellular carcinoma by LINC01391-modulated Wnt/β-catenin pathway inactivation through ICAT. *Cancer Lett.* **460**, 119–127 (2019).

146. Li, D. *et al.* CADM2, as a new target of miR-10b, promotes tumor metastasis through FAK/AKT pathway in hepatocellular carcinoma. *J. Exp. Clin. Cancer Res. CR* **37**, 46 (2018).

147. Liu, N. *et al.* CADM2 inhibits human glioma proliferation, migration and invasion. *Oncol. Rep.* **41**, 2273–2280 (2019).